Investigation and discovery of targetable markers in urological tumors

Doctoral thesis

to obtain a doctorate (PhD)

from the Faculty of Medicine

of the University of Bonn

Miriam Saponaro

from Mirano, Italy

2025

Written with authorization of
the Faculty of Medicine of the University of Bonn

First reviewer: Prof. Dr. med. Michael Hölzel

Second reviewer: Prof. Dr. Nicola Aceto

Day of oral examination: 05/05/2025

From the Clinic and Policlinic for Urology and Pediatric Urology

Table of contents

List of abbreviations 6

1 Introduction 12

1.1 Cancers 14

1.1.1 Prostate cancer (PCa) 14

1.1.2 Bladder cancer (BCa) 16

1.2 Targets 20

1.2.1 CUB domain-containing protein 1 (CDCP1) 20

1.2.2 Epithelial growth factor receptor (EGFR) 23

1.2.3 Tumor-associated macrophages (TAMs) 25

1.2.4 Senescence 28

1.3 Therapeutical strategies 32

1.3.1 Nanobodies (Nbs) 32

1.3.2 TAM-targeting therapies 34

1.3.3 Senolytic drugs 37

2 Materials and methods 39

2.1 Solutions 39

2.2 Cell culture 41

2.3 Nb production 42

2.4 FACS staining with Nbs 44

2.5 Vectors for CDCP1 mutants and CDCP1 isoforms expression and transfection 44

2.6 SDS Gels preparation 45

2.7 Western blotting (WB) 45

2.8 Vitality assay 46

2.9 Immunohistochemistry (IHC) on MIBC and PCa tumor-microarray (TMA) 46

2.10 CRISPR/Cas9 47
2.11 Cytokine arrays 47
2.12 Human macrophage differentiation 48
2.13 Murine macrophage differentiation 48
2.14 Macrophage migration assays 49
2.15 Macrophage polarization assay 49
2.16 Anti-CDCP1 Ab production and treatments 50
2.17 Treatment with ERK inhibitor (iERK) 50
2.18 qPCR 51
2.19 Prostate and bladder murine organoids generation 52
2.20 FACS on mouse tumors PCa 53
2.21 Generation of LNCaP clones with the CRISPaint method 53
2.22 FACS analysis clones 55
2.23 mRNA sequencing 55
2.24 Statistical analysis 56
3 Results 57
3.1 Nbs targeting CDCP1 and EGFR reduce tumor growth *in-vitro* 57
3.2 CDCP1 expression is correlated with inflammatory cytokine production and TAM infiltration in urological cancers 63
3.3 Generation of a model for senescence evaluation with CRISPaint technology and identification of new senescence markers 71
4 Discussion 78
5 Abstract 88
6 List of figures 90
7 List of tables 91
8 References 92

9 Acknowledgements 112

10 Curriculum vitae 114

List of abbreviations

ADC	Antibody-drug conjugate
ADT	Androgen deprivation therapy
APC	Antigen-presenting cells
AR	Androgen receptor
Arg1	Arginase 1
ATF	Amino-terminal fragment
ATF5	Activating transcription factor 5
Ba/Sq	Basal/squamous
Bca	Bladder cancer
BCG	Bacillus Calmette-Guérin
BCL-2	B-cell lymphoma 2
BM	Bone marrow
BMDM	Bone marrow-derived macrophages
BMPs	Bone morphogenetic proteins
CAM	Chorioallantoic membrane
CAR	Chimeric antigen receptor
CCL2	CC-chemokine ligand 2
CD11b	Cluster of differentiation 11b
CD14	Cluster of differentiation 14
CD16	Cluster of differentiation 16
CD163	Cluster of Differentiation 163
CD19	Cluster of differentiation 19
CD200R	Cluster of Differentiation 200R
CD206	Cluster of Differentiation 206
CD3	Cluster of differentiation 3
CD318	Cluster of differentiation 318
CD38	Cluster of differentiation 38
CD45	Cluster of differentiation 45
CD49b	Cluster of differentiation 49b
CD68	Cluster of differentiation 68

CD80	Cluster of differentiation 80
CD86	Cluster of differentiation 86
CDCP1	CUB domain-containing protein 1
CDK2	Cyclin dependent kinase 2
CDK4	Cyclin dependent kinase 4
CDK6	Cyclin dependent kinase 6
CDKN1A	Cyclin-dependent kinase inhibitor 1A
CDKN2A	Cyclin-dependent kinase inhibitor 2A
CDKs	Cyclin-dependent kinases
cDNA	Complementary deoxyribonucleic acid
CDR	Complementarity-determining regions
Cet	Cetuximab
CH1	Immunoglobulin heavy chain gamma constant domain 1
CH2	Immunoglobulin heavy chain gamma constant domain 2
CH3	Immunoglobulin heavy chain gamma constant domain 3
CIS	Chemotherapy-induced senescence
CL	Immunoglobulin light chain gamma constant domain
CLU	Clusterin
CM	Conditioned media
CRPC	Castration-resistant prostate cancer
CSF-1	Colony stimulating factor 1
CTF	Carboxyl-terminal fragment
CUB1	CUB domain 1
CUB2	CUB domain 2
CXCL1	Chemokine (C-X-C motif) ligand 1
CXCL2	Chemokine (C-X-C motif) ligand 2
cynoCDCP1	Non-human primate CDCP1
DAMPs	Damage-associated molecular patterns
DDR	DNA damage response
delCUB1	Deletion CUB1
delCUB2	Deletion CUB2
delN-term	Deletion N-term

DER	Digital rectal examination
EGF	Epithelial growth factor
EGFR	Epithelial growth factor receptor
ELISA	Enzyme-linked immunosorbent assay
ERK	Extracellular signal-regulated kinases
ERK1/2	Extracellular signal-regulated kinases 1 and 2
Ex19Del	Deletions in exon 19
Fab	Fragment antigen-binding
FACS	Fluorescence-activated cell sorting
Fc	Fragment crystallizable
FGFR3	Fibroblast growth factor receptor 3
FGFs	Fibroblast growth factors
FlaB	Flagellin B
FR	Framework regions
GAPDH	Glyceraldehyde-3-phosphate dehydrogenase
GDF15	Growth differentiation factor 15
GS	Gleason score
HA	Hemagglutinin
HB-EGF	Heparin-binding EGF
HcAbs	Heavy-chain antibodies
HER1	Epidermal growth factor receptor 1
HER2	Human epidermal growth factor receptor 2
HGFR	Hepatocyte growth factor receptor
hCDCP1	Human CDCP1
iERK	ERK inhibitor
IFN-gamma	Interferon-gamma
IgG	Immunoglobulin G
IHC	Immunohistochemistry
IL10	Interleukin 10
IL13	Interleukin 13
IL1-alpha	Interleukin 1-alpha
IL1-beta	Interleukin 1-beta

IL4	Interleukin 4
IL6	Interleukin 6
IL8	Interleukin 8
IL8	Interleukin 8
iNos	Inducible nitric oxide synthases
IPTG	Isopropyl-β-D-thiogalactopyranosid
ISUP	Society of Urological Pathology
KIF14	Kinesin family member 14
KO	Knock-out
L858R	Arginine replacing leucine at codon 858
LHRH	Luteinizing hormone-releasing hormone
LPS	Lipopolysaccharide
LumNS	Luminal non-specified
LumP	Luminal papillary
LumU	Luminal unstable
mAbs	Monoclonal antibodies
MAPK	Mitogen-activated protein kinase
mCRPC	Metastatic castration-resistant prostate cancer
MIBC	Muscle-invasive bladder cancer
mCDCP1	Murine CDCP1
MMPs	Metalloproteases
mpMRI	Multiparametric magnetic resonance imaging
mRNA	Messenger ribonucleic acid
mTOR	Mammalian target of rapamycin
Nbs	Nanobodies
NE-like	Neuroendocrine-like
NMIBC	Non-muscle-invasive bladder cancer
PAMPs	Pathogen-associated molecular patterns
PBMCs	Peripheral blood mononuclear cells
Pca	Prostate cancer
PCR	Polymerase chain reaction
pEGFR	Phosphorylated EGFR

pERK	Phosphorylated ERK
PHLDA	Pleckstrin homology-like domain family A member 1
PI3K	Phosphoinositide 3 kinase
PKCδ	Protein kinase C delta
polyI:C	Polyinosinic:polycytidylic acid
PSA	Prostate-specific antigen
Pten	Phosphatase and ensin homolog
RB	Retinoblastoma tumor suppressor protein
rFc	Rabbit Fc
rFc-Nb	Rabbit Fc-nanobodies
RTK	Receptor tyrosine kinase
RT-PCR	Reverse transcription polymerase chain reaction
SASP	Senescence-associated secretory phenotype
SFKs	Src family kinases
sgRNA	Single guide RNA
SIMA135	Subtractive immunization associated 135 kDa
TAM	Tumor-associated macrophages
TB	Terific Broth
TGF-beta	Tumor growth factor-beta
TGF-α	Transforming growth factor α
TKIs	Tyrosine kinase inhibitors
TLR3	Toll-like receptor 3
TLR4	Toll-like receptor 4
TLR7	Toll-like receptor 7
TLR9	Toll-like receptor 9
TLRs	Toll-like receptors
TMA	Tumor-microarray
TME	Tumor microenvironment
TNF-alpha	Tumor necrosis factor-alpha
TNM	Tumor, node, metastases staging
TP53I3	Tumor protein p53 inducible protein 3
TRASK	Transmembrane and associated with Src kinases

TURBT	Transurethral resection of bladder tumor
UC	Urothelial carcinoma
UGT2B11	UDP glucuronosyltransferase family 2 member B11
VEGF	Vascular endothelial growth factors
VEGF	Vascular endothelial growth factor
VH	Immunoglobulin heavy chain gamma variable domain
VHH	Heavy chain variable domain from HcAbs
VL	Immunoglobulin light chain gamma variable domain
WB	Western blotting
WT	Wild-type
β-GAL	β-D-galactosidase

1 Introduction

Urological cancers account for roughly 10 % of all cancer cases globally (Bray et al., 2024; Zi et al., 2021, pp. 1990–2019). The most common types of urological cancers include prostate, bladder, and kidney cancer. Both men and women can be affected by bladder cancer (BCa) and kidney cancer, whereas prostate cancer (PCa), testicular, and penile cancers are exclusive to men. The etiology of these diseases is largely attributed to dietary habits and smoking (*Urological Cancers*, n.d.). As described in Fig. 1 the incidence and mortality of urological cancers are still very elevated. Therefore, urological cancers remain a major global health challenge (Zi et al., 2021, pp. 1990–2019).

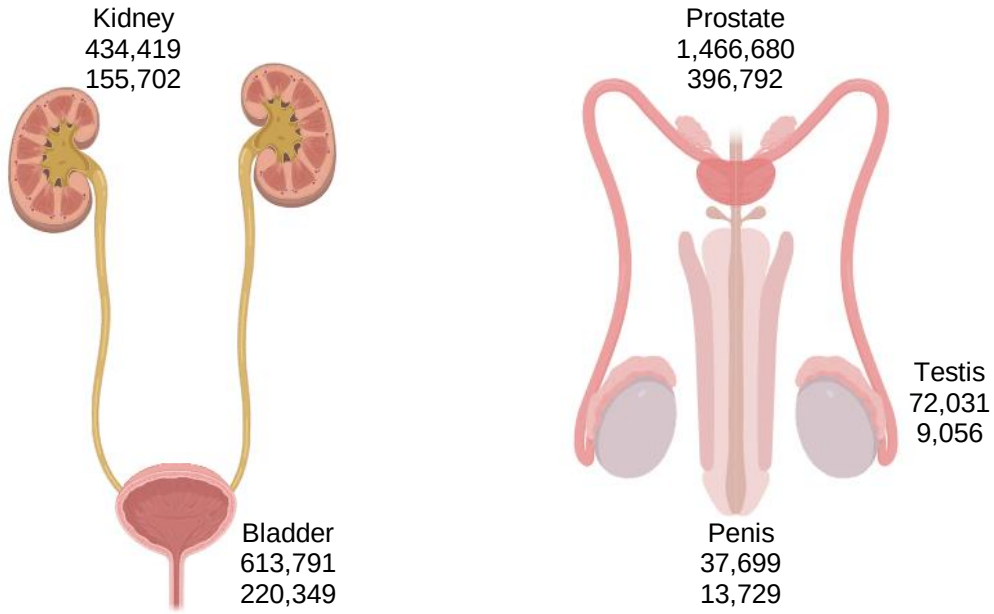

Fig. 1: Urological cancer incidence and mortality
Number of newly diagnosed cases (top) and deaths (bottom) of urological cancers in 2022. Data obtained from Bray et al. (Bray et al., 2024). Image created with BioRender.

Given that mortality in these cancers is often due to late diagnosis or the development of resistance to standard therapy, the scientific community has proposed solutions focused on earlier detection and the treatment of more advanced or resistant tumors. These solutions primarily involve discovering novel tumor markers or establishing more effective

or long-lasting therapies. In this line, the projects presented in this thesis aim to develop therapies that can effectively target advanced cancer stages and/or overcome therapy resistance in some of the most frequent urological lesions. In detail, three different scientific questions were explored: 1) Can CUB domain-containing protein 1 (CDCP1) and epithelial growth factor receptor (EGFR) be successfully targeted with nanobodies (Nbs) in urological cancers? 2) Is CDCP1 correlated with tumor-associated macrophages (TAM) infiltration and can CDCP1 be targeted to diminish TAM-negative effects in advanced urological cancers? 3) Can the biological features of senescence be characterized more appropriately to simplify the discovery of new senescence markers for the treatment of advanced PCa?

1.1Cancers

1.1.1 Prostate cancer (PCa)

PCa ranks as the second most common cancer overall, and the most common among men, with more than 1.4 million new diagnoses and 397,000 deaths worldwide in 2022 (Bray et al., 2024). Confirmed risk factors for PCa include aging, family medical history, and specific genetic alterations. Smoking, body weight, and certain dietary factors are potential risk factors that are still under investigation (Bray et al., 2024). The incidence of PCa has seen a significant rise in recent years, largely attributable to the effectiveness of screening programs that evaluate prostate-specific antigen (PSA) levels in blood. Despite this increase in diagnosis, survival rates remain high due to early detection, the typically indolent nature of the tumor, and advancements in treatment modalities (Leach, 2023). Initial detection of PCa is commonly achieved through PSA testing or digital rectal examination (DRE), with further investigation conducted via multiparametric magnetic resonance imaging (mpMRI) (Barber and Ali, 2022). An abnormal DRE or mpMRI necessitates a biopsy and the determination of the Gleason score (GS), recently replaced by the International Society of Urological Pathology (ISUP) grade (Barber and Ali, 2022). Another utilized tool for PCa classification is tumor, node, metastases (TNM) staging (*Urological Cancers*, n.d.). The integration of PSA levels, GS, and TNM staging facilitates the stratification of patients based on the risk level, which is crucial in guiding clinical decision-making for the most appropriate intervention (Tonry et al., 2020). The standard clinical approach for low-risk PCa, which is considered non-life threatening, typically involves a strategy of watchful waiting or active surveillance (Tonry et al., 2020). On the contrary, medium and high-risk PCa necessitate treatment. Curative treatment options for these cases include radical prostatectomy, radical radiotherapy, and androgen deprivation therapy (ADT) (Tonry et al., 2020). Specifically, ADT aims to reduce the bioavailability of androgens, which are the primary drivers of the growth and proliferation of epithelial prostatic cells (Tonry et al., 2020). This can be achieved via two strategies. The first is a surgical approach, known as orchiectomy or surgical castration, which involves the removal of the testes. The second is a chemical approach, also known as chemical castration, which employs the use of luteinizing hormone-releasing hormone (LHRH) agonists and antagonists to inhibit the production and release of androgens (Wadosky

and Koochekpour, 2016). Likewise, the standard therapeutic regimen for the metastatic form of the disease is ADT, either as a standalone treatment or combined with chemotherapy, specifically the taxanes docetaxel or cabazitaxel (Wadosky and Koochekpour, 2016). Despite the initial efficacy of ADT, a majority of patients ultimately develop resistance. This leads to the emergence of a more aggressive form of the disease known as castration-resistant prostate cancer (CRPC) (Wadosky and Koochekpour, 2016). The standard therapeutic approach for primary CRPC or metastatic castration-resistant prostate cancer (mCRPC) typically involves the administration of docetaxel/cabazitaxel or second-generation ADT, such as enzalutamide or abiraterone (Achard et al., 2021). A summary of the clinical progression of PCa and its elective treatments is represented in Fig. 2.

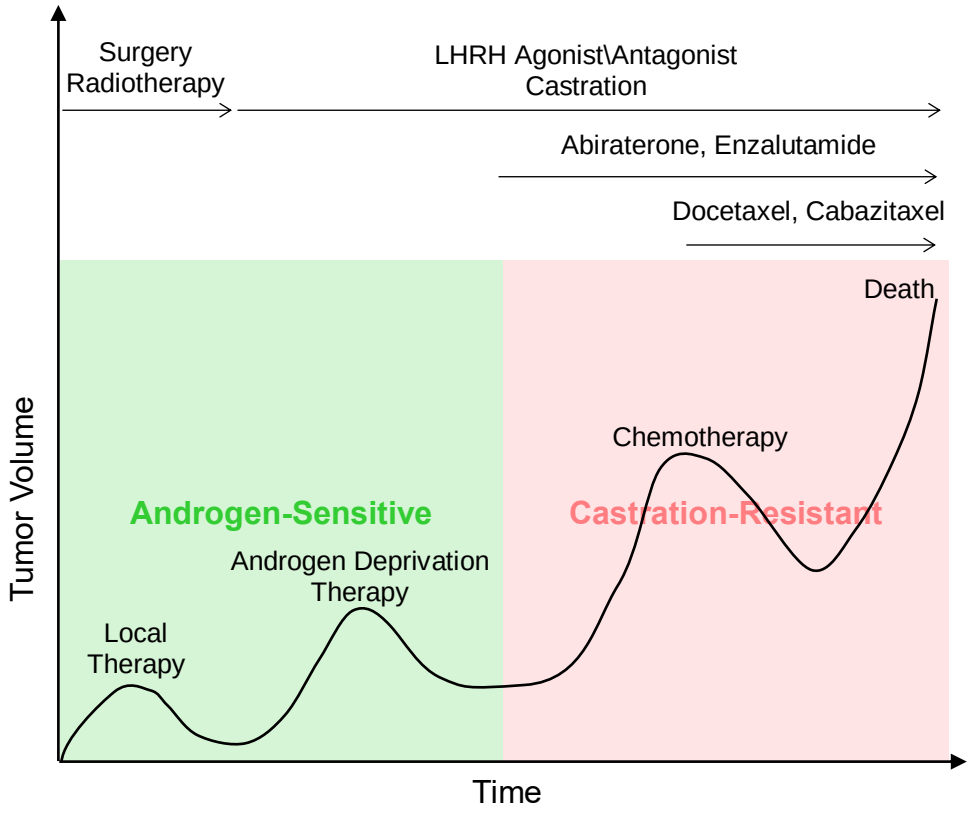

Fig. 2: Clinical progression and treatment of PCa
In summary, medium and high-risk PCa are treated with surgery, radiotherapy, and ADT. The tumor is stable for a relatively long period until the development of resistance to ADT. At this stage, treatment typically involves second-generation ADT and chemotherapy; however, resistance often develops, ultimately leading to the patient's death.

To briefly describe the standard treatments used in the clinic, taxanes, such as docetaxel and cabazitaxel, exert their antineoplastic activity by interacting with microtubules. This

interaction impedes the depolarization of microtubules and halts cell division, ultimately inducing apoptosis (Mosca et al., 2021). Enzalutamide is a selective antagonist that specifically targets the androgen receptor (AR), effectively blocking its activation by androgens, thereby disrupting the downstream signaling pathways that drive the growth and proliferation of PCa cells (Schalken and Fitzpatrick, 2016). Abiraterone, on the other hand, is designed to inhibit androgen biosynthesis within the adrenal gland. It accomplishes this by targeting and inhibiting the enzyme CYP17A1, crucial for producing androgens at this location (Achard et al., 2021).

1.1.2 Bladder cancer (BCa)

After PCa, BCa is the second most common urological tumor. In 2022, it was responsible for about 614,000 new cases and led to the death of 220,000 individuals (Bray et al., 2024). It predominantly affects males and the causes vary depending on the geographical region. In industrialized nations, the main factors are tobacco smoking, exposure to specific chemicals at work, and arsenic in drinking water (Bray et al., 2024). BCa typically presents clinically as painless gross hematuria, with cystoscopy serving as the gold standard for initial diagnosis (Lopez-Beltran et al., 2024). Any abnormal findings necessitate a pathological evaluation. Histopathological material can be procured via transurethral resection of bladder tumor (TURBT), which should be performed within 31 days from the diagnosis and also serves a therapeutic purpose (Lopez-Beltran et al., 2024). The most common histologic type of BCa is urothelial carcinoma (UC). It represents approximately 80-90 % of all BCa cases and involves the urothelium (Barber and Ali, 2022). Hence, it can also be present in the urethra and upper urinary tract, albeit in rarer instances. Non-urothelial bladder cancers, which are less common but more invasive, include squamous cell carcinoma and adenocarcinoma (Black and Black, 2020). The determination of the therapeutic approach relies both on the histological characteristics of the lesion and risk stratification. Pathologists stratify BCa into low-risk, intermediate-risk, or high-risk categories based on TNM staging. In the absence of nodal (N) or distant metastases (M), the classification relies on the primary tumor characteristics (T). It can be dichotomized into non-muscle-invasive bladder cancer (NMIBC) or muscle-invasive bladder cancer (MIBC) according to its penetration into the muscle layer surrounding the

bladder lumen (Matulewicz and Steinberg, 2020). NMIBC is typically low-risk, isolated tumors that are restricted to the bladder wall and are classified as T1 (Fig. 3). The standard treatment for these tumors involves TURBT followed by a single chemotherapy dose, which may include agents such as mitomycin C, gemcitabine, epirubicin, and docetaxel (Lopez-Beltran et al., 2024; Matulewicz and Steinberg, 2020). However, under certain circumstances, NMIBC can be classified as intermediate-risk or high-risk. In these cases, additional treatments may be required, which could include further chemotherapy, the use of bacillus Calmette-Guérin (BCG), or a radical cystectomy for the most aggressive forms (Matulewicz and Steinberg, 2020). On the other hand, MIBC is consistently categorized as high-risk due to its aggressive nature and tendency to spread beyond the bladder (Lopez-Beltran et al., 2024). All tumors that are exceeding T1 are classified as MIBC (T2, T3, T4) (Fig. 3).

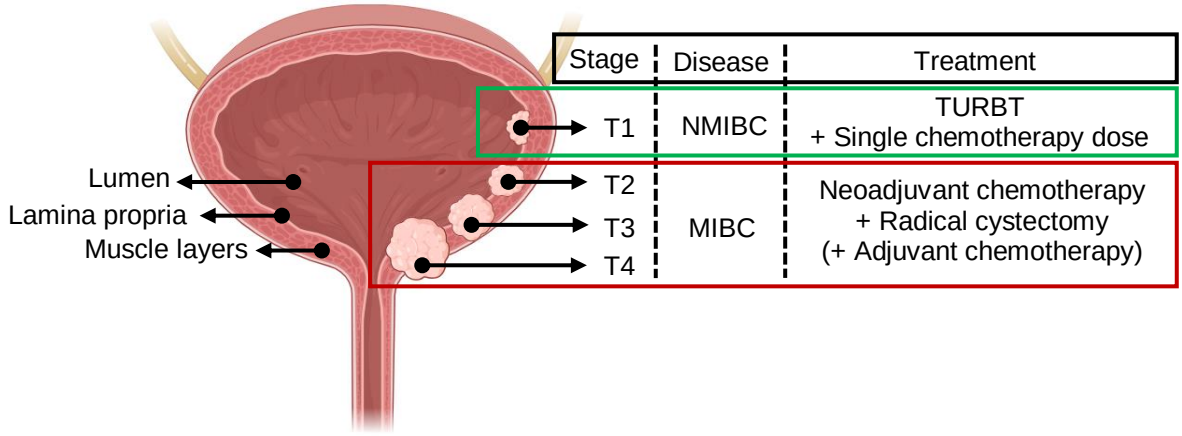

Fig. 3: Clinical progression and treatment of BCa
In summary, BCa is divided in NMIBC and MIBC. NMIBC is confined to the bladder lumen and is generally treated with TURBT. MIBC, which includes the most advanced stages, is infiltrating the muscle layer and treatment require radical cystectomy associated with chemotherapy. Image created with BioRender.

Recent transcriptome analysis has identified several molecular subtypes of MIBC that could potentially enhance patient stratification and provide insights into possible therapeutic strategies (Kamoun et al., 2020). These subtypes include luminal papillary (LumP), luminal non-specified (LumNS), luminal unstable (LumU), stroma-rich, basal/squamous (Ba/Sq), and neuroendocrine-like (NE-like) (Kamoun et al., 2020). Each subtype is characterized by unique differentiation patterns, oncogenic alterations, tumor microenvironments, and associations with specific histological and clinical features, all of

which are summarized in Fig. 4. LumP and Ba/Sq are the most common subtypes, representing 24 % and 35 % of patients respectively (Kamoun et al., 2020). Tumors of the LumP subtype are distinguished by their high levels of fibroblast growth factor receptor 3 (FGFR3) expression. This suggests that therapeutic strategies aimed at targeting FGFR3 could prove effective for these particular tumors (Kamoun et al., 2020). On the other hand, Ba/Sq tumors are characterized by high EGFR expression, increased immune infiltration, and a significantly lower survival rate compared to luminal variants (Kamoun et al., 2020).

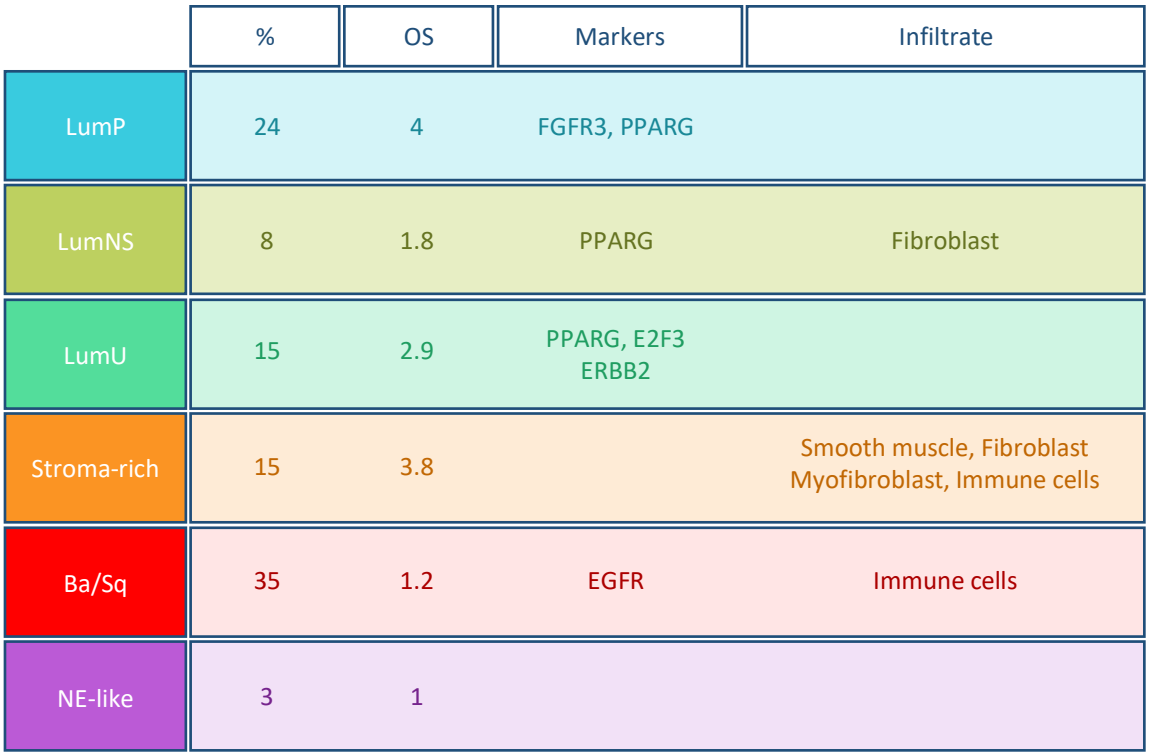

Fig. 4: MIBC molecular subtypes
Description of the most relevant characteristics of the six molecular subtypes recognized in MIBC. % refers to the percentage of MIBC patients affected by each subtype. OS refers to the average overall survival. Markers lists the most common markers characterizing each subtype. Infiltrate indicates the most common cell types infiltrating the tumor.

The standard treatment protocol for MIBC currently involves neoadjuvant chemotherapy, which may include drugs such as methotrexate, vinblastine, adriamycin, cisplatin, or a combination of gemcitabine and cisplatin, followed by radical cystectomy (Lopez-Beltran et al., 2024). Clinical trials showed that neoadjuvant can improve survival at 5 years for around 5-8 % of the patients (Lopez-Beltran et al., 2024; Sarkis et al., 2022; Stecca et al., 2023). Following surgery, patients with MIBC may undergo adjuvant chemotherapy,

although its efficacy in improving patient survival has yet to be proven (Lopez-Beltran et al., 2024). Despite therapeutic interventions, these tumors eventually relapse and metastasize beyond the anatomical confines of the bladder. Palliative care is administered to patients with locally advanced or metastatic BCa with the dual objectives of decelerating tumor progression and alleviating associated symptoms (Lopez-Beltran et al., 2024). The first-line therapeutic strategy typically involves platinum-based chemotherapy, such as cisplatin (Lopez-Beltran et al., 2024). However, recent advancements in the field have led to the emergence of novel treatment options, such as the combination of enfortumab-vedotin, an antibody-drug conjugate (ADC) targeting Nectin-4, and the immune checkpoint inhibitor pembrolizumab (Lopez-Beltran et al., 2024). In instances where platinum-based treatment proves ineffective, alternative therapeutic strategies may be employed, including tyrosine-kinase inhibitors like erdafitinib and immunotherapy (Lopez-Beltran et al., 2024).

1.2Targets

1.2.1 CUB domain-containing protein 1 (CDCP1)

CDCP1, also known as cluster of differentiation 318 (CD318), subtractive immunization associated 135 kDa (SIMA135), and transmembrane and associated with Src kinases (TRASK) is a cell surface glycoprotein composed of an amino-terminal signal peptide, an extracellular domain, a short transmembrane domain and a cytoplasmic domain (Wortmann et al., 2009) (Fig. 5). The extracellular domain has three CUB-like domains of unknown function and 14 consensus N-glycosylation sites that incorporate approximately 40 kDa of carbohydrate moieties (Wortmann et al., 2009) (Fig. 5). In turn, the cytoplasmic domain possesses five tyrosine phosphorylation sites required for downstream signaling (Khan et al., 2021) (Fig. 5). Indeed, upon tyrosine phosphorylation by Src family kinases (SFKs) at Y734, a subsequent phosphorylation at Y762 occurs, allowing protein kinase C delta (PKCδ) to bind and CDCP1 to form a complex with SFK and PKCδ (Benes et al., 2005; Wortmann et al., 2009).

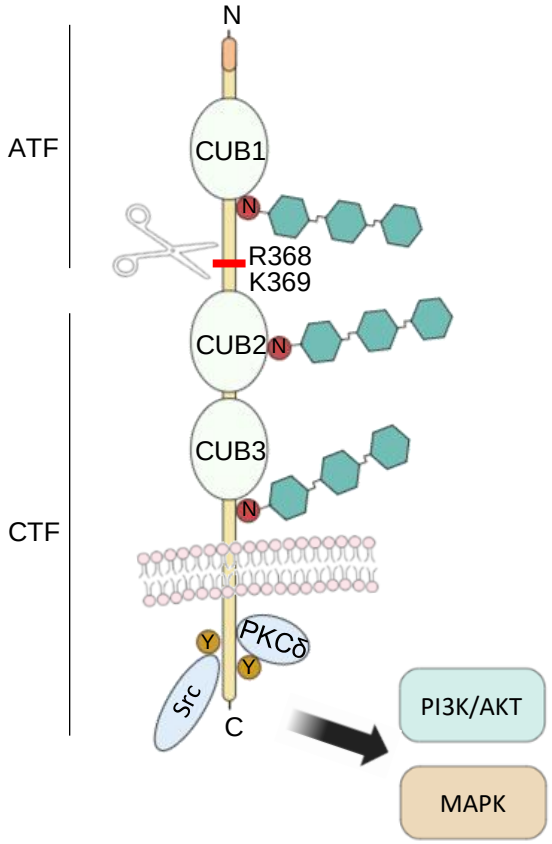

Fig. 5: Illustration of CDCP1 structure and downstream pathway.

This cascade of events can follow different situations. Firstly, it can be triggered by CDCP1 proteolysis. In this case, CDCP1 is cleaved by serine proteases in the extracellular region precisely at R368 and/or K369 (Khan et al., 2021). Proteolysis generates a free amino-terminal fragment (ATF) of 65 kDa and a carboxyl-terminal fragment (CTF) of 70 kDa spanning the cell membrane (He et al., 2010). After proteolysis the CTF undergoes phosphorylation at Y734 and, as mentioned above, it forms the multiprotein CTF-CDCP1/SFK/PKCδ, activating the pro-survival signaling (He et al., 2010). On the other hand, the destiny of ATF is still uncertain. Some articles reported ATF to be found in a free form in the serum of patients (Y. Chen et al., 2017), while others reported it to be binding to the CTF and not abandoning its original location on the cell surface (Kryza et al., 2020). Second, CDCP1 downstream pathway can be triggered by homodimerization or heterodimerization of CDCP1. Heterodimerization can happen with a plethora of proteins, and it is by now described to occur with some RTKs such as EGFR, hepatocyte growth factor receptor (HGFR), human epidermal growth factor receptor 2 (HER2) (Alajati et al., 2015; Kajiwara et al., 2021). Following the activation of CDCP1 and the formation of a multiprotein complex, several signaling cascades may be activated promoting cell growth and survival, such as the PI3K/AKT and the MAPK/ERK pathways (Khan et al., 2021). Since these pathways are known to be involved in tumor growth and metastasis formation, it is obvious to conclude that CDCP1 is involved in oncogenic mechanisms too. As such, several studies showed that CDCP1 is upregulated in many cancer types, such as breast, lung, colorectum, ovary, kidney, liver, pancreas, and hematopoietic system (Khan et al., 2021). Strikingly, elevated levels of this protein are generally associated with the most advanced disease stages, poorer prognosis, and/or reduced therapy response (Heitmann et al., 2020; Turdo et al., 2016). In our experience, the level of CDCP1 showed a tight correlation with the most advanced stages of PCa (Alajati et al., 2020). Indeed, Alajati et al. show that CDCP1 is highly expressed in CRPC and metastatic PCa in a human cohort and frequently associates with Pten loss, the most frequent genetic alteration found in PCa (Jamaspishvili et al., 2018). Moreover, thanks to the creation of a $CDCP1^{+}$; $Pten^{-/-}$ transgenic mouse model, it was proved that CDCP1 collaborates with

Pten loss for the advancement of PCa and metastasis formation (Alajati et al., 2020). Fig. 6 summarizes the mechanism of CDCP1 overexpression in such mouse model.

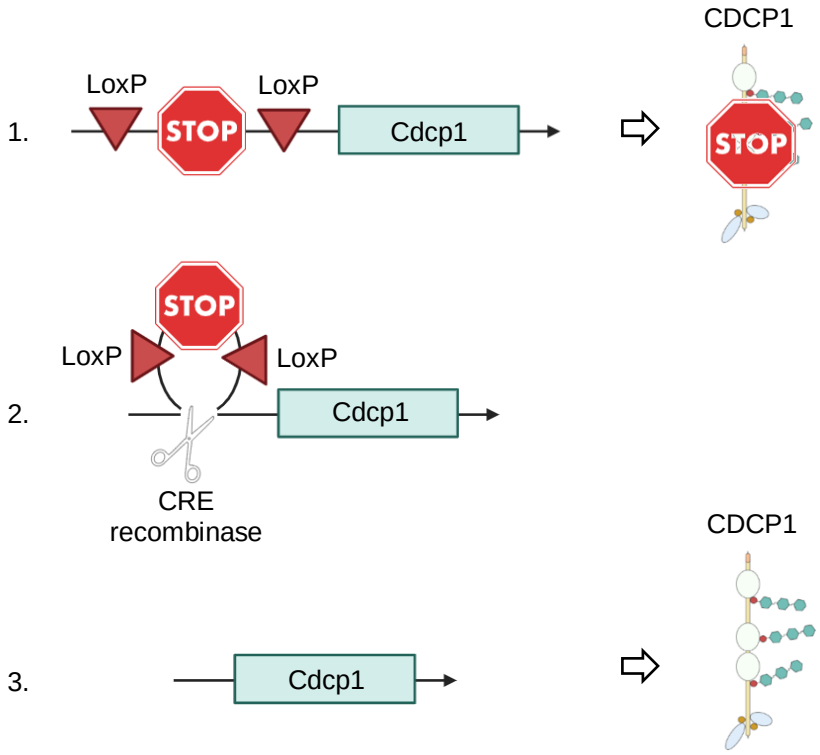

Fig. 6: CDCP1 overexpression in CDCP1^{+}; Pten$^{-/-}$ transgenic mouse model
Representation of the mechanism for CDCP1 overexpression in CDCP1^{+}; Pten$^{-/-}$ transgenic mouse model. Shortly, the STOP codon prevents the expression of CDCP1 in normal conditions (1). When Cre recombinase is introduced, the STOP codon is excised (2) and the mouse model, or *in-vitro* models derived from it, overexpress CDCP1 (3). Image created with BioRender.

Recently, we also studied the effects of CDCP1 overexpression in BCa (Saponaro et al., 2023). As observed in PCa, we noticed that CDCP1 is upregulated in the most advanced stages of BCa and correlates with the Ba/Sq subtype (Saponaro et al., 2023), which happens to be the most aggressive subtype among all MIBC (Kamoun et al., 2020). Based on the evidence suggesting the high relevance of CDCP1 in advanced oncological diseases, several hypotheses on its application in cancer diagnosis, prognosis, and treatment were explored. Interestingly, CDCP1 targeting, either with monoclonal antibodies or small molecule inhibitors, has already demonstrated effectiveness at inhibiting tumor growth and metastasis *in-vivo* (Alajati et al., 2020; Kollmorgen et al., 2013; Nakashima et al., 2017; Siva et al., 2008). Thus, it has proven to be a valid target, justifying the need for an enhanced effort in generating effective therapies that can target CDCP1.

1.2.2 Epithelial growth factor receptor (EGFR)

EGFR, also known as ErbB1 or human epidermal growth factor receptor 1 (HER1), is a receptor tyrosine kinase (RTK) found in the cell membrane and its structure consists of an intracellular region, a single transmembrane domain, and an extracellular ligand-binding domain (Guardiola et al., 2019). The intracellular region is divided into a small juxtamembrane region, which function is yet to be defined, a segment with tyrosine kinase activity, and a C-terminal regulatory tail, involved in the regulation of the receptor activation (Ferguson, 2008; Guardiola et al., 2019). The extracellular region is formed by four domains, two homologous ligand binding domains (domains I and III), and two cystine-rich domains (domains II and IV) (Ferguson, 2008). At the inactive state, the four extracellular domains are folded and the dimerization arm present in domain II is sequestrated by domain IV (Ferguson, 2008). However, ligands binding induces a conformational change exposing the dimerization arm (Ferguson, 2008). Epithelial growth factor (EGF) is the first ligand discovered for EGFR (Levantini et al., 2022; Ullrich et al., 1984). However, following research indicates other EGFR agonists, such as transforming growth factor α (TGF-α), heparin-binding EGF (HB-EGF), amphiregulin, betacellulin, epigen, and epiregulin (Linggi and Carpenter, 2006). All these ligands are present in the cell membrane as precursors. They are then cleaved and released in the extracellular space thanks to the proteolytic activity of the ADAM family of metalloproteases (Blobel, 2005). Upon interaction with one of its ligands and exposure of the dimerization arm, the canonical mechanism for EGFR activation requires its dimerization with a second EGFR molecule (homodimerization) or with another member of the ErbB family, such as ErbB2, ErbB3, ErbB4 (heterodimerization) (Ferguson, 2008; Linggi and Carpenter, 2006). Dimerization activates the intracellular tyrosine kinase region of the protein, which results in the auto-phosphorylation of tyrosine residues in the C-terminal tail segments (Sigismund et al., 2018; Zhang et al., 2006). The latter serve as docking sites for activating several signaling pathways that promote cell proliferation and survival, such as PI3K/AKT, MAPK, Ras/Raf/Mek/Erk, JAK/STAT, and PLCγ1/PKC pathways (Levantini et al., 2022;

Sigismund et al., 2018; Yarden and Sliwkowski, 2001). Fig. 7 summarizes the steps for EGFR activation and its function.

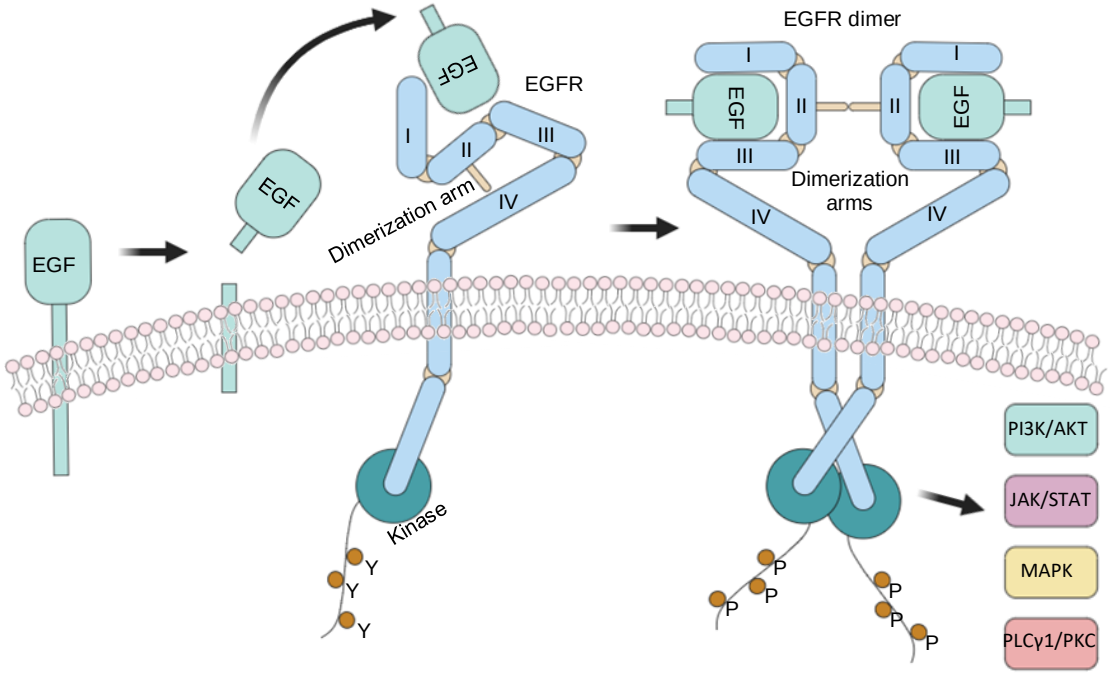

Fig. 7: EGFR
Illustration of EGFR structure and downstream pathway. Image created with BioRender.

EGFR downstream signaling plays a crucial function in tissue development and homeostasis (Sigismund et al., 2018). However, it can also act as a double-edged sword, supporting tumorigenesis and drug resistance in tumors (Sigismund et al., 2018). Indeed, EGFR dysregulation is frequently observed in cancer (Sigismund et al., 2018). Causes of EGFR dysregulation are mainly genetic alterations that increase receptor dimerization and activity (Levantini et al., 2022). Also, receptor amplification, transcriptional upregulation, or ligand overproduction have been reported (Levantini et al., 2022). Two major genetic alterations are described: short in-frame deletions in exon 19 (Ex19Del) and point mutations in exon 21, resulting in arginine replacing leucine at codon 858 (L858R) (Kobayashi et al., 2015; Ladanyi and Pao, 2008; Shi et al., 2014). At present, tumors with EGFR dysregulations are mainly managed with tyrosine kinase inhibitors (TKIs) such as gefitinib or erlotinib, or monoclonal antibodies (mAbs) like cetuximab (Chong and Jänne, 2013). However, durable complete response to these drugs is unusual due to the frequent acquisition of resistance mechanisms (Ladanyi and Pao, 2008). Treatment resistance is associated in 50 % of the cases with the development of a second EGFR mutation,

specifically T790M (Pao et al., 2005). Alternatively, tumor cells may respond to anti-EGFR therapies with amplification or activation of other RTKs that work synonymously to EGFR by activating common downstream effectors (Levantini et al., 2022). The most characterized mechanism in the promotion of resistance against anti-EGFR therapy is MET amplification (Bean et al., 2007). However, also HER2 or PIK3CA amplification (Papadimitrakopoulou et al., 2018), HER3 overexpression (Yonesaka et al., 2022) or AXL activation (Zhang et al., 2012) could promote resistance. In general, the selection and expansion of tumor cell clones carrying the resistant mutations potentially cause a more aggressive disease due to the lack of treatment options (Levantini et al., 2022). Currently, numerous studies focus on developing more effective, longer-lasting, and possibly mutation-specific drugs to improve the treatment of tumors with EGFR dysregulation (Levantini et al., 2022). From a clinical perspective, therapies targeting EGFR signaling are currently approved to treat lung, colorectal, pancreatic and head and neck cancers (Chong and Jänne, 2013). However, this receptor is correlated with poor prognosis also in ovarian, cervical, esophageal, gliomas, and bladder cancers (Chong and Jänne, 2013), suggesting that targeting EGFR may be beneficial for the treatment of these cancers too. Strikingly, several studies show that EGFR is upregulated in 27 - 53 % of MIBC cases (Chaux et al., 2012; Chow et al., 2001, 1997), and high expression of this receptor represents a distinct molecular characteristic of the Ba/Sq subtype (Kamoun et al., 2020). Clinical studies to test the application of EGFR inhibitors in recurrent or metastatic MIBC have already been proposed (Mooso et al., 2015).

1.2.3 Tumor-associated macrophages (TAMs)

Macrophages are mononuclear immune cells derived from the myeloid cell compartment and are present in most human tissues (Kadomoto et al., 2021; Sica et al., 2015). They can differentiate from circulating monocytes that are recruited to peripheral tissues upon exposure to local growth factors, cytokines, or microbial products, or, in the case of tissue-resident macrophages, they directly originate from the yolk sac during embryogenesis and are maintained in the adult tissues independently from monocyte replenishment (Kadomoto et al., 2021). The recruitment of monocytes to peripheral tissues occurs mostly via chemotaxis and the most common mechanism responsible for monocyte chemotaxis

to the tumor site is the presence of CC-chemokine ligand 2 (CCL2) in the tumor microenvironment (TME) (Kadomoto et al., 2021). In the peripheral tissues, macrophages have several functions, such as phagocytosis of pathogens, debris, infected and dead cells, antigen presentation, and production of inflammatory cytokines (Shapouri-Moghaddam et al., 2018). Some of these functions are crucial for controlling and eliminating infections as well as maintaining the homeostasis of certain tissues (e.g. microglia, lung alveolar macrophages, and Kupffer cells) (Kadomoto et al., 2021). However, macrophages can also play a negative role under certain circumstances. Indeed, they can sustain inflammatory diseases and cancer growth (Shapouri-Moghaddam et al., 2018). This is mainly possible because they are a highly plastic cell population, and their phenotype largely differs depending on the micro-environmental stimuli they encounter. Each phenotype exhibits a peculiar functional response, although the precise definition and characterization of macrophage phenotypes remain the subject of ongoing debate and vary across different scientific fields (Shapouri-Moghaddam et al., 2018). The process by which macrophages acquire a certain phenotype is called polarization and is extensively investigated in oncology. Recent publications indicate that gaining a deeper understanding of macrophage polarization may be crucial for improving tumor management (Josephs et al., 2015; Mantovani et al., 2017). In general, it is accepted that macrophages can play both anti-tumoral and pro-tumoral roles based on their polarization. Pro-tumoral macrophages, also known as TAM, anti-inflammatory macrophages, or M2 macrophages, constitute the main macrophage population infiltrating tumors (Zhang and Sioud, 2023). The pro-tumoral macrophage phenotype is generally induced by interleukin 4 (IL4), interleukin 13 (IL13), and colony stimulating factor 1 (CSF-1) (Locati et al., 2020; Yunna et al., 2020; Zhang and Sioud, 2023), and characterized by a high expression of cluster of differentiation 163 (CD163), cluster of differentiation 200R (CD200R), cluster of differentiation 206 (CD206), and arginase 1 (Arg1) (Mantovani et al., 2002; Yunna et al., 2020; Zhang and Sioud, 2023). Among the pro-tumoral attributes of TAMs, the production of anti-inflammatory cytokines plays a crucial role in tumor survival (Lahmar et al., 2016; Ocaña-Guzman et al., 2018; Zhang and Sioud, 2023). Indeed, anti-inflammatory cytokines such as interleukin 10 (IL10) or tumor growth factor-beta (TGF-beta) suppress the cytotoxic function of CD8(+) T cells, which are the main antitumoral effectors in the tumor microenvironment (TME) (Farhood et al., 2019). Moreover, TAMs

produce pro-angiogenic factors that sustain tumor vascularization and growth, such as vascular endothelial growth factor (VEGF) or interleukin 8 (IL8) (Kadomoto et al., 2021; Zhang and Sioud, 2023). On the contrary, anti-tumoral macrophages are far less common in the TME. Indeed, tumor cells tend to generate a cytokine milieu that supports tumor growth and survival, normally favoring pro-tumoral polarization of macrophages (Wang et al., 2021). However, recent publications show that TAMs can be re-programmed from a pro-tumoral to an anti-tumoral phenotype by targeting specific pathways involved in macrophage polarization (Gao et al., 2022; Rannikko and Hollmén, 2024). In physiological conditions, anti-tumoral macrophages develop upon exposure to interferon-gamma (IFN-gamma) or lipopolysaccharide (LPS) and generally express high levels of cluster of differentiation 38 (CD38), inducible nitric oxide synthases (iNos), cluster of differentiation 80 (CD80), and cluster of differentiation 86 (CD86) (Locati et al., 2020; Yunna et al., 2020). They produce pro-inflammatory cytokines, such as interleukin 1-beta (IL1-beta), IFN-gamma, and tumor necrosis factor-alpha (TNF-alpha) (Gao et al., 2022; Yunna et al., 2020). Fig. 8 highlights the key characteristics of polarized macrophages.

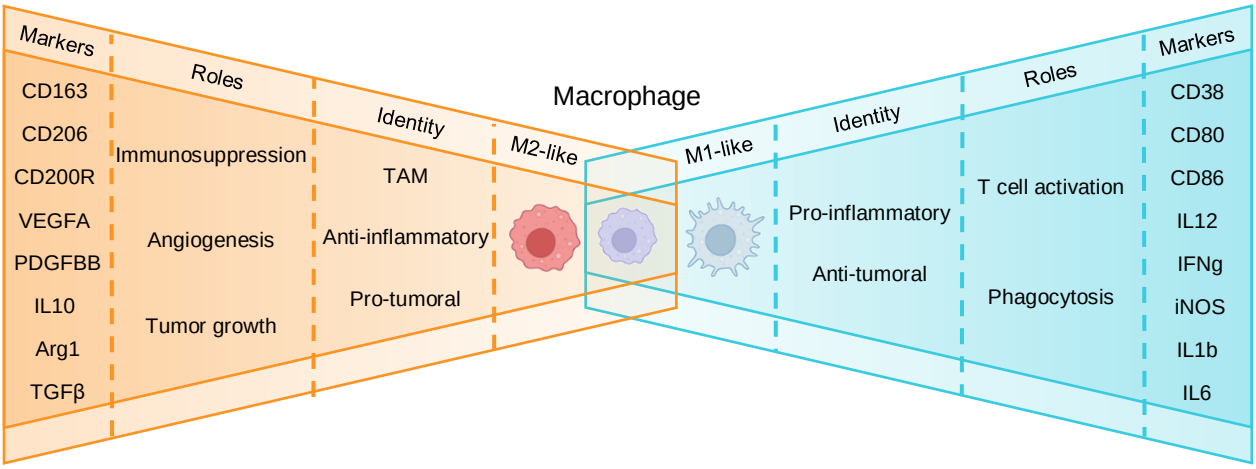

Fig. 8: Macrophage phenotypes
Introduction to macrophage phenotypes with relative roles and most common markers. Image created with BioRender.

1.2.4 Senescence

Cellular senescence is a cellular state that develops as self-defense against genomic alteration and cell transformation (Huang et al., 2022). In contrast to quiescence, which arrests the cell cycle in the G0 phase, senescence consists of the blockade in the G1 or G2 phase (Dan Sun and Buttitta, 2017; Gire and Dulić, 2015; Huang et al., 2022; Leonardo et al., 1994). It was originally proposed as a physiological regulatory mechanism occurring spontaneously upon extended cell proliferation, a process now specifically termed by the scientific community as replicative senescence (Gire and Dulić, 2015; Huang et al., 2022; Ohtani, 2022; Prasanna et al., 2021). Examples of specific systems where replicative senescence occurs are embryonic development and aging (Huang et al., 2022). In embryogenesis, senescence develops in a coordinated manner, functional to the embryo development (Muñoz-Espín et al., 2013; Storer et al., 2013). On the contrary, senescence develops during aging as a defensive mechanism caused by genetic exhaustion. Nonetheless, in both cases, replicative senescence is caused by telomere erosion (Huang et al., 2022). Telomeres are repetitive nucleotide-sequence motifs that protect the ends of chromosomes from deterioration or fusion with adjacent chromosomes (Calcinotto et al., 2019). Each cell division leads to the loss of 50–200 bp of unreplicated DNA at the 3′-end of chromosomes (Calcinotto et al., 2019). Telomeres progressively shorten over time. When they are nearly lost, the risk of exposing the free end of chromosomes is high (Herranz and Gil, 2018). Subsequent cell divisions would end in the deterioration of the genetic code. Thus, to prevent genetic mutations and the transmission of such mutations to the next generation of cells, DNA damage response (DDR) is activated. The function of DDR is to arrest the cell cycle progression while allowing for DNA repair (Dan Sun and Buttitta, 2017; Gire and Dulić, 2015; Leonardo et al., 1994; Rossiello et al., 2014). However, when telomeres are lost, DNA repair fails causing the persistence of DDR signaling (Rossiello et al., 2014). In turn, constant DDR signaling leads to senescence (Rossiello et al., 2014). Essentially, senescence prevents the accumulation of mutated cells, thereby also preventing tumor initiation (Huang et al., 2022; Rossiello et al., 2014). Since replicative senescence restricts the total number of cell divisions, it is reasonable to assume that it does not interfere only with tumor initiation but also with tumor growth (Roninson, 2003). However, this is not the case. Indeed, tumor cells often develop

mechanisms to bypass senescence, most commonly through the upregulation of telomerases, enzymes that inhibit telomere erosion during cell divisions (Roninson, 2003). Therefore, despite senescence having the potential to inhibit cancer growth, it does not occur spontaneously in this context. Nevertheless, senescence can be induced in tumor cells through several mechanisms, including radiation and some conventional anticancer drugs (chemotherapy-induced senescence; CIS) (Roninson, 2003). Specifically, evidence shows that cisplatin (Wang et al., 1998), doxorubicin (Schwarze et al., 2005; te Poele et al., 2002), and docetaxel (Schwarze et al., 2005), among others, can induce senescence in tumor cells. From a mechanistic perspective, the induction of senescence is mostly orchestrated by retinoblastoma tumor suppressor protein (RB). The phosphorylation level of RB dictates whether the cell cycle will continue and reach the M phase or stop beforehand (Weinberg, 1995). Preceding G1, RB is found in its active underphosphorylated form, which has an inhibitory activity on the progression of the cell cycle (Weinberg, 1995). As G1 progresses, RB becomes hyperphosphorylated and remains so throughout the rest of the cell cycle until emergence from phase M (Weinberg, 1995). Afterwards, should conditions be propitious for another cell division, RB would undergo phosphorylation again starting a new cell cycle (Weinberg, 1995). RB phosphorylation is the product of certain cyclin-dependent kinases (CDKs) upon their coupling with cyclins (Roger et al., 2021; Serrano et al., 1997; Weinberg, 1995). The most significant CDK-cyclin complexes promoting RB phosphorylation are cyclin A-CDK2, cyclin E-CDK2, cyclin D-CDK4, and cyclin D-CDK6 (Weinberg, 1995). During senescence, the function of those CDK-cyclin complexes is dampened by physiological inhibitors, resulting in RB hypophosphorylation, cell cycle arrest and blockade of cell division. Among the CDK-cyclin inhibitors that substantially impact senescence, p21 and p16 are the most significant. Indeed, these 2 CDKs are often upregulated in senescent systems, providing a strong inhibitory signal for the progression of the cell cycle (Huang et al., 2022). p21, also called cyclin-dependent kinase inhibitor 1A (CDKN1A), binds to cyclin A-CDK2 and cyclin E-CDK2 complexes, while p16, or cyclin-dependent kinase inhibitor 2A (CDKN2A), maintains RB hypophosphorylation through the inhibition of the cyclin D-CDK4/6 (Huang et al., 2022; Rossiello et al., 2014). Fig. 9 simplifies the mechanism responsible for cell cycle progression or senescence development.

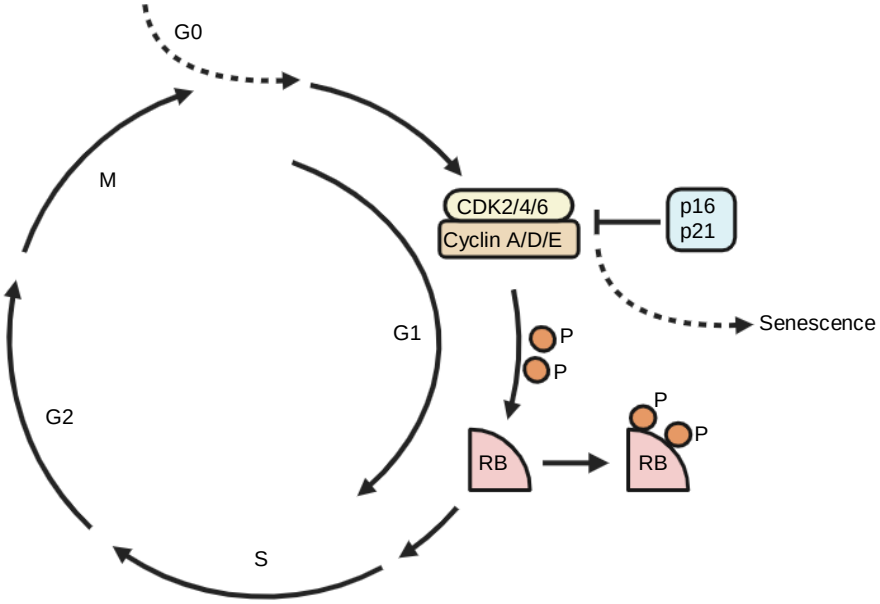

Fig. 9: Cell cycle and senescence
Representation of the mechanism for senescence development during the cell cycle. Image created with BioRender.

Despite senescence blocking cell growth, senescent cells are not completely dormant and exhibit some peculiar metabolic and morphological properties. First, compared to normal dividing cells they are characterized by enhanced activity of β-D-galactosidase (β-GAL), a hydrolase that cleaves β-linked terminal galactosyl residues from a wide range of naturally occurring substrates and resides in the lysosomes (Kurz et al., 2000). During senescence, the lysosomal content of β-GAL increases, together with lysosomal size. This characteristic can be easily recognized at the microscope as increased granularity. Other morphological features of senescent cells are enlarged and flattened cell shape and, sometimes, multi-nuclei (Roninson, 2003). In physiological conditions, β-GAL is active at the lysosome natural pH (pH=4-4.5) (Kurz et al., 2000). The overexpression of β-GAL during senescence causes this enzyme to become active at pH=6 (Kurz et al., 2000). The specific enzymatic activity of β-GAL in senescent cells has no well-understood function. However, it proved crucial for the development of tests that allow fast identification of senescent cells, such as the X-gal staining (Roninson, 2003). Senescent cells also produce and secrete many cytokines (e.g. IL1-alpha, IL1-beta, IL6, IL8), chemokines (e.g. CCL2, CXCL1, CXCL2), extracellular matrix components (e.g. fibronectin), proteases (e.g. MMPs), and growth factors (e.g. amphiregulin, EGF, BMPs, FGFs, VEGF, WNTs)

that influences their neighboring cells as well as tissue organization (Gonzalez-Meljem et al., 2018; Herranz and Gil, 2018; Roninson, 2003). The ensemble of all these molecules is termed senescence-associated secretory phenotype (SASP) (Herranz and Gil, 2018). SASP has a dual function. On the one hand, it reinforces the senescence growth arrest in an autocrine and/or paracrine manner, inducing surrounding cells to undergo senescence (Herranz and Gil, 2018). On the other hand, it has an important proinflammatory nature that plays a negative role in the development of certain pathologies which are dependent on inflammatory stimuli. Therefore, SASP simultaneously enhances the tumor-suppressive function of senescence by enlarging the pool of tumor cells that do not divide anymore and promotes tumor progression via proinflammatory mediators (Herranz and Gil, 2018). However, it has been proven that the continuous presence of SASP in the TME is correlated with increased tumor cell proliferation and invasion (Angelini et al., 2013; Bhatia et al., 2008; Di et al., 2014; Zacarias-Fluck et al., 2015). Moreover, SASP components can affect other elements in the TME. Indeed, senescent cells produce proangiogenic factors that influence endothelial cell proliferation (Gonzalez-Meljem et al., 2018) and cytokines that induce myeloid cell infiltration, which potently suppress T-cell responsiveness (Ruhland et al., 2016). Considering all the listed pro-tumoral features of senescence and SASP, it is currently believed that the detrimental effects of senescence outweigh its protective properties in cancer (Herranz and Gil, 2018). Fig. 10 summarizes the senescent cell characteristics mentioned in this chapter.

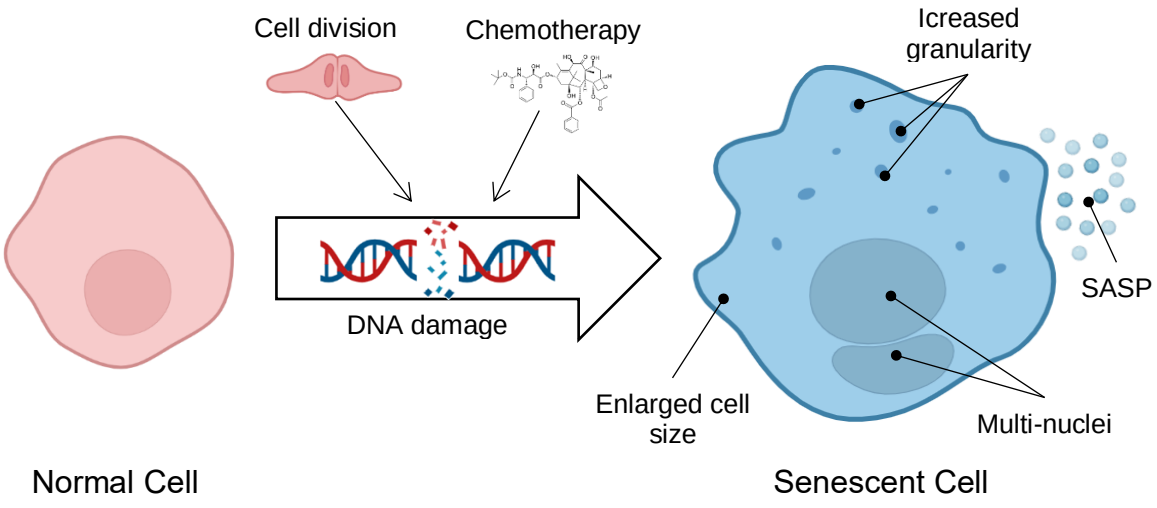

Fig. 10: Senescent cell characteristics
Summary of the main characteristics of senescent cells. Image created with BioRender.

1.3 Therapeutical strategies

1.3.1 Nanobodies (Nbs)

Nbs present many benefits compared to traditional mAbs. The size gap is the first and most striking difference between Nbs and mAbs. mAbs, particularly immunoglobulin G (IgG), have a molecular weight of approximately 150 kDa, whereas Nbs are about ten times smaller. The size reduction is clearly due to the structural differences between them. mAbs, composed of two heavy and two light chains, exhibit a complex structure. Each heavy chain consists of three constant domains (CH1, CH2, and CH3) and a variable domain (VH). The light chains consist of a constant domain (CL) and a variable domain (VL). CH2 and CH3 regions form the fragment crystallizable (Fc) region of the mAb, while CH1, VH, and light chains constitute the fragment antigen-binding (Fab) region. On the other hand, camelid heavy-chain antibodies (HcAbs) present a simpler structure. They possess an Fc region analogous to that of mAbs but lack the light chains and CH1 regions. Instead, they feature two single variable antigen-binding domains (VHH) in the Fab region (Jin et al., 2023). This structural simplification results in a substantial size reduction, bringing their molecular weight down to approximately 90 kDa (Jin et al., 2023). Nbs, which are essentially VHH monomers of the HcAbs, exhibit an even smaller size. Their molecular weight is around 15 kDa, making them significantly smaller than mAbs and HcAbs. Fig. 11 illustrates the structural differences between mAbs, HcAbs and Nbs. Despite the pronounced size difference between Nbs and mAbs, their antigen-binding regions present a comparable structure. Indeed, both Nbs and VH domains of mAbs are characterized by the presence of four conserved framework regions (FR) and three variable complementarity-determining regions (CDR) that are responsible for determining antigen specificity (Jin et al., 2023). However, the triad of CDRs in the VH domain of mAbs is generally inadequate for high-affinity antigen binding. This necessitates the conjoining of the mAb’s VH domain with the VL domain, requiring a sextet of CDRs to manifest full antigen-binding capability (Jin et al., 2023).

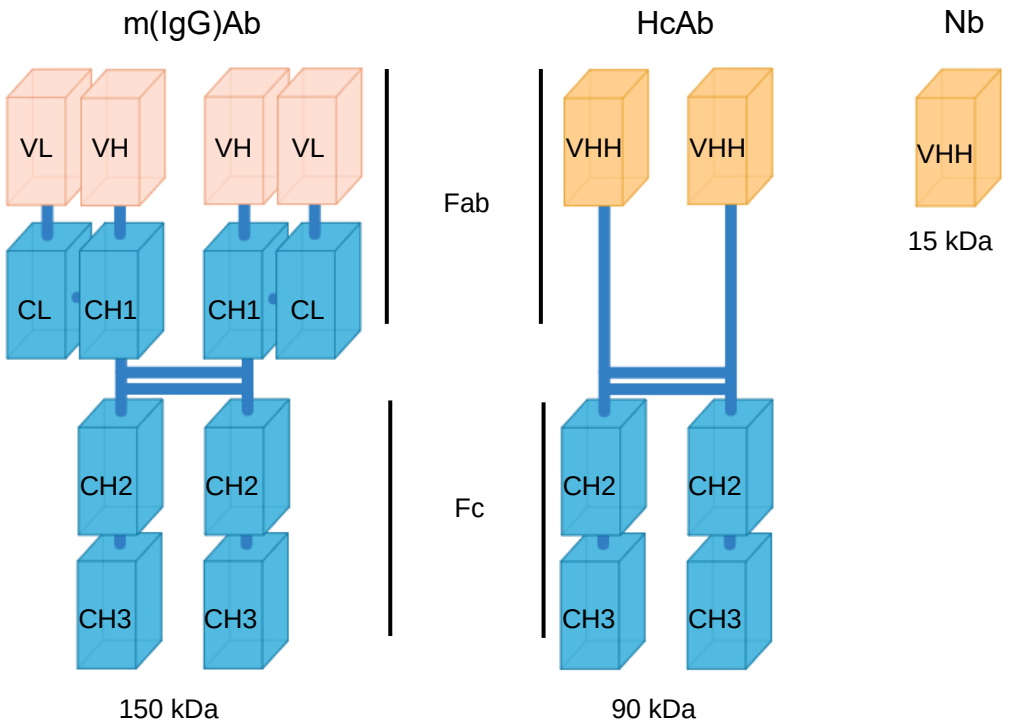

Fig. 11: mAb, HcAb, and Nb structure
Illustration of the structural features of mAbs, HcAbs, and Nbs.

In contrast, Nbs can preserve the antigen-binding capacity intrinsic to mAb while functioning as a monomeric entity equipped with only three CDRs (Bao et al., 2021). This is possible because Nbs present an extended paratope comprehensive of enlarged CDR1 and CDR3 (Jin et al., 2023). The capacity of maintaining a strong antigen-binding function while presenting a notably reduced size has profound implications for both therapeutic and imaging applications. Indeed, when compared to mAbs they present several advantages. First, Nbs are characterized by higher penetration and distribution within solid tumor masses, enhancing their therapeutic effectiveness (Oliveira et al., 2013). Besides, since their size is below the filtration threshold of the kidney's glomerular membrane, they can be quickly eliminated through urine (Bao et al., 2021). As a result, "off-target" toxicity is reduced. Moreover, thanks to the rapid clearance, the intensity of background signals rapidly decreases after the injection of imaging tracers derived from Nbs. Thus, early imaging of lesions is facilitated (Bao et al., 2021). An additional benefit of Nbs compared to mAbs is their remarkable stability, which ensures the preservation of their binding

affinity under various conditions (Bao et al., 2021). Indeed, Nbs are known for their superior ability to refold and revert to their original conformation even when subjected to harsh conditions like extreme pH levels and temperatures (Oliveira et al., 2013). Furthermore, the monomeric structure of Nbs do not require post-translational modifications to gain their active form. This greatly eases their molecular manipulation, enabling the straightforward creation of multivalent and multispecific Nb combinations (Oliveira et al., 2013). It also facilitates their production in bacteria, which offers rapid growth and cost advantages compared to the eukaryotic production systems required for mAb production (Oliveira et al., 2013). In conclusion, due to their small size, simple structure, high antigen binding affinity, and remarkable stability, Nbs have the potential to transform antibody-based therapy (Jin et al., 2023). Notably, Nbs have been successfully tested for treating various diseases, including cancer, autoimmune and infectious diseases (Jin et al., 2023). Caplacizumab, a Nb targeting von Willebrand factor, is currently approved for thrombotic thrombocytopenic purpura (Duggan, 2018; Hollifield et al., 2020). In Japan, the tetravalent Nb targeting tumor necrosis factor-alpha Ozoralizumab was approved for treating rheumatoid arthritis (Keam, 2023). Finally, Ciltacabtagene autoleucel, a Nb chimeric antigen receptor (CAR) T cell therapy, was approved for treating multiple myeloma in February 2022 (Mullard, 2022).

1.3.2 TAM-targeting therapies

The involvement of TAM in tumor-promoting mechanisms convinced the scientific community that elimination or reprogramming of TAMs could have a beneficial effect on patient prognosis. Elimination can be obtained via any strategy that diminishes the presence of macrophages in the tumor. The induction of apoptosis and the blockade of recruitment in the tumor site are the most typical examples of strategies for TAM elimination. On the other hand, reprogramming TAMs requires the identification of markers or pathways that can influence the phenotype of macrophages. When considering therapies that can hinder TAM infiltration in the tumor, the first recorded drugs with a proven effect are bisphosphonates (Ngambenjawong et al., 2017; Tang et al., 2013). This family of compounds can bind to tumor microcalcifications. They are then phagocyted from macrophages inducing apoptosis (Ngambenjawong et al., 2017).

Despite the effective tumor regression observed in murine models upon single treatment with bisphosphonates (Hiraoka et al., 2008; Miselis et al., 2008; Zeisberger et al., 2006), the same results haven´t been achieved in clinical trials (Ngambenjawong et al., 2017; Zeisberger et al., 2006). However, bisphosphonates showed some benefits in combination with other drugs (Ngambenjawong et al., 2017; Zeisberger et al., 2006). Another strategy that can eliminate TAM and consequently cause tumor shrinkage is the inhibition of CSF-1R, an RTK that promotes macrophage function and survival (Ngambenjawong et al., 2017). Since tumor cells and other TME components produce chemokines that attract macrophages to the tumor site, alternative strategies to reduce TAM infiltration involve blocking the activity or synthesis of these chemokines. One of the most remarkable strategies that block chemokine-induced recruitment of macrophages is targeting the CCL2/CCR2 axis. CCL2 is a key chemokine responsible for inducing macrophage chemotaxis. Targeting this chemokine or its receptor, CCR2, has proven effective in reducing TAM recruitment and promoting tumor regression in *in-vivo* models (Gazzaniga et al., 2007; Lim et al., 2016; Popivanova et al., 2009). However, all the aforementioned approaches affect macrophages without distinction. Achieving a complete tumor clearance may instead require preserving certain macrophage populations characterized by anti-tumoral properties (Ngambenjawong et al., 2017). Therefore, a more appropriate therapy should specifically target TAMs while sparing anti-tumoral macrophages. Hence, at the current state of research, reprogramming TAMs is a more appealing option compared to macrophage elimination. When evaluating therapeutic strategies that can reprogram TAM from a pro-tumoral to a tumoricidal phenotype, it is essential to mention mammalian target of rapamycin (mTOR) and toll-like receptors (TLRs) (Ngambenjawong et al., 2017). mTOR is a serine/threonine kinase. Its main role is to sense the presence of amino acids, glucose, lipids and ATP in order to regulate downstream metabolic processes (Byles et al., 2013; Weichhart et al., 2015). Activation of mTOR pathways usually promotes the synthesis of nucleic acids, proteins, and lipids, and stimulates glycolysis and mitochondrial respiration (Weichhart et al., 2015). Emerging data suggest that the metabolic reconfiguration promoted by mTOR can influence myeloid cell function (Weichhart et al., 2015). Accordingly, inhibition of mTOR has been proven effective in the polarization of macrophages towards the M1-like phenotype with an anti-tumor effect in a hepatocarcinoma mouse model (Chen et al., 2012). TLRs are

transmembrane receptors expressed from macrophages and other antigen-presenting cells (APC). Their physiological function is to recognize various pathogen-associated molecular patterns (PAMPs) and damage-associated molecular patterns (DAMPs) as part of the innate immune surveillance (Ngambenjawong et al., 2017). Surprisingly, different TLRs induce pro-inflammatory M1 polarization of macrophages in response to certain PAMPs (e.g. polyinosinic:polycytidylic acid (polyI:C) for TLR3, LPS for TLR4, imiquimod for TLR7, and CpG-oligonucleotide for TLR9) (Ngambenjawong et al., 2017). Therefore, scientists have investigated TLR activation as a tool for TAM reprogramming in the TME. For example, Zheng et al. developed a weakened strain of Salmonella typhimurium that secrete flagellin B (FlaB) and thus activates TLR4 and TLR5 simultaneously (Zheng et al., 2017). The engineered bacteria effectively suppressed tumor growth and metastasis in mouse models and prolonged animal survival (Zheng et al., 2017). Fig. 12 illustrates the most common strategies that target TAM infiltration.

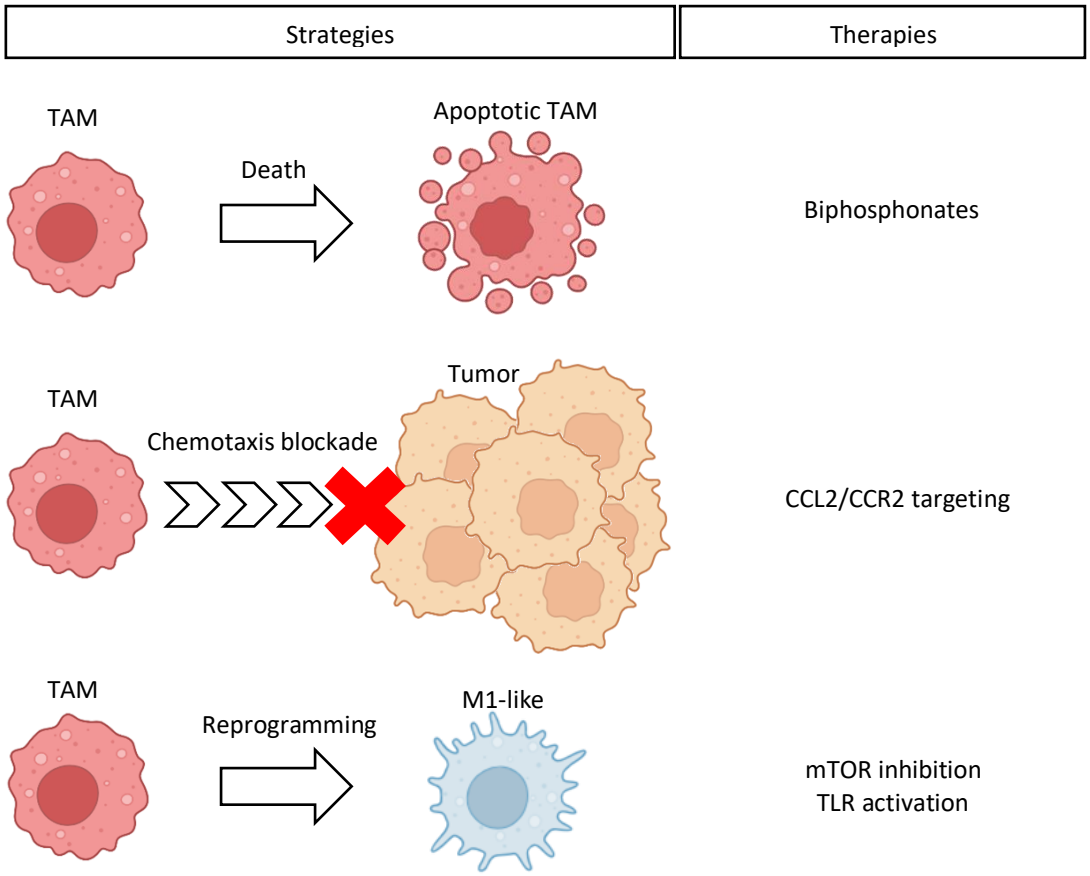

Fig. 12: TAM-targeting therapies
Illustration of the different strategies available for depleting TAMs in tumors. Image created with BioRender.

1.3.3 Senolytic drugs

Considering the relevance of senescence in tumor progression, scientists have proposed that eliminating senescent cells post-chemotherapy may be crucial to avoid tumor progression and/or relapse in patients (Gonzalez-Meljem et al., 2018; Ohtani, 2022; Prasanna et al., 2021). As a result, the search for senolytic drugs that could eliminate senescent cells gained increasing interest in the tumor field and the number of proposed senescence markers and senolytic therapy has been growing over time. However, due to the ubiquity of the selected markers, none of the proposed strategies have successfully met the challenge of targeting senescent cells while avoiding off-target toxicity. A clear example is navitoclax, a selective inhibitor of B-cell lymphoma 2 (BCL-2) family proteins. BCL-2, along with other members of the BCL-2 family, plays an important role in inhibiting apoptosis and it has been found upregulated in senescent cells (Yosef et al., 2016). This suggests that senescent cells switch off the apoptotic mechanism to survive after DDR failure. Re-activating such mechanism could help to clear the senescent cell population (Yosef et al., 2016). This intuition proved to be somewhat accurate, as navitoclax showed great effectiveness in senescent cell elimination in *in-vitro* and *in-vivo* models (Chang et al., 2016; Jochems et al., 2021; Wang et al., 2017; Zhu et al., 2016). This drug was also used as part of the innovative strategy named “one-two punch”, which involves a first hit with a pro-senescence drug (e.g. docetaxel) to induce senescence in tumor cells and a second hit with a senolytic compound (e.g. navitoclax) to eliminate senescent cells (L. Wang et al., 2022) (Fig.13).

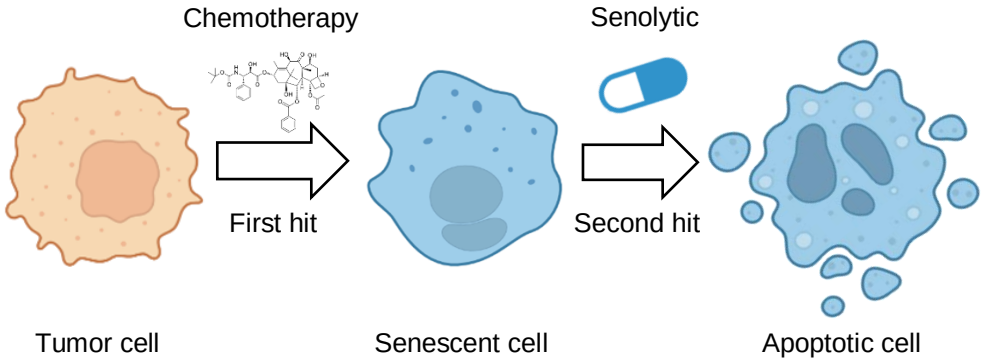

Fig. 13: One-two punch strategy
Illustration of the “one-two punch” strategy. Image created with BioRender.

Remarkably, navitoclax treatment proved great efficacy in combination with many pro-senescent drugs when the one-two-punch strategy was applied to cancer cell lines (Fleury et al., 2019; Hann et al., 2008; Saleh et al., 2020; Wang et al., 2017; Wu et al., 2014; Yosef et al., 2016). However, during phase I clinical trials, this drug showed high off-target toxicity, and further research was halted (Kaefer et al., 2014). Therefore, since the one-two punch therapy has been proven effective in preclinical models despite navitoclax toxicity, there is a pressing need to discover a senolytic drug characterized by an improved specificity for senescent cells.

2 Materials and methods

2.1 Solutions

Name	Recipe
1M Tris pH 6.8 (Stacking Gel)	121.1 g Tris-Base (#AE15, ROTH) in 500 mL demineralized H_2O, adjust pH to 6.8 with 32 % HCl (ROTH) and fill up to 1 L with demineralized H_2O
1M Tris pH 8.8 (Separation Gel)	121.1 g Tris-Base (#AE15, ROTH) in 500 mL demineralized H_2O, adjust pH to 8.8 with 32% HCl (ROTH) and fill up to 1 L with demineralized H_2O
10X SDS Running Buffer	30 g Tris-Base (#AE15, ROTH), 144 g Glycine (#3790, ROTH), 10 g SDS (#CN30, ROTH) and fill up to 1 L with demineralized H_2O
10X Tris-Glycine Buffer	30 g Tris-Base (#AE15, ROTH), 144 g Glycine (#3790, ROTH) and fill up to 1 L with demineralized H_2O
1X Transfer Buffer	200 mL 10x Tris-Glycine, 300 mL 2-propanol (#6752, ROTH) and fill up to 2 L with demineralized H_2O
10X TBS	24 g Tris-HCl (#9090, ROTH), 5,6 g Tris-Base (#AE15, ROTH), 88 g NaCl (#P029, ROTH), fill up to 1 liter with demineralized H_2O and adjust pH to 7.6 if necessary
1X TBST	100 mL 10x TBS, 900 mL demineralized H_2O, 500 µl Tween-20 (#A4974, PanReac Applichem)
4X WB Sample Loading Dye	2 g SDS (#CN30, ROTH), 5 mL 1 M Tris-HCl pH 6.5, 8 mL Glycerin (#6962, ROTH), 100 mg Bromphenol Blue (Carl Roth #A512.2), warm up to 37 °C until SDS dissolves, add 10 mL 1 M DTT

	(Carl Roth #6908.1) and fill up to 25 mL with demineralized H_2O
8 % SDS Gel Solution	8 % Acrylamide (#40-A515, ROTH), 37 % 1M Tris pH 8.8, 0.1 % SDS (#CN30, ROTH), 0.1 % APS (Carl Roth #9178.3), 0,8 µL / mLTEMED (#2367, ROTH) in demineralized H_2O
Stacking Gel Solution	3 % Acrylamide (#40-A515, ROTH), 13 % 1M Tris pH 6.8, 0.1 % SDS (#CN30, ROTH), 0.1 % APS (Carl Roth #9178.3), 0,8 µL / mLTEMED (#2367, ROTH) in demineralized H_2O
LB-Medium	25 g LB (#6673, Carl Roth) and fill up to 1 L with demineralized H_2O
LB-Agar	25 g LB (#6673, Carl Roth), 20 g Agar-Agar (#2266, Carl Roth), fill up to 1 L with demineralized H_2O, autoclave, let cool down to 56°C in water bath before adding 100 µg/mL ampicillin, pour in 10 cm bacteria dish (Greiner)
0.5 % Crystal Violet	2.5 mg Crystal Violet (#T123, ROTH) in 50 mL demineralized H_2O
1 % Crystal Violet	5 mg Crystal Violet (#T123, ROTH) in 50 mL demineralized H_2O
0.1 % Acetic Acid	0.5 mL 100 % Acetic Acid (ROTH) in 500 mL demineralized H_2O

Table 1: Solutions
List of solutions used in this work and their recipes.

2.2 Cell culture

All cells and organoids were maintained in a humid environment at 37°C and 5% CO_2 in a CO_2 incubator (PHCbi). The following table describes the composition of all used media:

Cells/Organoids	Name	Recipe
PC3 (ATCC), SCaBER (ATCC), 769p (ATCC)	RPMI complete	RPMI1640 (Thermo Fisher Scientific), 10% fetal calf serum (Thermo Fisher Scientific), 1% streptomycin/penicillin (10.000 units/ml Penicillin and 10.000 µg/ml Streptomycin; Thermo Fisher Scientific), 1% glutamine (Thermo Fisher Scientific)
LNCaP (ATCC)	LNCaP Media	RPMI1640 w/o phenol red (Thermo Fisher Scientific), 10% fetal calf serum, 1% streptomycin/penicillin (10.000 units/ml Penicillin and 10.000 µg/ml Streptomycin, 1% glutamine
	DMEM complete	DMEM 10% fetal calf serum, 1% streptomycin/penicillin
41-2 (ATCC)	41-2 Maintenance Media	10 % fetal calf serum (not heat inactivated),1 % streptomycin/penicillin,1 % non-essential amino acids (Thermo Fisher Scientific),1 % sodium pyruvate (Thermo Fisher Scientific)
41-2	41-2 Ab Production Media	PFHM-II (Thermo Fisher Scientific), 1 % streptomycin/penicillin
PBMC-derived macrophages	Human Macrophage Media	RPMI1640, 50 ng/mL human CSF1 (Peprotech), 10% fetal calf serum, 1% streptomycin/penicillin, 1% GlutaMax,

		(Thermo Fisher Scientific), 1% sodium pyruvate
BMDM	Murine Macrophage Media	DMEM, 20 ng/mL murine CSF1 (Peprotech), 10% fetal calf serum, 1% streptomycin/penicillin
Prostate murine organoids	Prostate Organoid Media	Advanced DMEM/F12 (Thermo Fisher Scientific), 1% GlutaMax, 1% HEPES (Thermo Fisher Scientific), 0.20% Primocin, 2% B27 (#17504-04, Life Technologies), 500 nM A83-01 (#2939, Tocris Bioscience), 200 µg/mL NAC (#A9165, Sigma-Aldrich), 0.5 ng/mL EGF (#AF-100-15, PeproTech), 100 ng/mL Noggin (#120-10C, Peprotech), 100 ng/mL R-Spondin (#4645-RS-025, R&D Systems), 10 µM Y-27632 (#M1817, Abmole Bioscience), 0.3 ng/mL DHT (#D-073-1ML, Sigma-Aldrich)
Bladder murine organoids	Bladder Organoid Media	Advanced DMEM/F12, 1% GlutaMax, 1% HEPES (Thermo Fisher Scientific), 0.20% Primocin, 2% B27, 500 nM A83, 200 µg/mL NAC, 0.5 ng/mL EGF, 100 ng/mL Noggin, 100 ng/mL R-Spondin, 10 µM Y-27632

Table 2: Cell line, primary cell and organoid media
List of in-vitro models used in this work and their media.

2.3Nb production

Nbs were generated from the Core Facility Nanobodies from the University of Bonn. The Landesuntersuchungsamt Rheinland-Pfalz (23 177- 07/A 17-20-005 HP) authorized all immunizations necessary for Nbs production. Within 10 weeks, alpacas (Vicugna pacos) were immunized by six subcutaneous injections of a 1:1 mixture composed by 200 µg of human CDCP1 protein (#CD1-H52H6, Acro Biosystems) or EGFR and GERBU-FAMA adjuvant. Subsequently, 100 mL of blood were drawn, and peripheral blood mononuclear

cells (PBMCs) were isolated. PBMCs messenger ribonucleic acid (mRNA) was extracted, and reverse transcription polymerase chain reaction (RT-PCR) was performed to obtain complementary deoxyribonucleic acid (cDNA). To generate a library for phage display, VHH sequences in the cDNA were amplified by polymerase chain reaction (PCR) and cloned into a phagemid vector. The phage display was performed using E. coli TG1 cells in combination with KM13 helper phages to enrich specific VHHs. The biotinylated bait protein was immobilized with magnetic streptavidin beads. After two rounds of panning, E. coli ER2738 cells were infected with the enriched phages and individual clones were picked in a 96-well plate. The clones were grown 4 h at 37 °C, protein expression was induced by isopropyl-β-D-thiogalactopyranosid (IPTG) and Nbs were produced overnight at 30 °C. The supernatants were then tested for specific binding of VHHs to CDCP1 and EGFR by enzyme-linked immunosorbent assay (ELISA) and positive hits were sequenced. Nb encoding genes were cloned into pHEN6 vectors with an N-terminal pelB signaling sequence and a C-terminal HA-His6 tag. The plasmids were transformed into chemically competent E. coli WK6 cells. Cells were grown in Terific Broth (TB) media (100 µg/ml Ampicillin), inoculated with 25 mL of an overnight preculture, and incubated at 37 °C in a shaking bacteria incubator until reaching an optical density of 1.2. Protein expression was induced by adding 0.4 mM IPTG and bacteria were further incubated for 4 h. The cells were harvested by centrifugation at 4,000 RCF and 10 °C for 25 min. The cell pellet was suspended in 25 mL TES buffer (200 mM Tris, 0.65 mM EDTA, 500 mM sucrose, pH 8.0), incubated for 1 h slowly mixing at 4 °C, diluted with 70 mL of 0.25 concentrated TES buffer and incubated at 4 °C overnight slowly mixing. Subsequently, the suspension was centrifuged at 70,000 RCF, 10 °C for 45 min and the supernatant was filtered through a 0.45 µm filter. Later, selected Nbs were cloned into the pCSE2.5 vector to obtain different Nb formats: HcAbs using the rabbit CH2 and CH3 domains (Nb-rFc), Nb homodimers or Nb heterodimers comprising an HA-Avi-6His Tag. Obtained plasmids were transfected in HEK293-6E cells using jetPEI® transfection reagent (Sartorius). Six days after transfection, cell suspension was centrifuged for 10 min at 4,600 rpm at 4 °C and the supernatant containing the Nb constructs were harvested and filtered with a Steriflip (Merck). Nb comprising a His Tag were purified by Ni2+-Affinity chromatography. Supernatants were mixed with equilibrated Ni2+-NTA beads and incubated for 2 h at 4 °C slowly mixing. Afterwards, Ni2+-affinity chromatography was carried out on a gravity

column. The flow through was discarded and the beads were washed with 100 mL wash buffer (50 mM Tris, 50 mM NaCl, 10 mM imidazole, pH 8.0). The protein was eluted in elution buffer (50 mM Tris, 50 mM NaCl, 500 mM imidazole, pH 8.0), the buffer was replaced using PD-10 columns to storage buffer (20 mM Hepes pH 7.4, 150 mM NaCl) and proteins were concentrated using an Amicon 3 kDa MWCO. Nb-rFc were purified by protein A affinity chromatograpy using HiTrap Protein A columns and a Äkta pure system. After Binding Nb-rFcs were eluted with glycin elution buffer (0,1 M Glycin•HCl, pH 2,5). Buffer was exchanged using PD-10 columns to storage buffer (20 mM Hepes pH 7.4, 150 mM NaCl) and proteins were concentrated using an Amicon 10 kDa MWCO. Purification steps were monitored by SDS-PAGE. Proteins were flash frozen in liquid nitrogen and stored at -80 °C.

2.4 FACS staining with Nbs

For the FACS staining performed with the Nbs, PC3 and SCaBER cells were first incubated for 30 min with the different Nbs (10µg/mL) and 1:1000 LIVE/DEAD™ Fixable Near IR (#L34993, Invitrogen™). Cells were then washed via centrifugation for 5 min, 300 RCF at room temperature, and incubated with 1:50 anti-HA secondary antibody (#901524, BioLegend) for 30 min. Cells were washed a second time for 5 min, 300 RCF at room temperature, and acquired with BD FACSCanto™ II Flow Cytometer (BD biosciences). Obtained data were analyzed with FlowJo™.

2.5 Vectors for CDCP1 mutants and CDCP1 isoforms expression and transfection

Vectors for the transmembrane expression of CDCP1 mutants (delN-term, delCUB1, delCUB2) and CDCP1 isoforms (*homo sapiens* CDCP1, *mus musculus* CDCP1, *macaca fascicularis* CDCP1) were generated in Hölzel lab and provided to us. HEK-293T cells (ATCC) were seeded at a density of $2.5*10^5$/well in 12-well plates (TPP). Transfection was performed on HEK-293T cells with Lipofectamine™ 3000 (#L3000001, Invitrogen™) as described by the provider. The day after transfection cells were detached with a scraper and processed as described in Chapter 1.4 for the fluorescence-activated cell sorting (FACS) analysis.

2.6 SDS Gels preparation

8 % SDS Gels for electrophoresis were prepared as follows. Glass plates for 1.0 mm thick gels were mounted in a casting stand. 8 % SDS Gel Solution was poured between the glass plates. Stacking Gel Solution was poured on top of the solidified 8 % SDS Gel Solution and 10-well combs or 15-well combs were inserted. After complete solidification, gels were conserved at 4 °C in distilled water until usage.

2.7 Western blotting (WB)

Cells were seeded in 6-well plates (TPP) at the following densities: PC3, 10^5 cells / well; 796p, 10^5 cells / well; SCaBER, $2*10^5$ cells / well. They were treated for 48 h with 0.7 µM Nbs or relative controls (mAb-CDCP1 or cetuximab). Cells were detached with the help of a scraper and lysed in RIPA buffer (#9806, Cell Signaling). Cell lysates were centrifuged at 14,000 RCF for 15 min at 4 °C to eliminate cell debris and protein concentration was measured in the supernatant with Pierce™ BCA Protein Assay Kit (#23225, Thermo Scientific™) as described by the manufacturer. 20 µg of protein were mixed 1:4 with 4X WB Sample Loading Dye and loaded on 8 % SDS Gels and electrophoresis was performed in a BioRad buffer tank filled with 1X SDS Running Buffer for 1 h and 45 min at 100 V using PowerPac™ HC Power Supply (BioRad). Gels were then mounted in sandwiches with 0.45 µm Hybond-P PVDF membranes (Amersham Biosciences). Each sandwich was hold together between two foam pads and filter paper sheets and inserted in a gel holder cassette (BioRad). The gel holder cassette was then inserted in the buffer tank filled with 1X Transfer Buffer and proteins were transferred on the membrane applying 100 V for 1 h and 45 min with a PowerPac™ HC Power Supply (BioRad). Membranes were blocked for 2 h at room temperature in a 5 % milk solution (neoFroxx) and cut as needed. Cut membranes were incubated with anti-pEGFR (#2236T, Cell Signaling), anti-EGFR (#4267, Cell Signaling), anti-CDCP1 (#4115, Cell Signaling), anti-pERK (#9102S, Cell Signaling), anti-ERK (#4377, Cell Signaling), and anti-β-actin (#A2228, Sigma-Aldrich) primary antibodies overnight at 4 °C and with the HRP-conjugated secondary antibodies (anti-rabbit, #170-6515 or anti-mouse, #170-6516; BioRad) for 2 h at room temperature. Finally, membranes were developed with

SuperSignal™ West Pico PLUS Chemiluminescence-Substrate (Thermo Fisher Scientific) and chemiluminescence was measured with ChemiDoc MP (BioRad).

2.8 Vitality assay

Vitality was assessed with crystal violet assay. Cells were seeded in a 12-well plate (TPP) with the following densities: PC3, $2.5*10^3$ cells / well; 769p, $1.5*10^3$ cells / well; SCaBER, $5*10^3$ cells / well. After 12 h, 0.7 µM treatment with Nbs and the relative controls (anti-CDCP1 Ab, cetuximab) was started. On day 3, the media was replaced with fresh media and treatment. The experiment was stopped after 6 days of treatment. Cells were fixed with 4 % PFA for 15 min and stained with 0.5 % Crystal Violet for 15 min. Plates were dried at room temperature for 2 days and crystal violet was then dissolved with 0.1 % Acetic Acid. The absorbance of the resulting solution was then analyzed at the wavelength of 570 nm with a spectrometer (Spectra Thermo, SLT).

2.9 Immunohistochemistry (IHC) on MIBC and PCa tumor-microarray (TMA)

CDCP1, cluster of differentiation 68 (CD68), and CD163 expression was analyzed on a cohort of 238 PCa patients and one of 184 MIBC patients. Samples for the establishment of the PCa cohort were collected at the University Hospital of Bonn according to the project 013/20. MIBC samples collection was instead approved by the ethical review board of the Friedrich-Alexander-University Erlangen-Nürnberg (Erlangen, Germany; approval number: 329_16B and 97_18Bc) and tumors were gathered at the Comprehensive Cancer Center Erlangen Metropole Region Nuremberg (CCC-EMN). Stainings for CDCP1, CD68, and CD163 were performed on the PCa cohort with the VENTANA BenchMark ULTRA autostainer (Ventana) according to an accredited staining protocol in a routine immunohistochemistry facility. In the MIBC cohort, CDCP1 staining followed the same protocol used for the PCa cohort, but CD68 and CD163 stainings were performed as described by Taubert et al. (Taubert et al., 2021). CDCP1 was then analyzed with a semi-quantitative scale from experienced uropathologists at the University Hospital of Bonn (low, 0.0-1.9, or high, 2.0-3.0). On the PCa cohort, CD68 and CD163 levels received an interpretation with the same scale used for CDCP1, while in the MIBC cohort, their level

was automatically detected as H-score (scale 0–300) via QuPath (Bankhead et al., 2017; Taubert et al., 2021). Median H-scores were log2-transformed. CD68 and CD163 Hlog2 values (MIBC cohort) or semi-quantitative values (PCa cohort) were compared between CDCP1-high tumors and CDCP1-low tumors with two-tailed unpaired t-test. $P < 0.05$ was considered statistically significant.

2.10 CRISPR/Cas9

CRISPR/Cas9 method was used to generate the knock-out (KO) of CDCP1 on TCCSUP and T24 cell lines as described in Saponaro et al (Saponaro et al., 2023). Briefly, a double-stranded oligonucleotide coding for a single guide RNA (sgRNA) which targets the third exon of CDCP1 was obtained by annealing the following single-stranded oligonucleotides: hCDCP1_KO_BS, 5′-AAACccgtggtcaggatcggaac-3′; hCDCP1_KO_TS, 5′-CACCgttccgatcctgaccacgg-3′. The double-stranded oligonucleotide was then ligated with T4 DNA ligase (NEB, Ipswich, MA, US) into pSpCas9(BB)-2A-Puro (PX459) (#48139, Addgene, Watertown, MA, US) after digestion with BbsI-HF (NEB, Ipswich, MA, US). The obtained vector was transfected into TCCSUP and T24 cells using Lipofectamine™ 3000 (#L3000001, Invitrogen™). Cells were finally treated with 0.6 µg/mL Puromycin for 4 days to select the successfully transduced clones and expanded with a polyclonal approach to obtain stable cell lines.

2.11 Cytokine arrays

Conditioned media (CM) was obtained by incubating 10^6 T24, TCCSUP, and the respective CDCP1-KO cells for 72 h in 75 cm^2 flasks (TPP). CM from murine organoids (WT and CDCP1-overexpressing) was instead collected after 14 days of incubation following complete organoid formation. The concentration of cytokines was measured with LEGENDplex™ Human Inflammation Panel 1 (13-plex) (#740809, Biolegend®) in CM collected from human cell lines. Later, for financial reasons, a custom solution from the same company comprehensive of CCL2 and IL6 beads only was preferred. Cytokines were detected in CM from murine organoids with LEGENDplex™ Mouse Inflammation Panel (13-plex) (#740446, Biolegend®). The execution followed the technical steps suggested in the official protocol provided by the manufacturer. In the final step, beads

were analyzed with BD FACSCanto™ II Flow Cytometer (BD biosciences). The obtained data were processed with the official software provided by Biolegend®.

2.12 Human macrophage differentiation

Buffy coats from healthy donors were provided by the Blutspendedienst of the University Hospital of Bonn. 35 mL of blood from buffy coats was carefully stratified on 15 mL of Ficoll-Paque™ PLUS (#17-1440, Cytiva, Marlborough, MA, US) in 50 mL tubes. Tubes were then centrifuged at 800 RCF for 20 min at room temperature without the break. Upon the centrifugation step, a Ficoll layer separated the white blood cell ring containing PBMCs from other blood components. The white blood cell rings were collected and pooled in a single 50 mL tube and PBS (Thermo Fisher Scientific) was added to top the tube volume. The cell suspension was then centrifuged for 5 min, 300 RCF at room temperature. The supernatant was discarded, and the cell pellet was suspended in 50 mL of pure RPMI. Cells were diluted 1:10 with trypan blue (#1680, ROTH) and counted with a Neubauer chamber. 10^6 cells were seeded in each well of 6-well plates and placed in the incubator for 1 h. During the incubation, monocytes adhered to the bottom of the well while lymphocytes stayed in suspension, allowing for lymphocyte elimination via media removal. After removing the RPMI, Human Macrophage Media was added to the adherent monocytes to induce differentiation to macrophages. After 4 days of incubation, PBMC-derived macrophages were obtained and used for polarization assays or detached from 6-well plates with a cell scraper to perform migration.

2.13 Murine macrophage differentiation

A hole was made in the bottom of a 0.5 mL tube, which was then inserted into a 1.5 mL tube. Femurs and tibias were dissected from C57BL/6J mice and one of their extremities was cut. Mouse bones were then inserted in the previously adapted 0.5 mL tube with the cut extremities on the downside, to allow bone marrow (BM) flushing via centrifugation for 10 sec, 10,000 RCF at room temperature. Following centrifugation, the BM settled in the 1.5 mL tube. It was then suspended with 5 mL complete DMEM and washed for 5 min, 300 RCF at room temperature. The BM pellet was suspended in Mouse Macrophage Media, filtered with a 40 µM strainer (Sarstedt) to eliminate coagulated particles, and

seeded at a density of $2*10^6$ cells per well in 6-well plates. After 4 days of incubation at 37 °C, 5 % CO_2, 1 mL of fresh Mouse Macrophage Media was added, and following an additional 3 days of incubation macrophages were fully differentiated. Finally, bone marrow-derived macrophages (BMDM) were used for polarization assays or detached with a scraper from the 6-well plates and used for migration assays.

2.14 Macrophage migration assays

8.0 µm transwell (#353097, Falcon, London, UK) were inserted in 24-well plates (TPP). 700 µL of CM from human cell lines or murine organoids were placed in the space between the wells and the transwells after collection. Human PBMC-derived macrophages or murine BMDM were detached, diluted 1:2 in trypan blue, and counted with a cell counter (TC20, BioRad). $5*10^3$ macrophages were suspended respectively in complete RPMI (human) or DMEM (murine) and positioned on top of the transwell. 24-well plates were incubated overnight at 37 °C, 5 % CO_2, and fixed the day after with 4 % PFA for 15 min. Staining with 1 % Crystal Violet was performed for 15 min and the macrophages that did not migrate were removed from the top membrane of the transwell with a cotton swab. Transwells were air-dried for 2 days. Membranes were then removed from the plastic support of the transwells with the help of scalpels and forceps, mounted on glass microscope slides (Marienfeld) with Aquatex (Merck), and covered with glass coverslides (Marienfeld). Slides were dried overnight at room temperature, pictures were taken with Olympus SC50 microscope, and migrated macrophages were counted in ImageJ.

2.15 Macrophage polarization assay

Human PBMC-derived macrophages or murine BMDM were exposed to 75 % cells or organoids CM for 3 days. After stimulation, human macrophages were detached and stained for 20 min at 4 °C with 1:1000 LIVE/DEAD™ Fixable Near-IR Dead Cell Stain Kit (Invitrogen) and the following antibodies 1:400 CD11b (#563553, BD biosciences), 1:400 CD14 (#301834, BioLegend), 1:400 CD16 (#612944, BD biosciences), 1:200 CD163 (#25-1639-41, Invitrogen, Thermo Fisher Scientific), 1:200 CD200R (#329308, BioLegend), 1:200 CD80 (#305207, BioLegend), 1:200 CD38 (#612824, BD Biosciences). Mouse macrophages were stained for 20 min at 4 °C with 1:1000 LIVE/DEAD™ Fixable

Near-IR Dead Cell Stain Kit (Invitrogen) and the following antibodies 1:400 CD11b (#101206, BioLegend), 1:400 F4/80 (#123131, BioLegend), 1:200 CD206 (#141720, BioLegend) and 1:200 CD38 (#102721, BioLegend). They were then treated with Cytofix/Cytoperm™ Fixation/Permeabilization Kit (#554714, BD biosciences) according to the manufacturer´s instruction and stained with 1:100 Arg1 (#17-3697-80, Invitrogen) and 1:100 Nos2 (#12-5920-80, Invitrogen) for 30 min at 4 °C. Stained macrophages were washed twice with PBS at 300 RCF for 5 min and finally acquired with BD LSRFortessa™ cell analyzer (BD biosciences). The obtained data were analyzed with FlowJo™.

2.16 Anti-CDCP1 Ab production and treatments

The monoclonal Ab targeting CDCP1 (mAb-CDCP1) was isolated from a hybridoma cell line 41-2 (#CRL-2695, ATCC). First, 41-2 cells were expanded in 150 cm^2 flasks (TPP) with 41-2 Maintenance Media until they reached a density of 10^6 cells / mL. Cells were then collected, pelleted, and suspended in PBS. They were counted with the cell counter (TC20, BioRad), suspended in 41-2 Ab Production Media at 10^6 cells / mL, and incubated for 4 days. Media was then collected and handed to the Core Facility Nanobodies of the University of Bonn for isolation. Isolation of mAb-CDCP1 from the media was performed with columns following the protocol provided by the manufacturer. Specifics of such antibody and its ability to effectively downregulate CDCP1 expression in the cell membrane were previously described in the literature (Harrington et al., 2020; Hooper et al., 2003). Thus, we adopted it as the gold standard for experiments investigating CDCP1 regulation. Any treatment with mAb-CDCP1 was performed at 0.7 µM. For WB or cytokine detection in the CM, the treatment lasted 48 h. For the vitality assays, the treatment was maintained for 6 days.

2.17 Treatment with ERK inhibitor (iERK)

T24 and TCCSUP cells were seeded 10^5 / well in 6-well plates and treated respectively with 1 µM and 5 µM iERK (SCH772984, #HY-50846, Fisher Scientific) (Kopczynski et al., 2021). Cells were treated for 48 h, 24 h, and 6 h, and results were analyzed with WB and qPCR. Cytokine detection was performed from CM collected after 48 h treatment.

2.18 qPCR

RNA was isolated from T24, TCCSUP, and LNCaP cells with the TRIzol method. 1 mL of TRIzol™ (#15596026, Invitrogen) was added in each sample in 0.5 mL tubes. Samples were incubated for 5 min on ice. 200 µL of chloroform (#Y015, ROTH) were added. The obtained TRIzol-chloroform solution was mixed with vortex, incubated for 2 min at room temperature and centrifuged for 15 min at 4°C, 12,000 RCF. The aqueous upper phase was transferred in a new 0.5 mL tube and 500 µL of 2-propanol (#6752, ROTH) were added. The solution was incubated for 10 min at room temperature and centrifuged for 10 min at 4°C, 12,000 RCF. Supernatant was discarded and mRNA pellet was suspended in 1 mL of 75% ethanol (ROTH). A centrifuge step of 5 min at 4°C, 7,500 RCF was performed. Supernatant was discarded carefully, mRNA pellet was air-dried and suspended in 20 µL RNase-free water (Thermofisher). mRNA concentration was quantified with Thermo Scientific™ NanoDrop™ 2000/2000c Spectrophotometer. Retro-transcription was performed with obtained mRNA using PrimeScript RT Reagent Kit (#RR037A, TaKara) in a thermocycler (Professional Trio Fa. Analytica Jena). Quantitative PCR (qPCR) reactions were performed using QuantStudio™ 5 (Invitrogen) with TB Green® Premix Ex Taq™ II (#RR82WR, TaKara) and the specific primers reported below. Primer sequences were obtained from PrimerBank (http://pga.mgh.harvard.edu/primerbank/index.html). GAPDH expression level was used as a reference for the normalization of each value. Used primer sequences were as follows: hIL-6 forward, 5′-TACATCCTCGACGGCATCTC-3′, reverse, 5′-TGCCTCTTTGCTGCTTTCAC-3; hCCL2, forward, 5′-CAGCCAGATGCAATCAATGCC-3′, reverse, 5′-TGGAATCCTGAACCCACTTCT-3′; hUGT2B11, forward 5′-TGATTTTGTTGGAGGATTCCACTG-3′, reverse, 5′-GTCAAATCTCCACAGAACCTTTT-3′; hGDF15, forward, 5′-CAACCAGAGCTGGGAAGATTCG-3′, reverse, 5′-CCCGAGAGATACGCAGGTGCA-3′; hCLU forward 5′-CCAATCAGGGAAGTAAGTACGTC-3′, reverse, 5′-CTTGCGCTCTTCGTTTGTTTT-3′; hRRM2 forward, 5′-CACGGAGCCGAAAACTAAAGC-3′, reverse, 5′-TCTGCCTTCTTATACATCTGCCA-3′; hTP53I3 forward, 5′-GGAGGACCGGAAAACCTCTAC-3′, reverse, 5′-CCTCAAGTCCCAAAATGTTGCT-3′; hKIF14 forward 5′-TGTAGGTAGATTGGCACTTCAGA-3′, reverse, 5′-

CGACGTTGTAATGTAAGACGTGT-3′; hPHLDA forward, 5′-CTGGATGGTCCCAGACTCTCAG-3′, reverse, 5′-CTAAGAGCAGTCTGCAGGACAG-3′; hATF5 forward, 5′-TGGCTCGTAGACTATGGGAAA-3′, reverse, 5′-ATCAACTCGCTCAGTCATCCA-3′; GAPDH forward 5′-AATCCCATCACCATCTTCCA-3′; reverse, 5′-TGGACTCCACGACGTACTCA-3′.

2.19 Prostate and bladder murine organoids generation

CDCP1$^{lox\text{-}STOP\text{-}lox}$ transgenic mouse model was previously generated by introducing in the mouse genome a copy of the gene coding for human CDCP1 with an upstream STOP sequence flanked by loxP sites (Alajati et al., 2020). To generate organoids, prostate and bladder were removed from CDCP1$^{lox\text{-}STOP\text{-}lox}$ mice. They were chopped with a scalpel and incubated for 2 h in 5 mg/mL collagenase type II (#17101-015, Life Technologies) at 37 °C and 5 % CO_2. The obtained cell suspension was pelleted at 300 RCF for 5 min and digested with TrypLE Express (#12605-010, Life Technologies) for 15 min at 37 °C and 5 % CO_2. DMEM complete was added to stop the digestion and the cell mixture was mechanically dissociated with a syringe and 18 G needle. The suspension was filtered with a 40 µm strainer; cells were counted and transduced with a CBA-CRE adenovirus produced in the Virus Facility of the Medical Faculty University of Bonn. The transduction was performed as follows. A suspension of $2*10^4$ cells was pipetted in each well of a 96-well plate. The virus was added on top; the plate was centrifuged for 1 h, 600 RCF, 32 °C, and subsequently incubated for 1 h, 37 °C, 5 % CO2. In the meantime, 24-well plates were pre-warmed at 37 °C in the cell incubator. After the incubation, cells were collected and transferred from the 96-well plate to a 15 mL tube. They were then centrifuged at 300 RCF, 4 °C, and media with virus was removed. The cell pellet was suspended in 40 µL Matrigel (#356231, Corning) / $2*10^4$ cells and 40 µL drops were formed in each 24-well from the obtained suspension. 24-well plates were incubated for 30 min, 37 °C, 5 % CO_2 upside down to let the Matrigel drop solidify before adding Prostate Organoid Media or Bladder Organoid Media and placing the plates in the incubator. After 14 days, organoids were formed, and the media was collected for cytokine array. Moreover, Matrigel was dissociated with a pipette after adding 1 mL of cold PBS (4 °C). The dissociated Matrigel

was centrifuged for 5 min, 300 RCF, 4 °C to pellet the organoids. Matrigel-PBS supernatant was removed, and RIPA was added for WB analysis.

2.20 FACS on mouse tumors PCa

CDCP1^{+}; Pten$^{-/-}$ double mutant mouse model is a conditional mouse model that overexpresses human CDCP1 in a Pten null background prostate inducing spontaneous development of aggressive PCa. This model was previously generated by Alajati et al. (Alajati et al., 2020). Tumors from CDCP1^{+}; Pten$^{-/-}$ mice and from mice bearing Pten$^{-/-}$ mutation only were isolated. A scalpel was used to chop the tumors. The tissue was chemically digested with collagenase type II for 2 h, 37 °C, 5 % CO_2, and with 15 min incubation in 0.25 % Trypsin (Thermo Fisher Scientific). The final cell suspension was then obtained using a syringe with an 18 G needle and filtered with a 40 µm strainer. Finally, cells were stained with 2 different FACS panels for 20 min at 4 °C. The first panel: 1:1000 Zombie UV™ Fixable Viability Kit (#423107, BioLegend), CD45 (#103131, BioLegend), 1:400 CD3 (#100305, BioLegend), 1:400 CD19 (#115505, BioLegend), 1:400 CD11c (#117305, BioLegend), 1:400 Ly6G (#127605, BioLegend), 1:400 CD49b (#103503, BioLegend), 1:400 NK1.1 (#108705, BioLegend), 1:400 CD11b (#101291, BioLegend), 1:400 F4/80, 1:200 CD206 (#141727, BioLegend), 1:200 CD163 (#155307, BioLegend). The second panel: 1:1000 Zombie UV™ Fixable Viability Kit, 1:400 EpCAM (#118240, BioLegend), 1:400 CD45 (#103131, BioLegend), 1:200 CDCP1 (#324017, BioLegend). After staining, cells were washed twice at 300 RCF for 5 min and acquired with BD LSRFortessa™ cell analyzer (BD biosciences). The obtained data were analyzed with FlowJo™.

2.21 Generation of LNCaP clones with the CRISPaint method

The CRISPaint method is a three-plasmid tagging system that enables site-specific insertion of heterologous genetic material. The three plasmids are the target selector, which codes for the expression of Cas9 and a sgRNA; the frame selector, which allows re-introducing amino acids that are lost during the restrictions of the target site; the universal donor, which carries the gene of the fluorescent protein before its introduction in the host genome by Cas9. The specific application of this method is the creation of

chimeric proteins composed of a protein of interest and a fluorescent protein (e.g. mNeon). This method is described in detail in a previous publication (Schmid-Burgk et al., 2016). As a first step for the creation of LNCaP clones with this method, the double-stranded oligonucleotides coding for CDKN1A, CDKN2A, and GLB1 sgRNAs were generated via annealing of the following one-strand oligonucleotides: CDKN1A-top, 5′-CACCGGGCGGATTAGGGCTTCCTCT-3′, CDKN1A-bottom, 5′-AAACAGAGGAAGCCCTAATCCGCCC-3′; CDKN2A-top, 5′-CACCGGCCTCTCTGGTTCTTTCAAT-3′, CDKN2A-bottom, 5′-AAACATTGAAAGAACCAGAGAGGCC-3′; GLB1-top, 5′-CACCGCAGGCTTTCATCATCATACA-3′, GLB1-bottom, 5′-AAACTGTATGATGATGAAAGCCTGC-3′. The annealing phase required a step of 4 min at 90 °C and one of 8 h at room temperature. The double-stranded oligonucleotides for CDKN1A, CDKN2A, and GLB1 were then cloned separately in the Target selector via restriction with BbsI-HF® (#R3539, NEB) at 37 °C for 15 min and ligation with T4 DNA ligase (#M0202, NEB) overnight at 16 °C. Ligated plasmids were transformed in NEB® Stable Competent *E. coli* (High Efficiency) (#C3040, NEB). To do that, bacteria were thaw on ice and plasmids were pipetted in the bacteria suspension. Heat shock was performed on bacteria at 42°C for 30 seconds. Bacteria were incubated for 5 min in ice, spread onto pre-warmed LB-Agar plates and incubated overnight at 37 °C in a bacteria incubator. Bacteria colonies grown on the LB-Agar plate, were inoculated in 5 mL LB-Medium and grown overnight at 37 °C, 200 RPM shaking, in a bacteria incubator. QIAGEN Plasmid Mini Kit (QIAGEN) was performed with the bacteria suspensions to isolate the plasmids. Plasmids were sent to Microsynth in a pre-mixed solution with the following primer (5′-AGGGCCTATTTCCCATGATTC-3′) to confirm that the sgRNAs were efficiently cloned into the Target selector with sanger sequencing. Target selector plasmids positive for sgRNAs integration were transformed once again in NEB® Stable Competent *E. coli* (High Efficiency) (#C3040, NEB), expanded in 150 mL of LB-Media, and isolated with QIAGEN Plasmid Maxi Kit (QIAGEN). Finally, 3 independent LNCaP clones expressing p16-mNeon, p21-mNeon, and β-GAL-mNeon chimeric proteins were generated. To do that, LNCaP cells were seeded in 96-well plates at a density of $5*10^3$ cells / well. The day after, they were transfected with the 3-plasmid system (50 ng Target selector + 50 ng Frame selector + 100 ng mNeon Universal donor) using Lipofectamine™ 3000. Transfection

reagents were removed from the cells after 6 h and replaced with LNCaP Media. 24 h after transfection, efficiently transfected cells were selected using 1 µg / mL puromycin for 4 days. Obtained clones were then expanded in a polyclonal approach.

2.22 FACS analysis clones

Senescence was induced in LNCaP-p16-mNeon, LNCaP-p21-mNeon, and LNCaP-β-GAL-mNeon for 6 days with 0.6 nM docetaxel. Cells were then detached and stained with LIVE/DEAD™ Fixable Near-IR Dead Cell Stain Kit (Invitrogen) for 20 min at 4 °C. Analysis was performed with BD FACSCanto™ II Flow Cytometer (BD biosciences) and data were analyzed with FlowJo™.

2.23 mRNA sequencing

LNCaP-p16-mNeon, LNCaP-p21-mNeon, and LNCaP-β-GAL-mNeon were treated for 6 days with 0.6 nM docetaxel to induce senescence. Cells were then detached with 0.025 % trypsin (Thermo Fisher Scientific), collected, and handed to the Flow Cytometry Core Facility of the Medical Faculty University of Bonn for sorting. Per clone, 3 different cell populations (mNeon1+, mNeon2+, and mNeon3+) were sorted with BD FACSAria™ III Cell Sorter (BD biosciences). RNA was then extracted with TRIzol and mRNA sequencing was performed from the Next Generation Sequencing (NGS) core facility of the Medical Faculty University of Bonn. QuantSeq 3′ mRNA-Seq Library Prep Kit (Lexogen, Vienna, Austria) was used for enrichment and sequencing was performed on a NovaSeq 6000 (Illumina, San Diego, CA, USA) device with a read length of 1 × 100 bp. Data were provided in FastQ format and further analyzed by the Core Unit for Bioinformatics Data Analysis (CUBA) of the Medical Faculty University of Bonn. Statistical analysis was performed in the R environment with the Bioconductor package DESeq2 (Huber et al., 2015; Love et al., 2014). Benjamini–Hochberg method was used to calculate multiple testing adjusted p values. Data visualization was generated upon TMM normalized data (Robinson and Oshlack, 2010) using R packages ggplot2 (Wickham, 2016) and ComplexHeatmap (Gu et al., 2016), respectively.

2.24 Statistical analysis

The statistical evaluation of the experimental results was performed with GraphPad Prism 8 software (GraphPad, San Diego, CA, USA). The paired and unpaired Student’s t-test was used and p values < 0.05 were considered statistically significant.

3 Results

3.1 Nbs targeting CDCP1 and EGFR reduce tumor growth *in-vitro*

Anti-CDCP1 Nbs were produced in collaboration with the nanobody facility of the University of Bonn and were then tested for their affinity to CDCP1. Since Nbs are tagged with an HA-tag, we detected wheter the Nbs were binding to CDCP1 via immunostaining and FACS analysis on PC3. First, we incubated the cells with our Nbs and then with an APC secondary antibody against HA-tag. Eight out of nine Nbs showed specific affinity to our protein of interest (Fig.14). C07 did not show affinity to CDCP1 and was used in following experiments as a negative control (Fig.14).

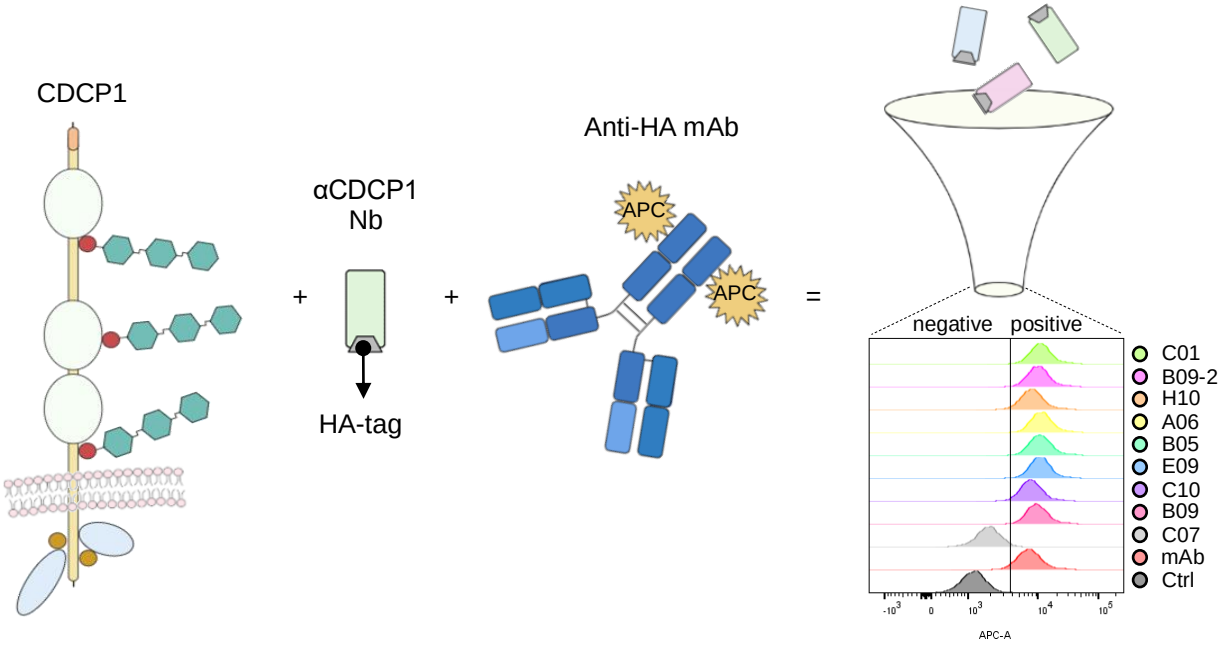

Fig. 14: FACS analysis of different Nbs targeting CDCP1
The different Nbs generated to target CDCP1 were tested for their ability to bind to the antigen on PC3 cell line. Cells were incubated with Nbs and then with secondary anti-HA mAb conjugated with APC. APC signal was detected via FACS. Positive hits, effectively binding to CDCP1, are on the right side of the vertical black line in the FACS panel. The mAb condition in red refers to the anti-CDCP1 mAb used as a positive control for the binding. Image created with BioRender.

We then tried to characterize the binding specificity of each Nb that showed affinity to CDCP1 via expressing CDCP1 homologs or variant of human CDCP1 in HEK293T cells.

Upon transfection of cells with each CDCP1 construct, we used the same strategy described in Fig. 14. When comparing the Nbs reactivity to human (hCDCP1), murine (mCDCP1) and non-human primate CDCP1 (cynoCDCP1) we observed that all Nbs could bind to human and non-human primate CDCP1 (Fig. 15). However, only four of them could bind to mCDCP1 (Fig. 15).

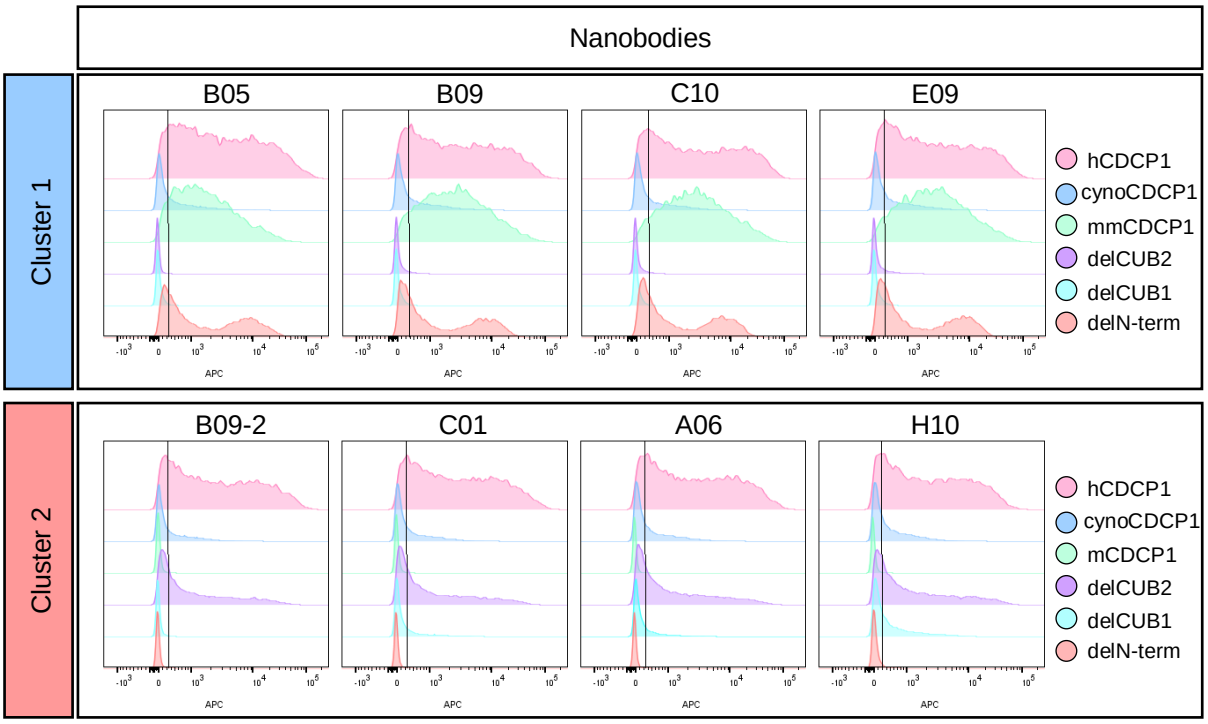

Fig. 15: Study of the binding of anti-CDCP1 Nbs to different species and epitopes
HEK293T cells were transfected with different CDCP1 isoforms (human, murine, non-human primate) and CDCP1 mutants (deletion for CUB2, deletion for CUB1, deletion for N-term). Transfected cells were incubated with Nbs and secondary anti-HA mAb conjugated with APC. Signal was detected via FACS. Positive signal stands on the right side of the black vertical line present in the FACS panels.

On the other hand, employing cells expressing different human CDCP1 variants allowed us to predict the epitope where each Nb is binding. The different CDCP1 mutants we employed are as follows: CDCP1 missing the N-terminal region (delN-term), CDCP1 missing CUB1 (delCUB1), CDCP1 missing CUB2 (delCUB2). Four Nbs showed a clear affinity to the CDCP1 variant missing the N-terminal region, while the other Four exhibited effective binding to delCUB2 CDCP1 (Fig. 15). None of them showed affinity to delCUB1 CDCP1 (Fig. 15). Interestingly, the pattern observed in the species affinity reflected also in the epitope affinity. Indeed, results suggest that the eight selected Nbs targeting CDCP1

can be clustered in two distinctive groups. We will refer to these groups as Cluster 1 and Cluster 2. As a general conclusion, Cluster 1 has affinity with human, monkey and murine CDCP1, while Cluster 2 only with human and monkey. This information becomes important when considering to perform toxicity studies in in-vivo models. Moreover, Cluster 1 binds CDCP1 in absence of its N-terminal region, but not in absence of its CUB1 and CUB2 region. Thus, the specific binding epitope of this cluster is probably in between the CUB1-CUB2 domains. On the contrary, Cluster 2 binds delCUB2 CDCP1 rather than delN-term CDCP1. Hence, Cluster 2 binds to an epitope that is present in between the Nterm-CUB1 region. After characterizing the binding pattern of the Nbs, we tested their effect on CDCP1 regulation and cell vitality. We observed no downregulation of CDCP1 nor anti-proliferative effect when Nbs were used in their single domain format at 10 µg/mL or 100 µg/mL (data not shown). Thus, we decided to produce rFc-Nb dimers in an attempt to improve their biological activity. In rFc-Nb dimers, the Fc region of rabbit antibodies links two identical Nb monomers. This format proved decisively more effective. Indeed, rFc-Nbs from Cluster 2 induced clear CDCP1 downregulation in PC3 cells (Fig. 16A). Moreover, rFc-H10 and rFc-A06 were able to reduce PC3 proliferation similarly to our gold standard (Fig. 16B), an anti-CDCP1 mAb previously published as effective in reducing cell growth. However, since the rFc format did not represent a clear improvement from the point of view of the size reduction when compared to common mAbs, we planned to produce Nb dimers characterized by a smaller linker of 963.87 Da (sequence: GGGGSGGGGSGGGGS). We produced such dimers with a biased approach, selecting H10 and A06 as the most promising Nbs. The final dimers were H10-H10 and A06-A06 homodimers, and H10-A06 and A06-H10 heterodimers. When testing H10-H10 and A06-A06 homodimers on PC3 cell line we noticed that their activity on CDCP1 deregulation was comparable to the rFc-Nb, while H10-A06 and A06-H10 heterodimers showed an enhanced ability to downregulate CDCP1 (Fig. 16C). Moreover, all Nb dimers showed a decisively improved ability to block cell proliferation (Fig. 16D).

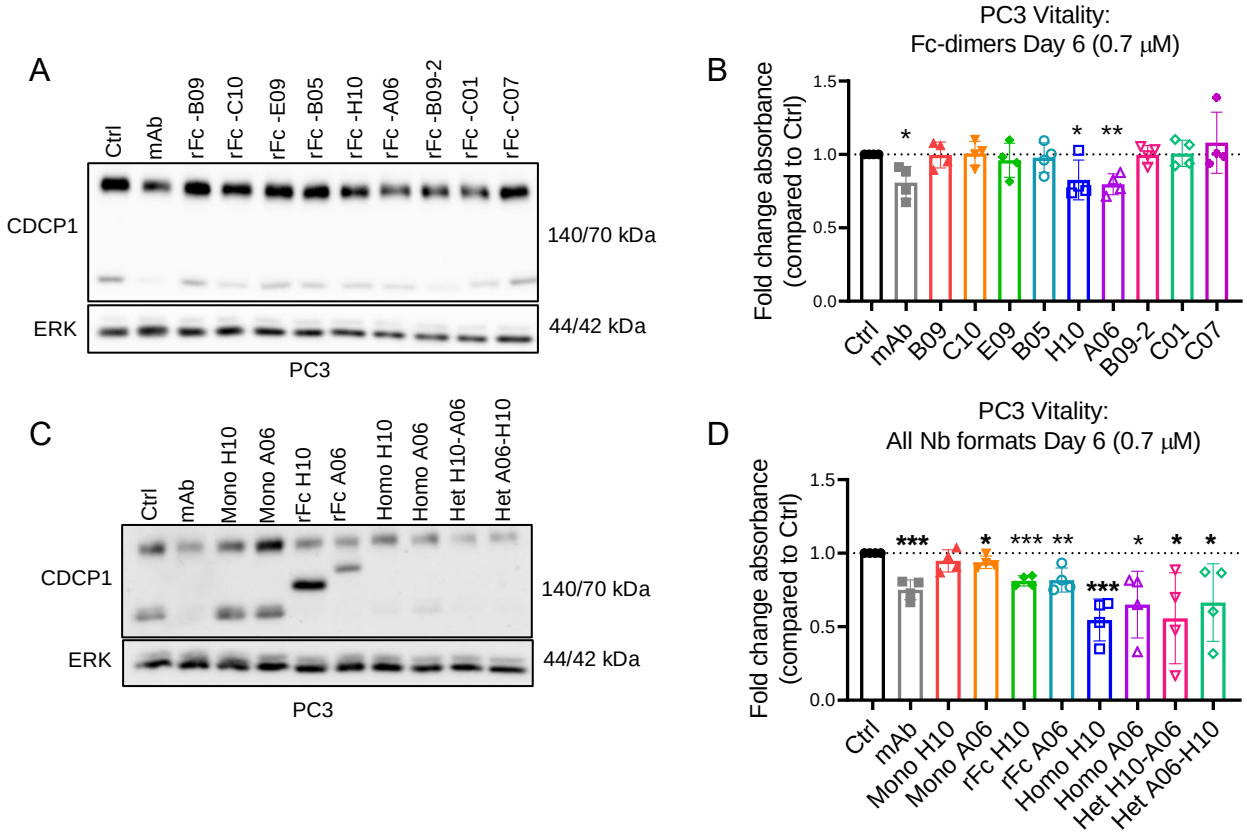

Fig. 16: Biological effect of anti-CDCP1 Nbs
(A) WB for CDCP1 and ERK in PC3 cells treated with rFc-Nbs for 2 days. (B) Graph of cell vitality performed with crystal violet method after treatment of PC3 with rFc-Nbs for 6 days. n=4. Error bars indicate SD. *P < 0.05, **P < 0.01. Statistical test: two-tailed unpaired t test. (C) WB for CDCP1 and ERK in PC3 cells treated with different Nb formats (Nb-monomers, rFc-Nbs, Nb-dimers) for 2 days. (D) Graph of cell vitality performed with crystal violet method after treatment of PC3 with Nb-monomers, rFc-Nbs, and Nb-dimers for 6 days. n=4. Error bars indicate SD. *P < 0.05, **P < 0.01, ***P < 0.001. Statistical test: two-tailed unpaired t test.

Since we published that CDCP1 is upregulated in Ba/Sq subtype of BCa and this subtype is characterized by high levels of EGFR, we hypothesized that targeting both CDCP1 and EGFR in such cancers could efficiently block tumor growth. For this reason we first produced Nbs against EGFR in collaboration with the Nbs facility and then tested for their affinity to EGFR with immunostaining and FACS analysis in SCaBER cell line, a Ba/Sq BCa cell model. Results show that ten Nbs out of twelve bind to EGFR successfully (Fig. 17).

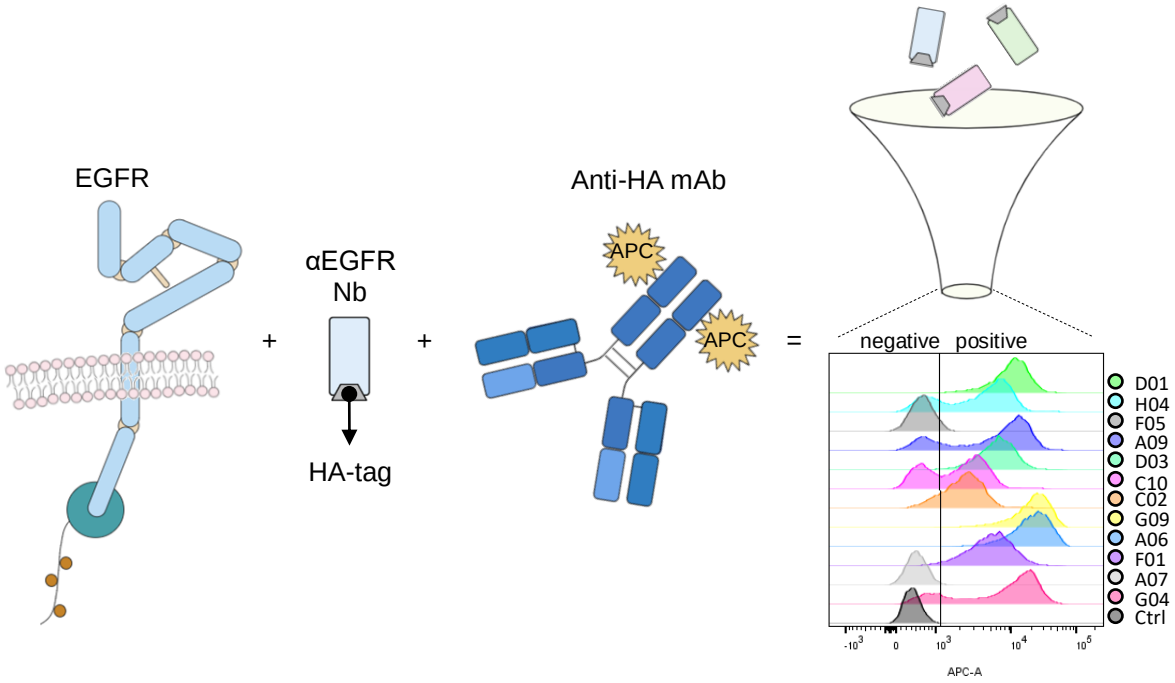

Fig. 17: FACS analysis of different Nbs targeting EGFR
The binding to EGFR was tested for Nbs generated to target EGFR on SCaBER cell line. Cells were incubated with Nbs and then with secondary anti-HA mAb conjugated with APC. APC signal was detected via FACS. Positive hits are on the right side of the vertical black line in the FACS panel. Image created with BioRender.

The Nbs showing affinity with EGFR were then tested for their ability to affect EGFR activation and cell proliferation in order to select the best candidates for further applications. Fig. 18A shows that Nbs G04, C10, D03 and D01 are the strongest inhibitors of EGFR phosphorylation upon EGF stimulation. The same Nbs also show a stark reduction of cell viability after 6 days of treatment, comparable to the one of our gold standard Cetuximab (Cet) (Fig. 18B).

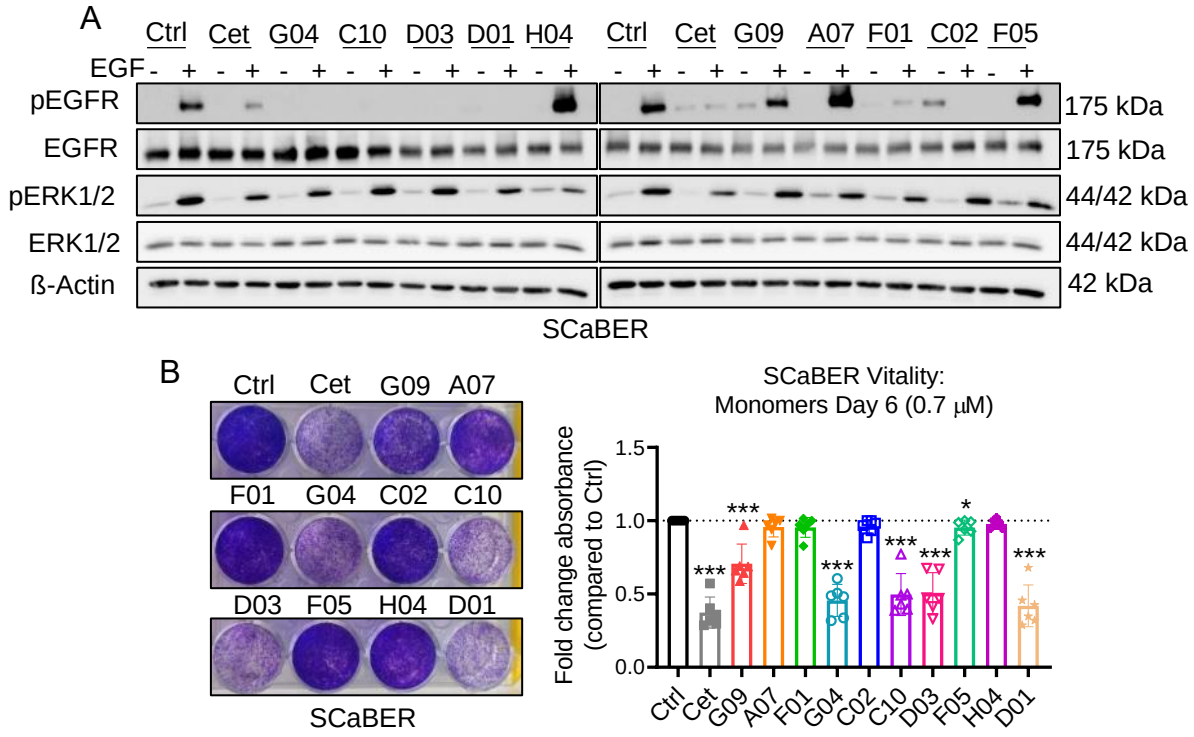

Fig. 18: Biological effect of anti-EGFR Nbs
(A) WB analysis for pEGFR, EGFR, pERK1/2, ERK1/2, ß-Actin on SCaBER cells pretreated with anti-EGFR Nbs and subsequently activated with EGF. (B) Cristal violet assay on SCaBER cells treated for 6 days with anti-EGFR Nbs (0.7 µM). Left: representative picture of the assay. Right: Bar plot. n=6. Error bars indicate SD. *P < 0.05, ***P < 0.001. Statistical test: two-tailed unpaired t test.

Altogether, our results showed that anti-CDCP1 Nb dimers can efficiently downregulate CDCP1 and reduce PC3 cell growth. Besides, anti-EGFR Nbs bind efficiently to EGFR and block EGF binding, making them suitable for the creation of bispecific Nbs that target at the same time CDCP1 and EGFR. Anti-EGFR Nbs also reduce SCaBER cell growth, adding to their potential effect.

3.2 CDCP1 expression is correlated with inflammatory cytokine production and TAM infiltration in urological cancers

Basing on in-house and external publications we hypothesized that CDCP1 may have some sort of liaison with TAM infiltration in bladder and prostate cancers (Brina et al., 2023; Saponaro et al., 2023). To probe this hypothesis we first screened a MIBC and a PCa TMA for CD68 and CD163 expression. Results prove that tumors expressing high levels of CDCP1 are also the most infiltrated with CD163+ and CD68+ cells (Fig. 19A, 19C). We observed a ~20% increase in high-CDCP1 tumors coexpressing high levels of CD68 and CD163 when compared to the low-CDCP1 tumors in both MIBC and PCa (Fig. 19B, 19D).

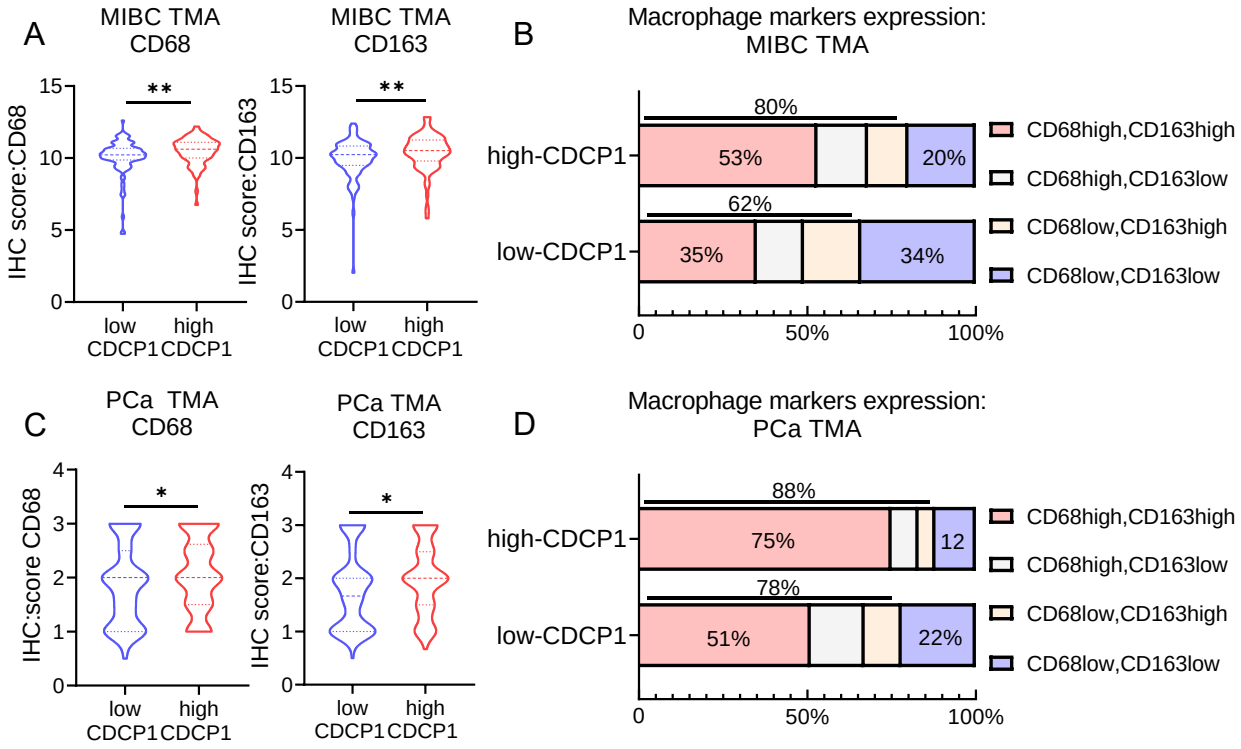

Fig. 19: Expression of CDCP1, CD68, and CD163 in MIBC and PCa TMAs
(A) Violin plot for CD68 and CD163 levels in low-CDCP1 and high-CDCP1 tumors on a MIBC TMA. n=184. Error bars indicate SD. **P < 0.01. Statistical test: two-tailed unpaired t test. (B) Representation of the percentage of low-CDCP1 and high-CDCP1 MIBC tumors expressing high/low levels of CD68 and CD163. (C) Violin plot for CD68 and CD163 levels in low-CDCP1 and high-CDCP1 tumors on a PCa TMA. n=238. Error bars indicate SD. *P < 0.05. Statistical test: two-tailed unpaired t test. (D) Representation of the percentage of low-CDCP1 and high-CDCP1 PCa tumors expressing high/low levels of CD68 and CD163.

Since the presence of inflammatory cytokines can influence deeply the fitness of TAM and their migration to the tumor site, we decided to investigate whether tumor cells expressing CDCP1 are characterized by a peculiar secretome. We first induced the knock-out (KO) of CDCP1 in 2 MIBC cell lines (T24 and TCCSUP) using CRISPR/Cas9 technology (Fig. 20A). Then, we tested the CM of control (Ctrl) and CDCP1-KO cells for inflammatory cytokine levels with a multiplex assay. Result show a consistent IL6 and CCL2 reduction in the media collected from both the cell lines knocked-out for CDCP1 (Fig. 20B), suggesting that CDCP1 may participate to TAM recruitment. Indeed, CCL2 is fundamental for macrophage chemotaxis. Besides, as expected, when performing migration assays with the CM from Ctrl and CDCP1-KO cells we observed a reduced macrophage migration towards CDCP1-KO CM (Fig. 20C).

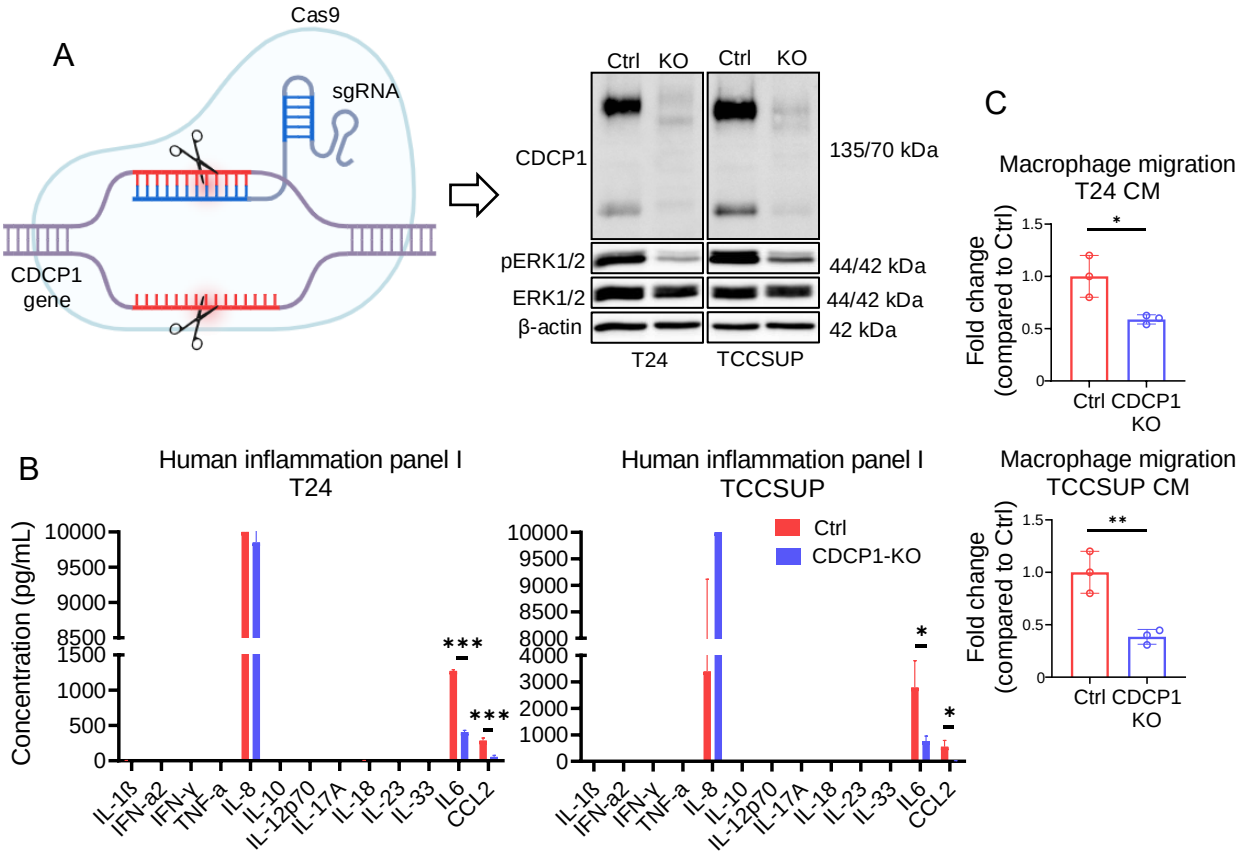

Fig. 20: KO of CDCP1 reduces cytokine expression
(A) WB for CDCP1, pERK1/2, ERK1/2, β-actin on T24 and TCCSUP cells knocked out for CDCP1 and relative Ctrl. (B) Bar plot of cytokine levels in CM collected from CDCP1-KO T24 and TCCSUP, and relative Ctrl. n=3. Error bars indicate SD. *P < 0.05, ***P < 0.0001. Statistical test: two-tailed unpaired t test. (C) Bar plot of macrophage migration towards CM collected from CDCP1-KO T24 and TCCSUP, and relative Ctrl. n=3. Error bars indicate SD. *P < 0.05, **P < 0.001. Statistical test: two-tailed unpaired t test.

We repeated the evaluation of CCL2 and IL6 production and macrophage migration upon the treatment of MIBC cell lines with a mAb targeting CDCP1 (Harrington et al., 2020; Hooper et al., 2003). We aimed to investigate CDCP1 targeting as a possible strategy to decrease TAM infiltration and ameliorate the TME conditions in MIBC tumors expressing high levels of CDCP1. The experimental setup is represented in Fig. 21A. Shortly, we isolated PBMC from donors´ buffy coats and differentiated them into macrophages. Meanwhile, we treated T24 and TCCSUP cells with anti-CDCP1 mAb for 48 hours and then collected the CM. Treatment with the Ab successfully downregulated CDCP1 expression in all tested cell lines (Fig. 21B). Consequently, MIBC cell lines showed decreased CCL2 and IL6 levels in the CM (Fig. 21C). Moreover, the CM collected from MIBC cell lines treated with anti-CDCP1 mAb induced a lower migration of PBMC-derived macrophages (Fig. 21D).

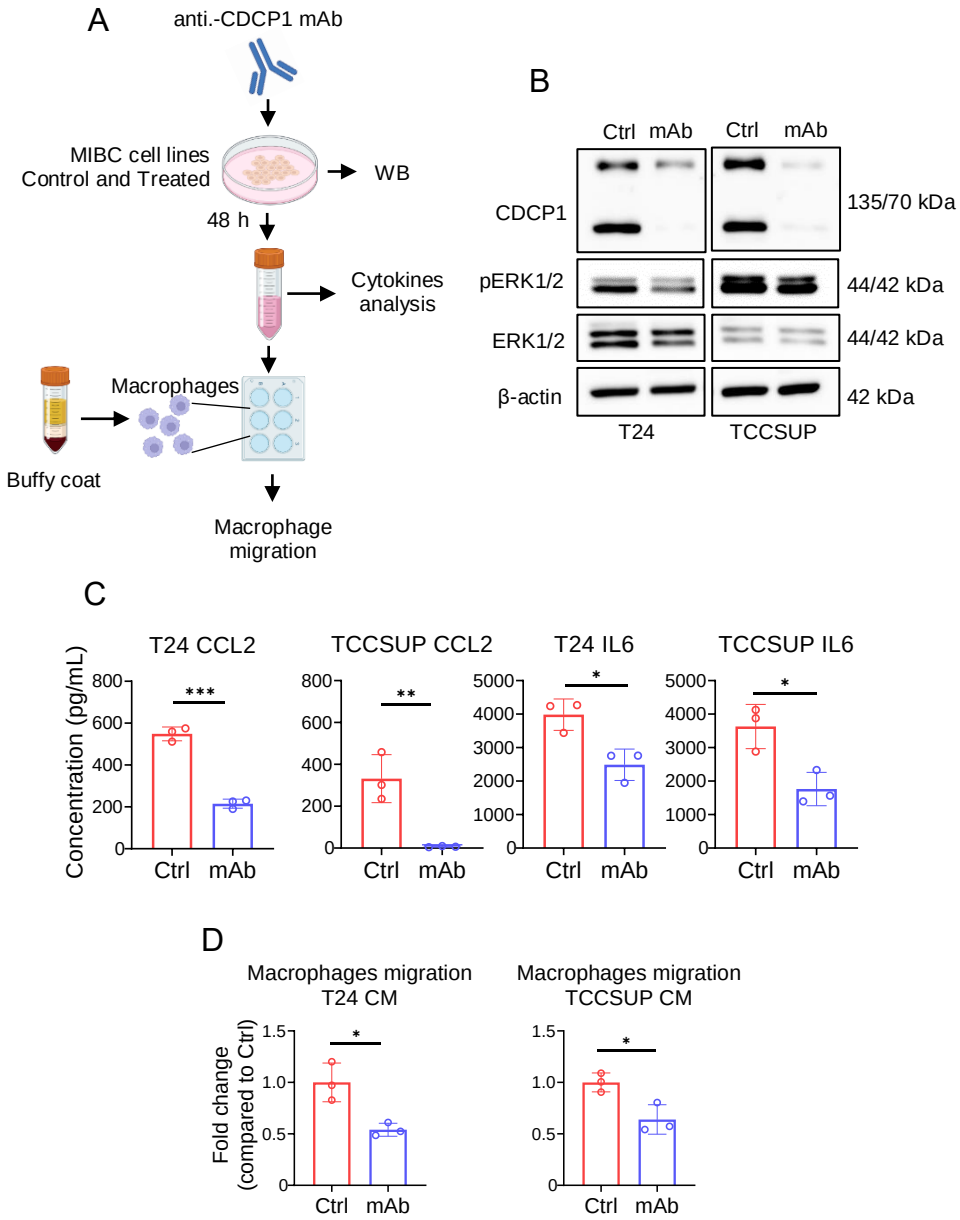

Fig. 21: Cytokine level upon treatment with mAb targeting CDCP1
(A) Illustration of the experiments performed with anti-CDCP1 mAb. Briefly, MIBC cell lines were treated with anti-CDCP1 mAb and WB was performed. CM was harvested from treated and untreated cells and cytokine analysis was performed. CM was used to assess the migration of PBMC-derived macrophages. Image created with BioRender. (B) WB for CDCP1, pERK1/2, ERK1/2, β-actin on T24 and TCCSUP after treatment with mAb (0.7 µM) for 48 h. (C) Bar plot of CCL2 and IL6 concentration in T24 and TCCSUP CM after treatment with anti-CDCP1 mAb (0.7 µM) for 48 h. n=3. Error bars indicate SD. *P < 0.05, **P < 0.001, ***P < 0.0001. Statistical test: two-tailed unpaired t test. (D) Bar plot of PBMC-derived macrophage migration towards CM of T24 and TCCSUP treated with anti-CDCP1 mAb (0.7 µM) for 48 h. n=3. Error bars indicate SD. *P < 0.05. Statistical test: two-tailed unpaired t test.

Importantly, the dependency of the MAPK/ERK pathway on CDCP1 is already fully consolidated in several cancer types (Khan et al., 2021) and our results confirm it in BCa too. Indeed, it is evident that ERK phosphorylation decreases when knocking out CDCP1 or targeting this protein with the Ab in MIBC cell lines (Fig. 20A and Fig. 21B). Since ERK1/2 activation is reported to be responsible for cytokines transcription in different circumstances (Chang et al., 2023; C.-Y. Chen et al., 2017) and ERK1/2 inhibition can reduce CCL2 and IL6 production (Hu et al., 2024; Tan et al., 2023), we hypothesized that CDCP1/ERK pathway could be responsible for CCL2 and IL6 production in CDCP1-expressing tumor cells. To verify this assumption we treated T24 and TCCSUP cell lines with the ERK inhibitor SCH772984 (iERK) (Kopczynski et al., 2021). We first confirmed that ERK phosphorylation was reduced after the treatment. Precisely, iERK effect was strong after 24h and 6h of treatment (Fig. 22A). Afterwards, we assessed CCL2 and IL6 mRNA expression observing a clear reduction after 24h and 6h of treatment with iERK (Fig. 22B). Finally, the media from cells treated with iERK was collected after 48h and tested for cytokines level via Legendplex™. The concentration of CCL2 and IL6 in the CM was strongly reduced (Fig. 22C).

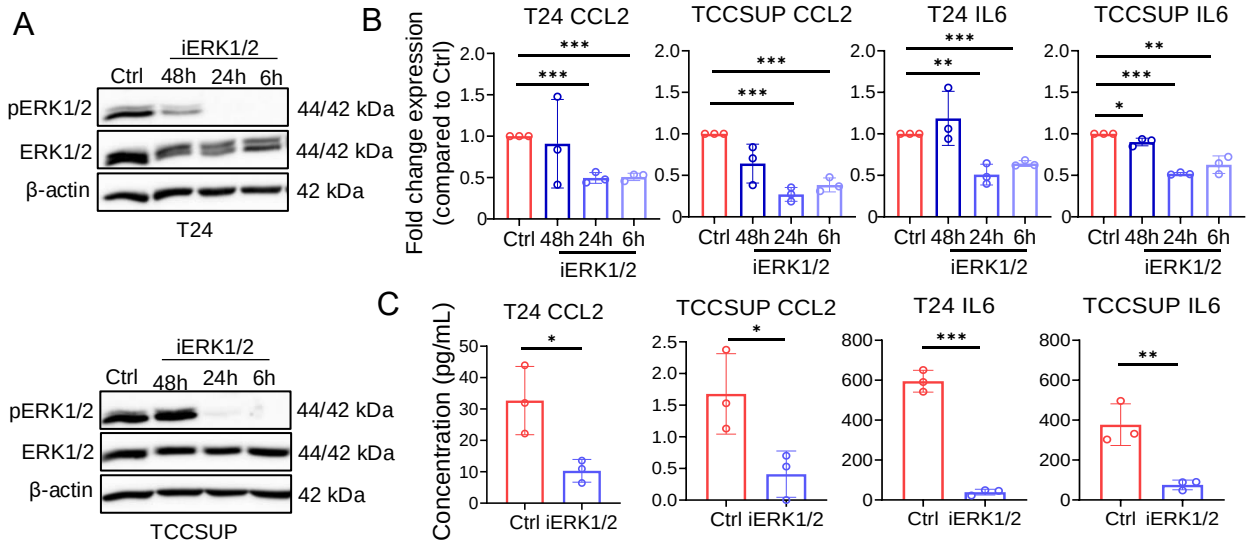

Fig. 22: Cytokine expression upon ERK inhibition
(A) WB for pERK1/2, ERK1/2, β-actin on T24 and TCCSUP after treatment with ERK inhibitor (1 μM and 5 μM) for 48, 24 and 6 h. (B) Bar plot of CCL2 and IL6 mRNA expression in T24 and TCCSUP after treatment with ERK inhibitor (1 μM and 5 μM) for 48, 24 and 6 h. n=3. Error bars indicate SD. *P < 0.05, **P < 0.001, ***P < 0.0001. Statistical test: two-tailed unpaired t test. (C) Bar plot of CCL2 and IL6 concentration in T24 and TCCSUP CM after treatment with ERK inhibitor (1 μM and 5 μM) for 48. n=3. Error bars indicate SD. *P < 0.05, **P < 0.001, ***P < 0.0001. Statistical test: two-tailed unpaired t test.

To confirm the results obtained on MIBC cell lines following CDCP1 KO or blockade we performed CDCP1 overexpression in murine organoid models of bladder and prostate. The procedure for the organoids generation is described in Fig. 23A and involves the excision of the bladder and the prostate from our CDCP1$^{lox\text{-}stop\text{-}lox}$ mouse model, which can overexpress CDCP1 in any tissue following the activity of CRE recombinase, as explained in Fig. 6. The organoids obtained upon the introduction of CRE recombinase in cells isolated from the bladder and prostate via virus transduction show a successful CDCP1 overexpression and ERK1/2 activation (Fig. 23B). Moreover, cytokine analysis on the media obtained from the organoids demonstrate that CDCP1 introduction triggered an increased production of CCL2 and IL6 in both organ-derived organoids (Fig. 23C).

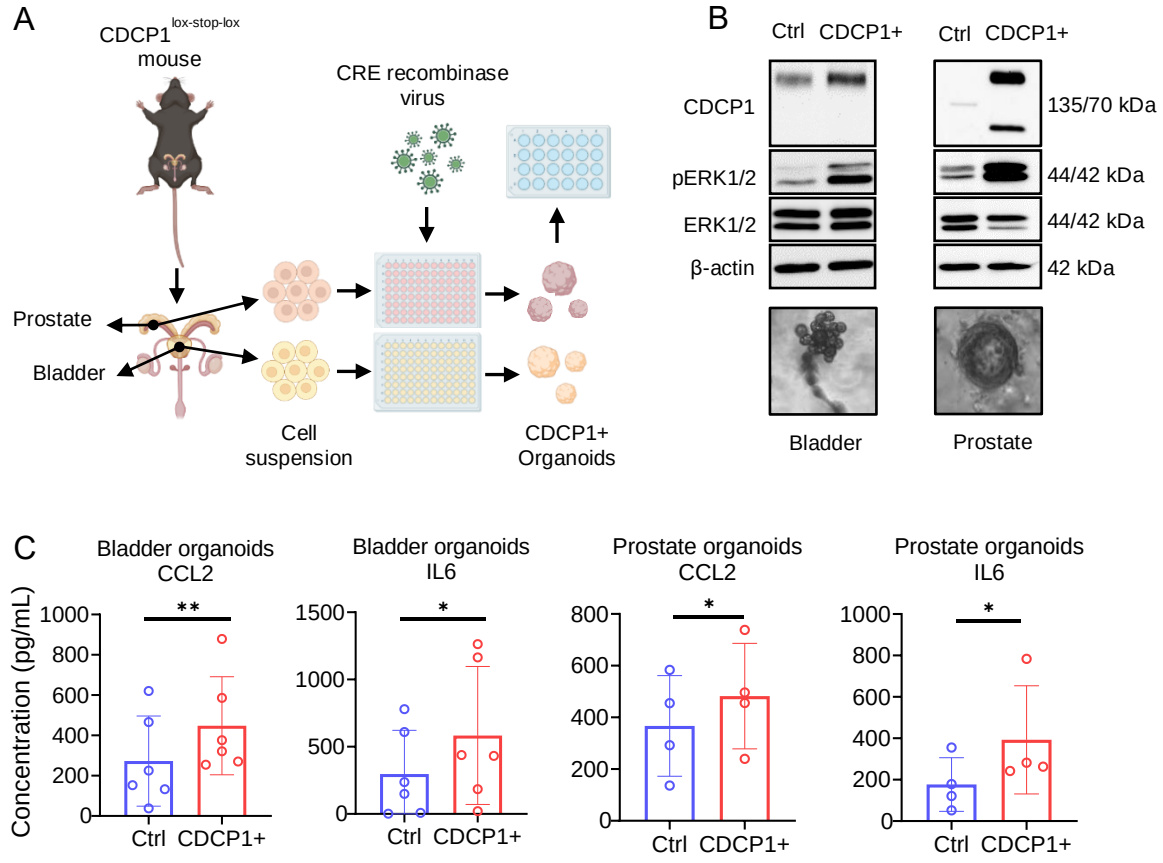

Fig. 23: Cytokine level in murine organoids overexpressing CDCP1
(A) Generation of murine organoid models of CDCP1 overexpression in bladder and prostate. Briefly, bladder and prostate were dissected from CDCP1$^{lox\text{-}stop\text{-}lox}$ mice and dissociated. Bladder and prostate cells were then transduced with CRE recombinase virus and seeded in Matrigel to form organoids. (B) Top: WB for CDCP1, pERK1/2, ERK1/2, β-actin on murine bladder and prostate organoids. Bottom: representative pictures of bladder and prostate organoids. (C) Bar plot of CCL2 and IL6 concentration in bladder and prostate organoids CM after 14 days incubation. Bladder, n=6; prostate, n=4. Error bars indicate SD. *P < 0.05, **P < 0.001. Statistical test: two-tailed unpaired t test.

Next, we analyzed whether macrophages infiltrating CDCP1-expressing tumors present pro-tumoral features. To do that, we first examined the macrophage phenotype induced by exposure to the media from CDCP1 KO and WT MIBC cell lines. Results show that the media collected from CDCP1-KO cells induces a reduced expression of $CD163^{+}$; and $CD200R^{+}$ in the macrophage population when compared to the media from cells expressing CDCP1 (Fig. 24A). A similar effect is observed when MIBC cell lines are pre-incubated with the anti-CDCP1 Ab (Fig. 24B). Moreover, to test whether this phenotype is also confirmed in a complex organism, we characterized the macrophage population in our mouse model for PCa that overexpress CDCP1 in a $Pten^{-/-}$ background and compared it with controls carrying only the $Pten^{-/-}$ genetic modification. As expected, mice with the $Pten^{-/-}$; $CDCP1^{+}$ genotype showed higher expression of CDCP1 in the epithelial cell population ($EpCAM^{+}$;$CD45^{-}$) when compared to the $Pten^{-/-}$ controls (Fig. 24C). The macrophage population expressing CD206 and CD163 was nearly 10 times bigger in $Pten^{-/-}$;$CDCP1^{+}$ mice compared to $Pten^{-/-}$ (Fig. 24D), confirming that the presence of CDCP1 is correlated with an increased infiltration of pro-tumoral macrophages in the tumor site.

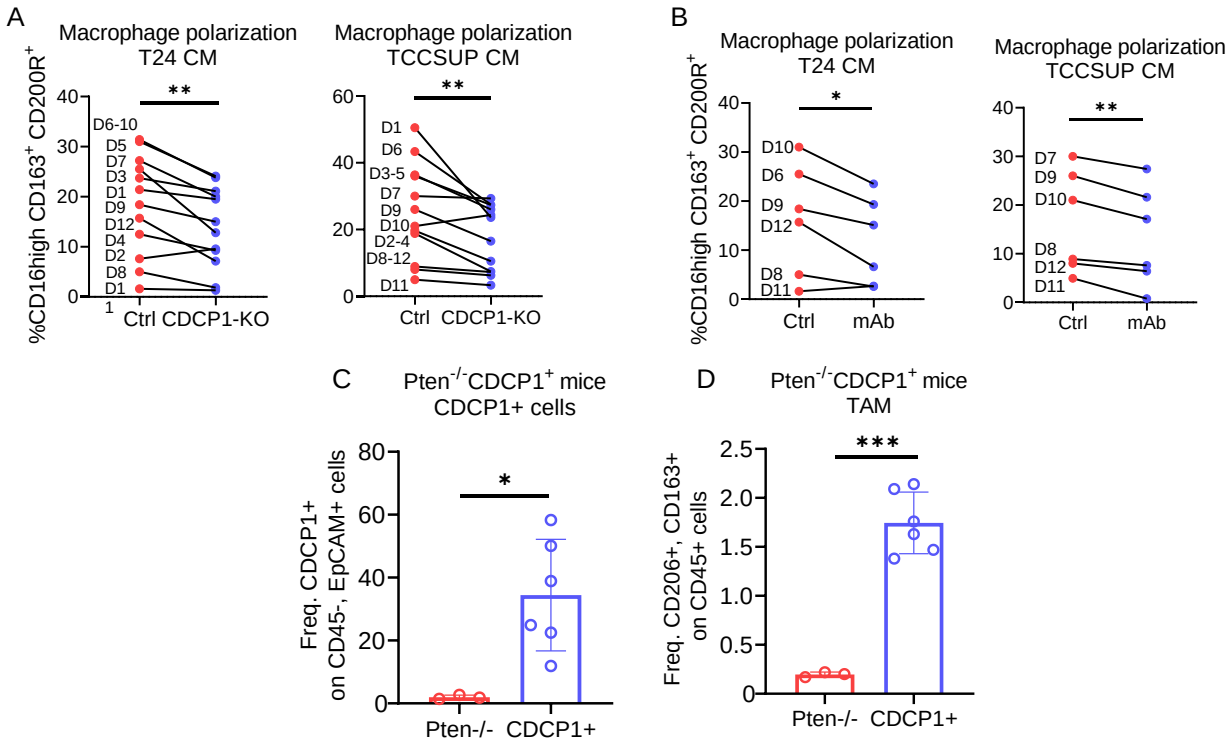

Fig. 24: Macrophage polarization

(A) FACS analysis for the percentage of CD163+, CD200R+ cells on PBMC-derived macrophages exposed to CM from CDCP1-KO and WT MIBC cells. n=12. Error bars indicate SD. **P < 0.001. Statistical test: two-tailed unpaired t test. (B) FACS analysis for the percentage of CD163+, CD200R+ cells on PBMC-derived macrophages exposed to CM from MIBC cells treated with anti-CDCP1 mAb vs. Ctrl. n=6. Error bars indicate SD. **P < 0.001. Statistical test: two-tailed unpaired t test. (C) FACS analysis of the frequency of CD45-, EpCAM+, CDCP1+ cells. Data obtained analyzing the prostate of our transgenic mouse model for CDCP1-overexpressing PCa. n=9. Error bars indicate SD. *P < 0.05. (D) FACS analysis of the frequency of CD45+, CD206+, CD163+ cells. Data obtained analyzing the prostate of our transgenic mouse model for CDCP1-overexpressing PCa. n=9. Error bars indicate SD. ***P < 0.0001.

3.3 Generation of a model for senescence evaluation with CRISPaint technology and identification of new senescence markers

As a first step for the identification of targetable senescence markers, we decided to establish a new *in-vitro* model that allows easy detection of senescent cells. The crucial aspect of this model is that established senescence markers, such as p16, p21 and β-GAL, are fused to mNeon, a green fluorescent protein. Thus, when senescence is triggered, cells carrying the fusion proteins emit an enhanced fluorescence signal caused by the upregulation of senescence markers. Our plan was then to sort low-mNeon cells (non-senescent) and high-mNeon cells (senescent) and compare their transcriptome with mRNA sequencing for the identification of new senescence targets. The concept of the whole project is briefly represented in Fig. 25.

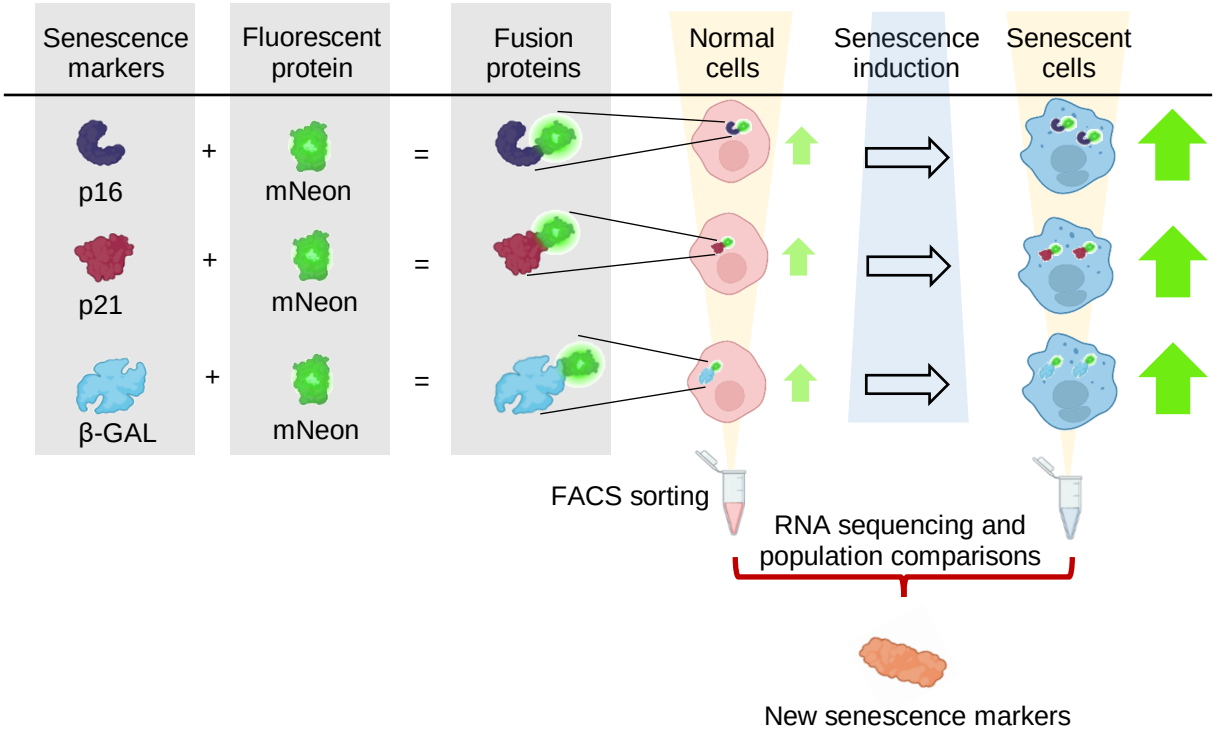

Fig. 25: LNCaP CRISPaint model for senescence detection and marker discovery
Representation of the cell model for detecting senescence. The model was created using CRISPaint technology, which allows the introduction of exogenous DNA in specific genetic locations. In this way, fusion proteins composed by a renowned senescence marker and the fluorescent protein mNeon were generated. The transcription of such fusion proteins depends on the promoter of the specific senescence markers. Thus, fusion proteins mRNA levels correspond to the mRNA level of the endogenous senesce markers. Image created with BioRender.

The fusion proteins were obtained in LNCaP cells via the CRISPaint methodology (Effern et al., 2022; Schmid-Burgk et al., 2016) for three different senescence markers (p16, p21, β-GAL). The three LNCaP clones were named LNCaP-p16-mNeon, LNCaP-p21-mNeon and LNCaP-β-GAL-mNeon, and were analyzed via FACS for mNeon fluorescence intensity before and after senescence induction with docetaxel treatment. Results show that LNCaP clones treated with docetaxel successfully increase their mNeon fluorescence (Fig. 26A). Moreover, we observed that all the clones had the tendency to cluster into three different cell populations with increased mNeon intensity after the treatment, that we named mNeon1+, mNeon2+, mNeon3+ (Fig. 26B). Interestingly, mNeon1+ and mNeon2+ are present in the Ctrl and Doce conditions, while mNeon3+ population only appear after senescence induction with docetaxel.

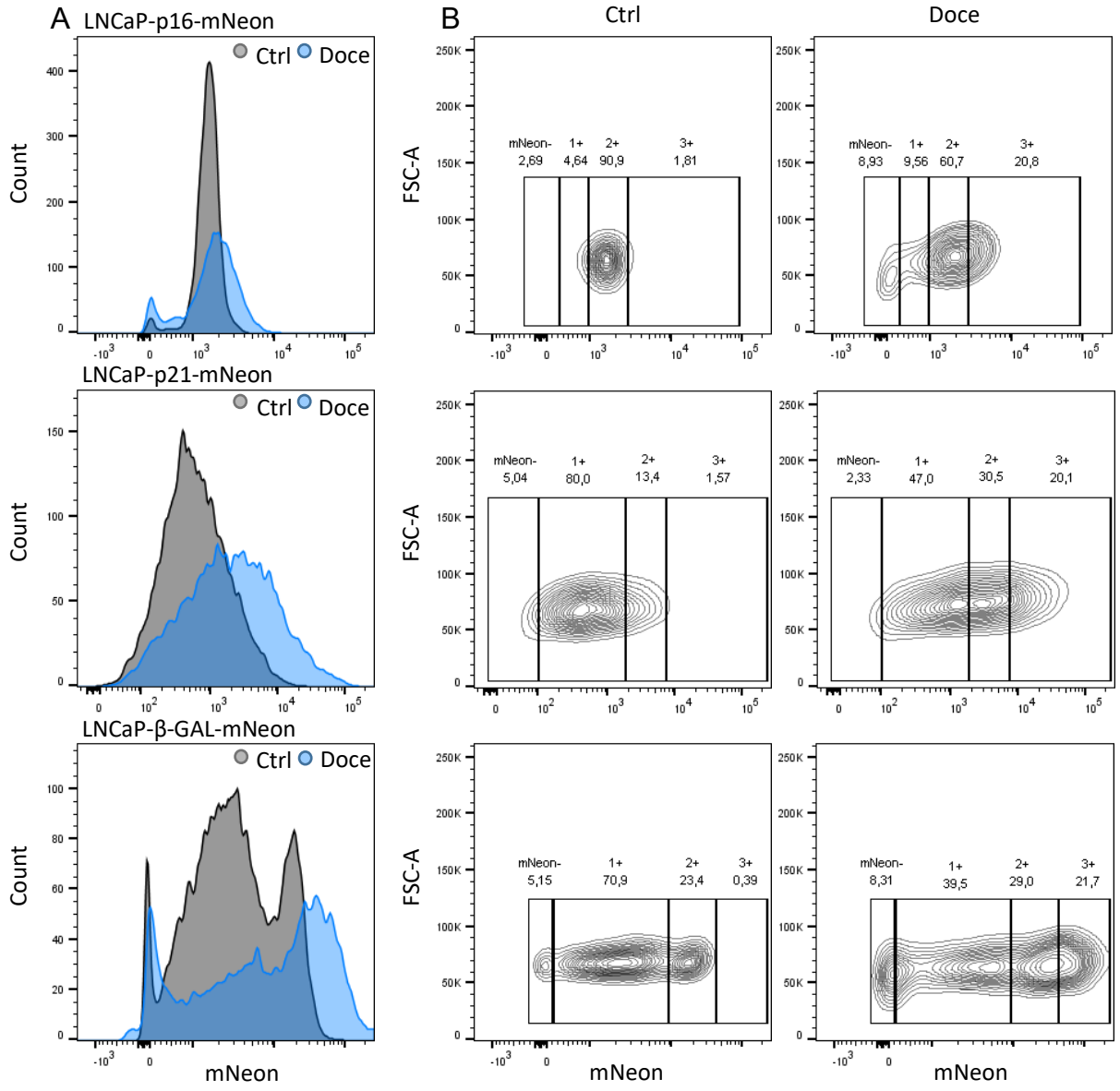

Fig. 26: Senescence induction in LNCaP CRISPaint clones
(A) Flow cytometry histograms indicating mNeon fluorescent intensity in LNCaP-p16-mNeon, LNCaP-p21-mNeon and LNCaP-β-GAL-mNeon after senescence induction. Senescence was induced with docetaxel treatment (0.6 nM) for 6 days. (B) Flow cytometry graphs indicating the three cell populations observed after senescence induction with docetaxel (0.6 nM) for 6 days. mNeon- are cells negative for mNeon, excluded from further analysis because they include cells that failed the DNA insertion with CRISPaint. 1+, 2+, 3+ are the mNeon1+, mNeon2+ and mNeon3+ populations.

To study the transcriptomic differences between the three cell populations (mNeon1+, mNeon2+, mNeon3+), we FACS-sorted them starting from each of the 3 LNCaP clones (LNCaP-p16-mNeon, LNCaP-p21-mNeon, LNCaP-β-GAL-mNeon) and performed mRNA sequencing. The plot in Fig. 27A shows that the three cell populations have a similar gene expression in all the 3 clones. Moreover, we identified a cluster of genes that are significantly different between mNeon-1+ and mNeon-3+ populations. Particularly, we observed that those genes have a tendency to increase along the mNeon-1+, mNeon-2+ and mNeon-3+ populations (Fig. 27B).

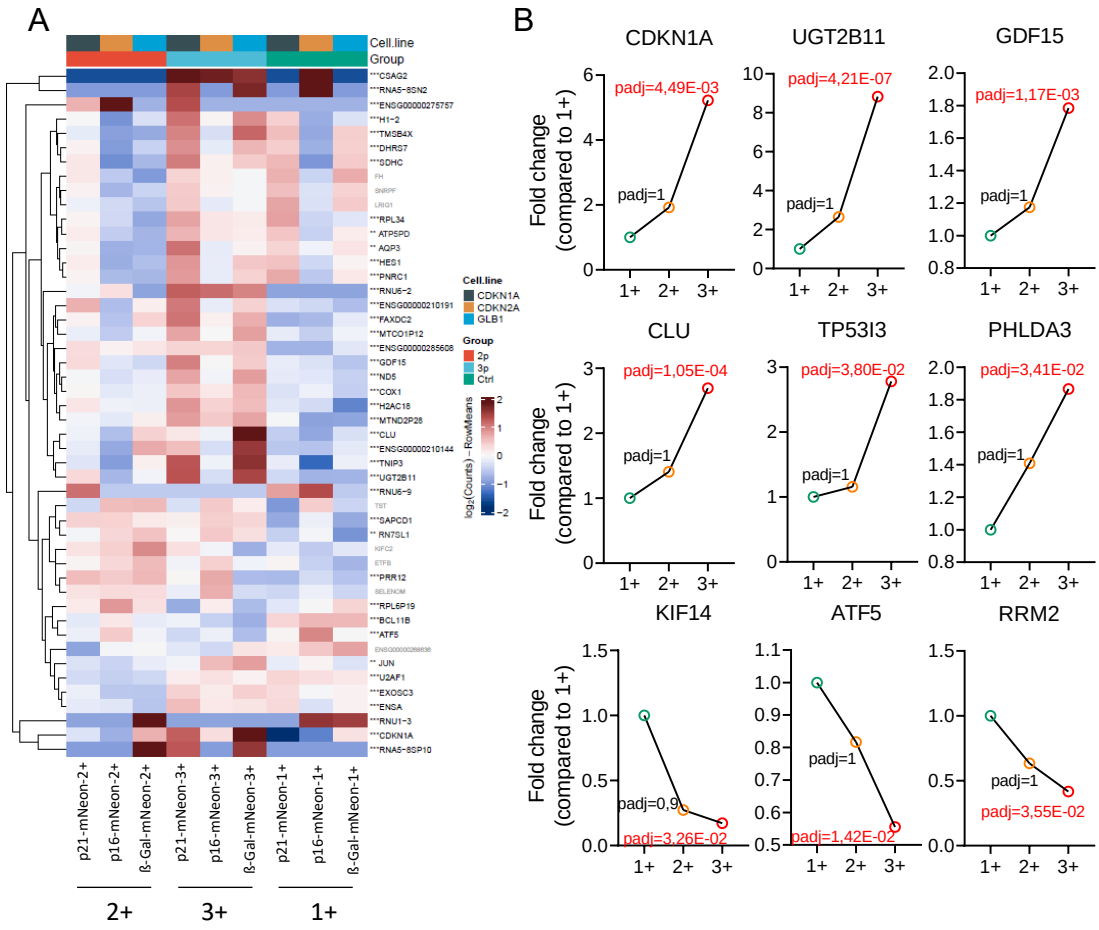

Fig. 27: mRNA sequencing in LNCaP CRISPaint clones
(A) Heat-map of the most differentially expressed genes in the three populations (mNeon1+, mNeon2+, mNeon3+) for the three different clones (LNCaP-p16-mNeon, LNCaP-p21-mNeon, LNCaP-β-GAL-mNeon). (B) Graphs of a selected cluster of genes that have a stark expressional difference when comparing the mNeon1+ and mNeon3+ populations.

We sorted again the different cell populations both from the Ctrl condition and the docetaxel-treated condition (Doce) and analyzed with qPCR the cluster of genes identified with the RNA sequencing (UGT2B11,GDF15, CLU, TP53I3, PHLDA3, KIF14, ATF5, RRM2). The LNCaP-p21-mNeon shows the same pattern observed in the mRNA sequencing. Indeed, all the genes variate gradually along the three cell populations in the treated condition (Fig. 28, Fig. 29). In this clone, UGT2B11 and PHLDA are significantly different also between the 1+ and 2+ populations of the untreated condition (Ctrl). The LNCaP-ß-Gal-mNeon shows a more variable pattern, but always maintains the same tendency observed in the LNCaP-p21-mNeon clone (Fig. 28, Fig. 29). Lastly, the LNCaP-p16-mNeon clone rarely shows any difference between the 1+ and 2+ population in the Doce condition, but still has a distinct 3+ population (Fig. 28, Fig. 29).

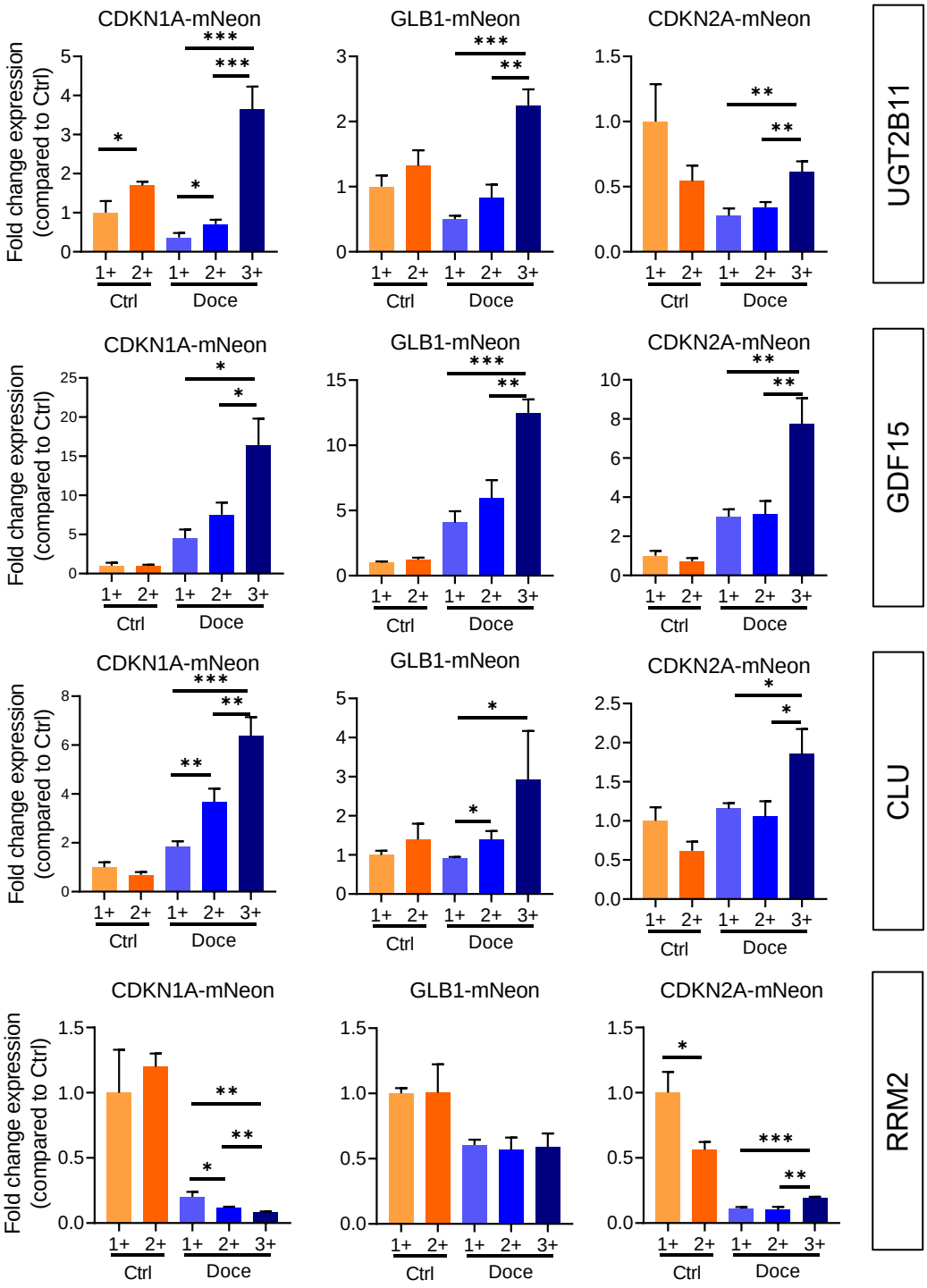

Fig. 28: qPCR analysis of LNCaP CRISPaint clones
qPCR analysis of a selected cluster of genes (UGT2B11, GDF15, CLU, RRM2, TP53I3, KIF14, PHLDA, ATF5) in the different populations sorted from docetaxel treated (0.6 µM, 6 days) and Ctrl LNCaP clones. The figure continues with Fig. 29.

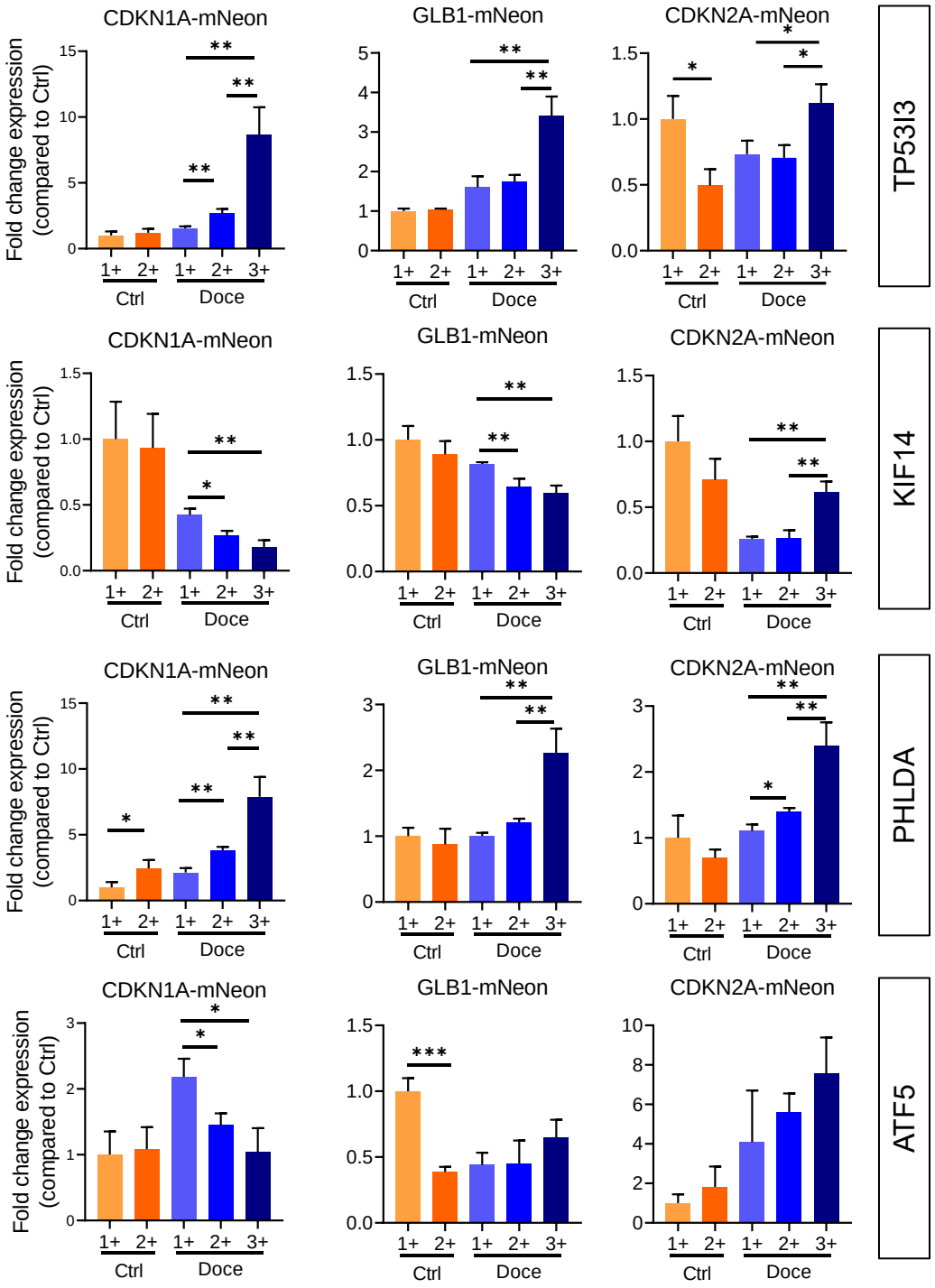

Fig. 29: qPCR analysis of LNCaP CRISPaint clones
qPCR analysis of a selected cluster of genes (UGT2B11, GDF15, CLU, RRM2, TP53I3, KIF14, PHLDA, ATF5) in the different populations sorted from docetaxel treated (0.6 µM, 6 days) and Ctrl LNCaP clones. The first part of this figure is in Fig. 28.

4 Discussion

Tumors that either acquire resistance or are unresponsive to conventional therapies represent a major challenge. Resistant or unresponsive clusters of tumor cells quickly expand, leading to a more aggressive form of the disease, as in the case of CRPC. Typically, CRPC develops from locally advanced or metastatic PCa within 2-3 years from the start of the conventional therapy (Chandrasekar et al., 2015; Wadosky and Koochekpour, 2016), which involves androgen deprivation through orchiectomy or ADT (Tonry et al., 2020). Treating CRPC generally requires chemotherapy, which can prolong survival by about 18 months (Calabrò and Sternberg, 2007). However, resistance to chemotherapy often occurs, requiring further adjustment to the treatment plan. Despite the possibly indefinite treatment adjustments employed to manage advanced PCa, the disease remains barely treatable and is associated with high mortality. Likewise, the long-term survival rates for patients affected by the most advanced stages of MIBC (T3, T4) or metastatic BCa are poor despite the use of current therapies (Abufaraj et al., 2016). The first-line treatment for MIBC is radical cystectomy, sometimes combined with neoadjuvant chemotherapy (Leach, 2023; Lopez-Beltran et al., 2024). While this approach has seemingly good oncological outcomes, many patients still experience recurrence. Therefore, stabilizing their condition after cystectomy with adjuvant chemotherapy seems crucial. At the state of the art, the clinical practice suggests treating bladder-resected patients with cisplatin-based adjuvant therapy, which can give a 6 % survival improvement at 5 years (Lopez-Beltran et al., 2024). However, the relevance of adjuvant treatment with cisplatin is still unclear due to the ambiguity of available clinical data, and the lack of effective therapy for relapse containment after radical cystectomy partly defines the high mortality for MIBC. Cisplatin is also the first-line treatment for metastatic BCa. Nevertheless, nearly all patients with a partial or complete response to treatment ultimately progress and die because of the disease (Lopez-Beltran et al., 2024). In conclusion, advanced and metastatic forms of CRPC and MIBC still lack efficient treatment options. Thus, the scientific community currently dedicates its efforts to finding new targets for therapies that offer improved outcomes compared to the available therapies. In this thesis, we contributed to this effort by analyzing novel therapeutic options

for known markers of advanced urological cancers, such as CDCP1 and EGFR, and by developing a system for identifying novel markers.

Expression of membrane proteins CDCP1 and EGFR frequently correlate with advanced cancer stages, particularly in urological cancers (Alajati et al., 2020; Chaux et al., 2012; Chow et al., 2001, 1997; Kamoun et al., 2020; Saponaro et al., 2023; Sigismund et al., 2018). Their classical downstream pathways involve the activation of different protein kinases that play an essential role in cancer cell growth and survival, such as AKTs, MAPKs, and STATs (Khan et al., 2021; Levantini et al., 2022; Sigismund et al., 2018; Yarden and Sliwkowski, 2001). Due to their pro-tumorigenic role and their transmembrane localization, which makes them easily accessible to targeted therapies, they stand out as good targets for developing novel anti-cancer therapies. Of note, CDCP1 and EGFR are already established as targets for different therapeutic approaches. Especially, the use of EGFR antibody-based therapies has already been approved in the clinic for treating metastatic non-smal-cell lung cancer, colorectal cancer, squamous-cell carcinoma of the head and neck, and pancreatic cancer (Chong and Jänne, 2013; Ciardiello and Tortora, 2008). Moreover, antibodies targeting CDCP1 have already been produced and tested *in-vitro* showing good responses in pre-clinical models of prostate and breast cancers (Alajati et al., 2020; Kollmorgen et al., 2013; Siva et al., 2008). To improve the potential effects of targeting CDCP1 and EGFR, we decided to generate Nbs against these proteins. Our decision was mainly influenced by evidence showing the several advantages of Nbs over mAbs. In the first place, Nbs are characterized by an impressively smaller size, which facilitates their penetration in solid tumors resulting in higher bioavailability of the drug directly inside the tumor mass (Jin et al., 2023). Moreover, the high water solubility of Nbs grants a short half-life and fast elimination. Therefore, they are excellent for reducing side effects due to “on-target” and/or “off-target” toxicity (Bao et al., 2021). We must also consider that urological tumors, especially BCa and kidney cancer, are in contact with the urine flow. Thus, the high water solubility of Nbs may also be indirectly advantageous for facilitating their migration to the tumor site via urine flow. Considering all these factors, we produced Nbs against CDCP1 and EGFR. After identifying Nbs with high affinity for our targets (Fig. 14, 17), we tested their biological effect on cell lines. Nbs targeting CDCP1 were initially tested on PC3 and SCaBER without showing any effect on CDCP1

expression or cell growth (data not shown). On the other hand, four Nbs targeting EGFR showed strong inhibition of EGFR signaling (Fig. 18A). Since the experiment required the incubation of cells with Nbs for 2 h and consequent stimulation with EGF for 10 min, we concluded that Nbs antagonism to EGF is most probably responsible for the observed effect. As a logical consequence of EGFR signaling deregulation, these four Nbs also successfully inhibited cell growth in a long-term experiment (Fig. 18B). When analyzing the lack of response to anti-CDCP1 Nbs, we must consider that CDCP1 has no identified physiological ligand. Therefore, it is probable that its regulation may require influencing the protein turnover, a much more complex mechanism than simply antagonizing the ligand. Among the classical mechanisms regulating membrane protein expression, endocytosis followed by proteolysis (Tsao et al., 2001) sounds appropriate for inducing the reduction of CDCP1 levels. Importantly, evidence proves that it is possible to trigger the endocytosis-proteolysis process via aggregation of membrane proteins utilizing mAbs (Paul et al., 2023). To study whether CDCP1 downregulation may also benefit from aggregation, endocytosis, and proteolysis, we decided to couple our Nbs with rFc to generate rFc-Nbs, which substantially present the same structure as Hc-Abs. In this format, four Nbs strongly affected CDCP1 levels (Fig. 16A), and two of them (H10 and A06) also reduced cell growth (Fig. 16B). This result suggests that dampening the tumor-promoting effect driven by CDCP1 may require the aggregation and internalization of the protein. Interestingly, based on our results in Fig. 15, all the rFc-Nbs that showed an effect on CDCP1 downregulation and/or cell growth target the same region of CDCP1. Later, since rFc-Nbs do not represent a real improvement compared to mAbs, we planned to generate smaller Nb dimers that could maintain the protein-aggregating property in a reduced format. We linked two Nb monomers with a 963.87 Da amino acidic linker generating four different dimer combinations with the two Nbs that showed cell growth inhibition in the rFc format. Two homodimer-Nbs, H10-H10 and A06-A06, and two biparatopic heterodimer-Nbs, H10-A06 and A06-H10, were generated. Heterodimer-Nbs showed increased CDCP1 downregulation compared to the rFc-Nbs (Fig. 16C). Homodimer-Nbs had comparable efficacy (Fig. 16C). Interestingly, the four dimers further reduced cell growth compared to rFc-Nbs (Fig. 16D). rFc-Nbs and Nb dimers were obtained quite easily via cloning the sequence of our Nbs into specific vectors. Indeed, manipulation of Nbs only requires a fast and easy approach due to their simple structure.

This quality further emphasizes the advantage of a Nb approach over mAbs and allows us to be more flexible and creative with the format design. For instance, we plan to generate bi-specific Nbs targeting CDCP1 and EGFR simultaneously, starting from our positive hits. The conceptualization of this strategy is based on the two proteins sharing common downstream pathways and even dimerizing to activate the MAPK/ERK pathway. Moreover, both CDCP1 and EGFR are upregulated in the Ba/Sq subtype of MIBC (Alajati et al., 2020; Chopra et al., 2023; Kamoun et al., 2020), strongly suggesting a possible interrelation between these two proteins. Altogether, anti-EGFR Nbs and anti-CDCP1 Nb-dimers show promising characteristics for developing innovative Nb-based therapies.

Immune components of the TME represent an additional cause for drug resistance in urological cancers. Specifically, the infiltration of TAMs in MIBC is strongly associated with poorer patient outcomes and increased resistance to adjuvant chemotherapy (Koll et al., 2023). A similar conclusion was also drawn in our previous publication concerning CDCP1 levels. Indeed, we observed a correlation between CDCP1 expression and shorter survival for patients treated with adjuvant chemotherapy (Hooper et al., 2003). Moreover, higher CDCP1 expression was observed in the Ba/Sq subtype of MIBC (Chopra et al., 2023; Saponaro et al., 2023), which is known to be infiltrated by a larger number of immune cells among the MIBC subtypes (Saponaro et al., 2023). Considering the observed liaison between CDCP1, TAMs and drug resistance in MIBC, we speculated that CDCP1 and TAM infiltration might be correlated too. The first insight that our hypothesis may hold biological value emerged about a year after our publication when Brina et al. showed that, in PCa transgenic mouse models, tumors overexpressing CDCP1 have high F4/80 and CD11b expression compared to tumors harboring different backgrounds (Brina et al., 2023). This evidence led us to hypothesize that CDCP1 may play an active role in macrophage recruitment thereby influencing tumor progression. If true, CDCP1 not only promotes tumor growth through its downstream signaling but also by creating an immune-suppressive TME. The first analysis we performed was IHC for macrophage markers CD68 and CD163 on an MIBC TMA and a PCa TMA. Results obtained for both sets of patients showed that CDCP1 expression correlates with CD163 and CD68 expression (Fig. 19A, 19C), validating our hypothesis from the clinical point of view. Strikingly, more than half of patients expressing high levels of CDCP1 have

combined high CD68 and high CD163 expression, while there is a 20 % reduction of CD68high, CD163high tumors in patients with low CDCP1 levels (Fig.19B, 19D). We investigated further the biological mechanism favoring the CDCP1-TAM correlation. It is widely accepted that the most straightforward mechanism explaining macrophage trafficking to target sites is chemotaxis, which is induced by specific cytokines (Hughes and Nibbs, 2018). At the same time, several studies reported the pivotal role of tumor cell-derived cytokines in monocyte/macrophage recruitment (Candido and Hagemann, 2013; Szebeni et al., 2017). Therefore, we investigated whether tumor cells expressing CDCP1 may be directly responsible for TAM recruitment via cytokines production. We generated MIBC cell lines KO for CDCP1 and analyzed their CM to compare the production of inflammatory cytokines with the CDCP1-expressing wild-type cell lines. Our results showed that CDCP1 KO importantly impairs the production of CCL2 and IL6 (Fig. 20B). Notably, CCL2 is the most important chemokine responsible for macrophage chemotaxis (Gazzaniga et al., 2007; Lim et al., 2016; Popivanova et al., 2009). Accordingly, CM collected from CDCP1-KO cell lines reduced macrophage migration when tested on PBMC-derived macrophages (Fig. 20C). We later showed reduction of CCL2/IL6 production and macrophage migration with media collected from the same cell lines upon treatment with an anti-CDCP1 mAb, observing comparable effect to the KO of CDCP1 (Fig. 21). Consistent with previous publications showing that CDCP1 levels correlate with ERK phosphorylation (Alajati et al., 2020; Khan et al., 2021; Saponaro et al., 2023), both CDCP1 KO and the mAb reduced the activation of ERK1/2 (Fig. 20A, 21B). Hence, we tested whether ERK inhibition alone could downregulate the expression of CCL2 and IL6 in MIBC cells, obtaining affirmative results (Fig. 22). Since there is also alternative evidence showing that ERK1/2 can be correlated with cytokines production (Cui et al., 2021; He et al., 2022; Jain et al., 2014; Peter et al., 2020; C. Wang et al., 2022; Yokota et al., 2022), we concluded that CDCP1/ERK axis may be responsible for CCL2 and IL6 production in tumor cells expressing CDCP1. The generation of bladder and prostate murine organoids overexpressing CDCP1 further confirmed our hypothesis. Indeed, when CDCP1 was upregulated, ERK showed increased phosphorylation (Fig. 23B), and the levels of CCL2 and IL6 also rose (Fig. 23C). Despite the gained clarity regarding the mechanism correlating CDCP1 and macrophage recruitment, the exact phenotype of macrophages infiltrating CDCP1-high tumors was still uncertain. The expression of CD163

is generally considered a pro-tumoral macrophage marker, and as previously mentioned we observed increased CD163 in tumors expressing high CDCP1 levels (Fig. 19A, 19C). Moreover, we observed high expression of CCL2 and IL6 in CDCP1-high tumor cells (Fig. 20B). This cytokine combination was previously reported to polarize macrophages towards a pro-tumoral phenotype (Roca et al., 2009). However, we aimed to confirm the macrophage phenotype experimentally. We collected the CM from WT and CDCP1-KO MIBC cells to stimulate PBMC-derived macrophages isolated from twelve different donors. Results show that the CM from WT cells polarize a higher % of macrophages towards a pro-tumoral phenotype compared to the CM from CDCP1-KO cells (Fig. 24A). The same conclusion was drawn when the anti-CDCP1 mAb was used on MIBC cells before collecting the CM (Fig. 24B). Moreover, the analysis of macrophage markers on the PCa isolated from our mouse model for CDCP1 overexpression showed high expression of CD206 and CD163 compared its control (Fig. 24C). CD206 is, along with CD163, one of the most relevant pro-tumoral macrophage markers. Overall, our results demonstrate that CDCP1 actively promotes TAM infiltration in the tumor. This finding proves quite novel since no previous report about an existing liaison between CDCP1 and TAM exists. However, it has been shown that CDCP1 already influences the activity of certain immune cells. Indeed, CDCP1 is listed among the endogenous ligands of CD6 (Aragón-Serrano et al., 2023). CD6 is a transmembrane protein expressed by CD8+ T cells, B cells, and NK cells, and can act as a negative regulator of their function upon ligand binding (Aragón-Serrano et al., 2023). A study conducted by Ruth et al. explored the use of 3a11 (anti-human CDCP1) mAbs in the co-culture of PBMCs and different tumor cell lines expressing CDCP1 (e.g. prostate, breast, lung) (Ruth et al., 2021). The authors observed an enhanced killing of cancer cells by PBMCs (Ruth et al., 2021). Moreover, the blockade of CD6 with anti-CD6 mAb showed a greater effect compared to interrupting the programmed cell death 1 (PD-1)/PD-1 ligand 1 (PD-L1) axis, the most common target of available immunotherapies (Ruth et al., 2021). Based on these evidences and our findings, targeting CDCP1 could integrate effector cells-induced tumor cell killing and a reduction of TAM infiltration, promoting the development of a strong anti-tumor microenvironment. Of note, targeting TAM is already considered a promising approach to antagonize tumor growth and advancement, reduce the development of drug resistance, and improve patient outcomes (Ngambenjawong et al., 2017; Tang et al., 2013). The

future perspective that we specifically envision for our research involves targeting CDCP1-associated TAM infiltration with the Nb-dimers against CDCP1 that we developed and characterized (Fig. 16). We would then suggest their application for the enhancement of immunotherapies in advanced PCa and the Ba/Sq subtype of BCa.

The next mechanism that can promote drug resistance and progression in tumors is senescence. As previously mentioned, senescent cells produce SASP, a bustling source of cytokines and growth factors, supporting the growth and survival of post-chemotherapy residual tumor cells (Angelini et al., 2013; Bhatia et al., 2008; Di et al., 2014; Gonzalez-Meljem et al., 2018; Ruhland et al., 2016; Zacarias-Fluck et al., 2015). Eliminating senescent cells was suggested as a possible solution to this problem (Gonzalez-Meljem et al., 2018; Ohtani, 2022; Prasanna et al., 2021). However, accomplishing this effectively is still complicated due to the ubiquity of senescence markers. Thus, we initially aimed to find new targets that could be useful for developing more specific senolytic therapies. To do so, we focused on developing a good model for identifying docetaxel-induced senescence *in-vitro*. Our model consists of three distinct transgenic LNCaP cell clones generated using the CRISPaint technology. Each clone expresses a different fusion protein that combines a renowned senescence marker with the green fluorescent protein mNeon and is regulated by the endogenous promoters of the specific senescence marker. The three chosen senescence markers were p16, p21, and β-GAL, and the resulting cell clones were unequivocally named LNCaP-p16-mNeon, LNCaP-p21-mNeon, and LNCaP-β-GAL-mNeon. These clones expressed increased levels of senescence markers upon senescence induction with docetaxel (data not shown). Consequently, we detected increased intensity of mNeon when analyzing them via FACS (Fig. 26A). After generating an appropriate model for senescence detection, our original aim was to analyze the transcriptome of low mNeon-expressing cells and high mNeon-expressing cells, expecting that the scenario would be dichotomized between non-senescent cells and senescent cells. However, following senescence induction, the scenario was quite different. Indeed, docetaxel treatment on our cell model induced the presence of three different cell populations, which we named mNeon1+, mNeon2+, and mNeon3+. This indicated that the situation is slightly more convoluted than anticipated and supported the notion of a heterogeneous senescent population, a concept also suggested by earlier studies (Cohn

et al., 2023). Therefore, we decided to separate the three different populations with FACS sorting for each LNCaP clone and analyze them with mRNA sequencing. Results showed that gene levels in mNeon1+ and mNeon2+ are similar, although not completely identical (Fig. 27A). mNeon3+ exhibited the most significant differences from the other two populations (Fig. 27A). This was unsurprising since the mNeon3+ population is the only one present exclusively after docetaxel treatment (Fig. 26B). In contrast, mNeon1+ and mNeon2+ are also present in the untreated condition (Fig. 26B). The major observation we made in our results is that the cluster of genes that are differentially expressed between mNeon1+ and mNeon3+ are also progressively upregulated/downregulated across the three populations (Fig. 27B). Basing on this particular behavior we developed two different hypotheses. The first hypothesis describes the three populations as three different senescence stages, where mNeon1+ is the non-senescent (normal cells), mNeon3+ is the senescent, and mNeon2+ is an intermediate stage. In the second hypothesis, mNeon1+ persists as the non-senescent population, while mNeon2+ and mNeon3+ are two different types of senescence. Specifically, mNeon3+ corresponds to the chemotherapy-induced senescent population and mNeon2+ to the naturally occurring senescent population. It has been demonstrated that a certain degree of senescence develops spontaneously in *in-vitro* and *in-vivo* systems. Thus, the concept that senescence develops in cancer exclusively upon chemotherapy or radiotherapy is nowadays obsolete. (Mikuła-Pietrasik et al., 2020). *In-vitro*, tumor cells can undergo senescence when subjected to inadequate culture conditions, or following the accumulation of mutations or the activation of oncogenes (Mikuła-Pietrasik et al., 2020). Besides, the study from Poele et al. provides a clear example of non-chemotherapy-related senescence directly in human tumors (te Poele et al., 2002). Here they analyzed untreated breast cancer samples for SA-ß-Gal expression and concluded that 10 % of the cells exhibited a senescent pattern. Altogether, these considerations suggest that a deeper examination of senescent cell heterogeneity is essential to differentiate between peculiar senescence stages or populations before attempting the identification of senescence markers by simply analyzing their transcriptome or proteome. Thus, our next plan is to dissect the heterogeneity of senescent cells after docetaxel treatment via single-cell sequencing. Confirming that senescent cells present different stages/populations after treatment may be crucial for developing a more thoughtful senolytic strategy. Indeed, the

presence of a heterogeneous population after senescence induction may imply that the “one-two-punch” strategy needs deep rearrangements. Specifically, senolytic therapies that target senescence universally may require replacement with senolytic therapies that target specific senescent populations that are relevant for tumor management. An additional aspect that we will analyze with single-cell sequencing is whether the post-chemotherapy senescent population, in our system identified as mNeon3+, develops starting from a time-0 specific cluster of cells that is, for example, more susceptible to chemotherapy or characterized by a higher “commitment” to senescence rather than apoptosis. Therefore, we will not exclusively address heterogeneity after docetaxel treatment but also disclose the specific cell cluster that converts into senescent cells upon chemotherapy in the tumor cell miscellany. We will try to map the dynamics of senescent cell subpopulations throughout senescence development and the specific variations occurring in their transcriptome during time. Ultimately, we aim to identify targets for eliminating senescent-to-be cells before administrating any cytotoxic agent, thus avoiding the emergence of senescence *a priori*. This approach would subvert the therapeutic strategy previously suggested for senescent cell clearance, which is commonly subsequent to chemotherapy.

Altogether, this study offers several suggestions for developing new therapies against urothelial cancers that are unresponsive to traditional treatments. The Nb-based strategy presented in this work showed promising results for targeting CDCP1 in locally advanced PCa. Besides, results observed upon testing anti-EGFR Nbs *in-vitro* suggest their application in the Ba/Sq subtype of MIBC. These preliminary statements require further investigation in *in-vivo* systems, such as chorioallantoic membrane (CAM) assay or murine models. Additionally, the investigation of TME in CDCP1 tumors revealed that targeting CDCP1 may be indicated as a TAM-targeting strategy. Indeed, this protein seems responsible for TAM infiltration in MIBC and PCa tumors, and its depletion reduces macrophage recruitment and pro-tumoral phenotype. In the future, this treatment option will be evaluated in preclinical models too. Lastly, generating a PCa model for senescence visualization upon chemotherapy induction revealed that the senescence population in cancer cells is heterogeneous. This observation suggested that a deeper characterization of the senescent cell populations post-chemotherapy is essential for finding new

senescence markers and improving the senolytic therapy. In a future scenario, the joint effort between the clinic and research could allow the identification of high-CDCP1/high-EGFR tumors or tumors with a high propensity for developing senescence. Such tumors could then be treated accordingly. Indeed, targeting CDCP1, EGFR, and/or senescence could be integrated in precision medicine, following the development of novel therapies that can replace the high-range traditional therapies on the basis of our findings and similar other studies.

5 Abstract

Urological cancers are among the cancers with the highest incidence. In recent years, several therapeutic solutions have been suggested and accepted in the clinic for treatment, but tumors, especially the most aggressive forms, frequently develop resistance to the available therapies. Thus, we focused on investigating novel solutions for treating the most aggressive forms of urological cancers. Specifically, we aimed to:

1) Investigate the application of nanobodies (Nbs) as targeting agents for CUB domain-containing protein 1 (CDCP1) in prostate cancer (PCa) and epithelial growth factor receptor (EGFR) in the basal/squamous (Ba/Sq) subtype of bladder cancer (BCa).
2) Study the correlation of CDCP1 with tumor-associated macrophage (TAM) infiltration in PCa and BCa.
3) Characterize senescence for the discovery of new senescence markers in advanced PCa.

CDCP1 is a transmembrane protein that correlates with tumor stage in several cancers. In our experience, CDCP1 is a promising target for treating advanced PCa. Thus, we tested Nbs as an innovative strategy for its targeting. Nbs are the smallest existing region of an antibody (Ab) that maintains the binding to their target and have several advantages compared to Abs. They are 10 times smaller, making them ideal for treating solid tumors since they can diffuse better in the tumor mass. Moreover, they are characterized by cheaper and easier production and higher stability. We also considered the application of Nbs for targeting EGFR, a transmembrane receptor known for sustaining tumor growth. Drugs targeting EGFR are already used in lung and head and neck cancers. In this work, we investigated EGFR targeting in the Ba/Sq subtype of BCa. This subtype is characterized by high levels of EGFR and greater aggressiveness. Both targeting CDCP1 and EGFR with Nbs in these cancers revealed promising results. Indeed, Nb dimers targeting CDCP1 reduced tumor growth in a PCa cell model, and Nbs targeting EGFR reduced cell growth in a Ba/Sq BCa cell model.

In the second part of this work, we studied the correlation of CDCP1 with TAM infiltration. CDCP1 correlates with the Ba/Sq subtype of BCa which is typically infiltrated by immune

cells. Our results showed that CDCP1-expressing tumor cells produce high levels of CCL2 and IL6, contributing to macrophage recruitment. Macrophages infiltrating CDCP1 tumors in our PCa mouse model overexpressing CDCP1 have the typical characteristics of tumor-associated macrophages (TAMs), which are reported to create an environment that promotes tumor growth and reduces immune responses. Thus, their elimination from the tumor microenvironment (TME) proves essential to dampen tumor aggressiveness and improve tumor responsiveness to immune therapy. Treatment with mAbs targeting CDCP1 efficiently reduced CCL2 and IL6 production and the migration potential of macrophages.

In the final part of this work, we aimed to discover new senescence markers to combine chemotherapy, such as docetaxel, with more efficient senolytic drugs. This proves fundamental since senescent cells could cause tumor relapse or aggravate tumor growth due to the production of growth factors and cytokines. However, targeting senescent cells is challenging due to their similarities with normal cells. To find a suitable marker for senescent cell elimination, we first developed a new model for senescence individuation using the CRISPaint technology. This technology allowed for the visualization of senescent cells in real-time and suggested that the situation after treatment with docetaxel in PCa is more complicated than expected. Indeed, we did not observe the formation of a senescent population but the presence of 3 different populations. We separated these populations and performed mRNA sequencing to identify specific population markers. We obtained a set of 8 genes that are progressively up- or down-regulated along the 3 populations, suggesting that different levels of senescence characterize these populations. To investigate this further, we plan to perform single-cell sequencing.

Altogether, the results presented in this thesis suggest some solutions for treating aggressive BCa or PCa. In particular, using Nbs to target CDCP1 or EGFR and targeting CDCP1 to reduce TAM infiltration. Finally, this thesis reveals the complexity of the senescent phenotype that requires a deeper investigation and an improved definition before being targeted efficiently.

6 List of figures

Fig. 1: Urological cancer incidence and mortality 12
Fig. 2: Clinical progression and treatment of PCa 15
Fig. 3: Clinical progression and treatment of BCa 17
Fig. 4: MIBC molecular subtypes 18
Fig. 5: Illustration of CDCP1 structure and downstream pathway. 20
Fig. 6: CDCP1 overexpression in CDCP1^{+}; Pten$^{-/-}$ transgenic mouse model 22
Fig. 7: EGFR 24
Fig. 8: Macrophage phenotypes 27
Fig. 9: Cell cycle and senescence 30
Fig. 10: Senescent cell characteristics 31
Fig. 11: mAb, HcAb, and Nb structure 33
Fig. 12: TAM-targeting therapies 36
Fig. 13: One-two punch strategy 37
Fig. 14: FACS analysis of different Nbs targeting CDCP1 57
Fig. 15: Study of the binding of anti-CDCP1 Nbs to different species and epitopes 58
Fig. 16: Biological effect of anti-CDCP1 Nbs 60
Fig. 17: FACS analysis of different Nbs targeting EGFR 61
Fig. 18: Biological effect of anti-EGFR Nbs 62
Fig. 19: Expression of CDCP1, CD68, and CD163 in MIBC and PCa TMAs 63
Fig. 20: KO of CDCP1 reduces cytokine expression 64
Fig. 21: Cytokine level upon treatment with mAb targeting CDCP1 66
Fig. 22: Cytokine expression upon ERK inhibition 67
Fig. 23: Cytokine level in murine organoids overexpressing CDCP1 68
Fig. 24: Macrophage polarization 70
Fig. 25: LNCaP CRISPaint model for senescence detection and marker discovery 71
Fig. 26: Senescence induction in LNCaP CRISPaint clones 73
Fig. 27: mRNA sequencing in LNCaP CRISPaint clones 74
Fig. 28: qPCR analysis of LNCaP CRISPaint clones 76
Fig. 29: qPCR analysis of LNCaP CRISPaint clones 77

7 List of tables

Table 1: Solutions 40
Table 2: Cell line, primary cell and organoid media..... 42

8 References

Abufaraj, M., Gust, K., Moschini, M., Foerster, B., Soria, F., Mathieu, R., Shariat, S.F., 2016. Management of muscle invasive, locally advanced and metastatic urothelial carcinoma of the bladder: a literature review with emphasis on the role of surgery. Translational Andrology and Urology 5, 73544–73744. https://doi.org/10.21037/tau.2016.08.23

Achard, V., Putora, P.M., Omlin, A., Zilli, T., Fischer, S., 2021. Metastatic Prostate Cancer: Treatment Options. Oncology 100, 48–59. https://doi.org/10.1159/000519861

Alajati, A., D'Ambrosio, M., Troiani, M., Mosole, S., Pellegrini, L., Chen, J., Revandkar, A., Bolis, M., Theurillat, J.-P., Guccini, I., Losa, M., Calcinotto, A., Bernardis, G.D., Pasquini, E., D'Antuono, R., Sharp, A., Figueiredo, I., Rodrigues, D.N., Welti, J., Gil, V., Yuan, W., Vlajnic, T., Bubendorf, L., Chiorino, G., Gnetti, L., Torrano, V., Carracedo, A., Camplese, L., Hirabayashi, S., Canato, E., Pasut, G., Montopoli, M., Rüschoff, J.H., Wild, P., Moch, H., Bono, J.D., Alimonti, A., 2020. CDCP1 overexpression drives prostate cancer progression and can be targeted in vivo. J Clin Invest 130, 2435–2450. https://doi.org/10.1172/JCI131133

Alajati, A., Guccini, I., Pinton, S., Garcia-Escudero, R., Bernasocchi, T., Sarti, M., Montani, E., Rinaldi, A., Montemurro, F., Catapano, C., Bertoni, F., Alimonti, A., 2015. Interaction of CDCP1 with HER2 Enhances HER2-Driven Tumorigenesis and Promotes Trastuzumab Resistance in Breast Cancer. Cell Reports 11, 564–576. https://doi.org/10.1016/j.celrep.2015.03.044

Angelini, P.D., Fluck, M.F.Z., Pedersen, K., Parra-Palau, J.L., Guiu, M., Bernadó Morales, C., Vicario, R., Luque-García, A., Navalpotro, N.P., Giralt, J., Canals, F., Gomis, R.R., Tabernero, J., Baselga, J., Villanueva, J., Arribas, J., 2013. Constitutive HER2 Signaling Promotes Breast Cancer Metastasis through Cellular Senescence. Cancer Research 73, 450–458. https://doi.org/10.1158/0008-5472.CAN-12-2301

Aragón-Serrano, L., Carrillo-Serradell, L., Planells-Romeo, V., Isamat, M., Velasco-de Andrés, M., Lozano, F., 2023. CD6 and Its Interacting Partners: Newcomers to the Block of Cancer Immunotherapies. Int J Mol Sci 24, 17510. https://doi.org/10.3390/ijms242417510

Bankhead, P., Loughrey, M.B., Fernández, J.A., Dombrowski, Y., McArt, D.G., Dunne, P.D., McQuaid, S., Gray, R.T., Murray, L.J., Coleman, H.G., James, J.A., Salto-Tellez, M., Hamilton, P.W., 2017. QuPath: Open source software for digital pathology image analysis. Sci Rep 7, 16878. https://doi.org/10.1038/s41598-017-17204-5

Bao, G., Tang, M., Zhao, J., Zhu, X., 2021. Nanobody: a promising toolkit for molecular imaging and disease therapy. EJNMMI Research 11, 6. https://doi.org/10.1186/s13550-021-00750-5

Barber, N., Ali, A. (Eds.), 2022. Urologic Cancers. Exon Publications, Brisbane (AU).

Bean, J., Brennan, C., Shih, J.-Y., Riely, G., Viale, A., Wang, L., Chitale, D., Motoi, N., Szoke, J., Broderick, S., Balak, M., Chang, W.-C., Yu, C.-J., Gazdar, A., Pass, H., Rusch, V., Gerald, W., Huang, S.-F., Yang, P.-C., Miller, V., Ladanyi, M., Yang, C.-H., Pao, W., 2007. MET amplification occurs with or without T790M mutations in EGFR mutant lung tumors with acquired resistance to gefitinib or erlotinib. Proceedings of the National Academy of Sciences 104, 20932–20937. https://doi.org/10.1073/pnas.0710370104

Benes, C.H., Wu, N., Elia, A.E.H., Dharia, T., Cantley, L.C., Soltoff, S.P., 2005. The C2 domain of PKCdelta is a phosphotyrosine binding domain. Cell 121, 271–280. https://doi.org/10.1016/j.cell.2005.02.019

Bhatia, B., Multani, A.S., Patrawala, L., Chen, X., Calhoun-Davis, T., Zhou, J., Schroeder, L., Schneider-Broussard, R., Shen, J., Pathak, S., Chang, S., Tang, D.G., 2008. Evidence that senescent human prostate epithelial cells enhance tumorigenicity: Cell fusion as a potential mechanism and inhibition by p16INK4a and hTERT. International Journal of Cancer 122, 1483–1495. https://doi.org/10.1002/ijc.23222

Black, A.J., Black, P.C., 2020. Variant histology in bladder cancer: diagnostic and clinical implications. Transl Cancer Res 9, 6565–6575. https://doi.org/10.21037/tcr-20-2169

Blobel, C.P., 2005. ADAMs: key components in EGFR signalling and development. Nat Rev Mol Cell Biol 6, 32–43. https://doi.org/10.1038/nrm1548

Bray, F., Laversanne, M., Sung, H., Ferlay, J., Siegel, R.L., Soerjomataram, I., Jemal, A., 2024. Global cancer statistics 2022: GLOBOCAN estimates of incidence and

mortality worldwide for 36 cancers in 185 countries. CA: A Cancer Journal for Clinicians 74, 229–263. https://doi.org/10.3322/caac.21834

Brina, D., Ponzoni, A., Troiani, M., Calì, B., Pasquini, E., Attanasio, G., Mosole, S., Mirenda, M., D'Ambrosio, M., Colucci, M., Guccini, I., Revandkar, A., Alajati, A., Tebaldi, T., Donzel, D., Lauria, F., Parhizgari, N., Valdata, A., Maddalena, M., Calcinotto, A., Bolis, M., Rinaldi, A., Barry, S., Rüschoff, J.H., Sabbadin, M., Sumanasuriya, S., Crespo, M., Sharp, A., Yuan, W., Grinu, M., Boyle, A., Miller, C., Trotman, L., Delaleu, N., Fassan, M., Moch, H., Viero, G., de Bono, J., Alimonti, A., 2023. The Akt/mTOR and MNK/eIF4E pathways rewire the prostate cancer translatome to secrete HGF, SPP1 and BGN and recruit suppressive myeloid cells. Nat Cancer 4, 1102–1121. https://doi.org/10.1038/s43018-023-00594-z

Byles, V., Covarrubias, A.J., Ben-Sahra, I., Lamming, D.W., Sabatini, D.M., Manning, B.D., Horng, T., 2013. The TSC-mTOR pathway regulates macrophage polarization. Nat Commun 4, 2834. https://doi.org/10.1038/ncomms3834

Calabrò, F., Sternberg, C.N., 2007. Current indications for chemotherapy in prostate cancer patients. Eur Urol 51, 17–26. https://doi.org/10.1016/j.eururo.2006.08.013

Calcinotto, A., Kohli, J., Zagato, E., Pellegrini, L., Demaria, M., Alimonti, A., 2019. Cellular Senescence: Aging, Cancer, and Injury. Physiological Reviews 99, 1047–1078. https://doi.org/10.1152/physrev.00020.2018

Candido, J., Hagemann, T., 2013. Cancer-related inflammation. J Clin Immunol 33 Suppl 1, S79-84. https://doi.org/10.1007/s10875-012-9847-0

Chandrasekar, T., Yang, J.C., Gao, A.C., Evans, C.P., 2015. Mechanisms of resistance in castration-resistant prostate cancer (CRPC). Transl Androl Urol 4, 365–380. https://doi.org/10.3978/j.issn.2223-4683.2015.05.02

Chang, J., Wang, Y., Shao, L., Laberge, R.-M., Demaria, M., Campisi, J., Janakiraman, K., Sharpless, N.E., Ding, S., Feng, W., Luo, Y., Wang, X., Aykin-Burns, N., Krager, K., Ponnappan, U., Hauer-Jensen, M., Meng, A., Zhou, D., 2016. Clearance of senescent cells by ABT263 rejuvenates aged hematopoietic stem cells in mice. Nat Med 22, 78–83. https://doi.org/10.1038/nm.4010

Chang, J.-W., Liu, S.-C., Lin, Y.-Y., He, X.-Y., Wu, Y.-S., Su, C.-M., Tsai, C.-H., Chen, H.-T., Fong, Y.-C., Hu, S.-L., Huang, C.-C., Tang, C.-H., 2023. Nesfatin-1 Stimulates CCL2-dependent Monocyte Migration And M1 Macrophage Polarization:

Implications For Rheumatoid Arthritis Therapy. International Journal of Biological Sciences 19, 281–293. https://doi.org/10.7150/ijbs.77987

Chaux, A., Cohen, J.S., Schultz, L., Albadine, R., Jadallah, S., Murphy, K.M., Sharma, R., Schoenberg, M.P., Netto, G.J., 2012. High epidermal growth factor receptor immunohistochemical expression in urothelial carcinoma of the bladder is not associated with *EGFR* mutations in exons 19 and 21: a study using formalin-fixed, paraffin-embedded archival tissues. Human Pathology 43, 1590–1595. https://doi.org/10.1016/j.humpath.2011.11.016

Chen, C.-Y., Fuh, L.-J., Huang, C.-C., Hsu, C.-J., Su, C.-M., Liu, S.-C., Lin, Y.-M., Tang, C.-H., 2017. Enhancement of CCL2 expression and monocyte migration by CCN1 in osteoblasts through inhibiting miR-518a-5p: implication of rheumatoid arthritis therapy. Sci Rep 7, 421. https://doi.org/10.1038/s41598-017-00513-0

Chen, W., Ma, T., Shen, X., Xia, X., Xu, G., Bai, X., Liang, T., 2012. Macrophage-Induced Tumor Angiogenesis Is Regulated by the TSC2–mTOR Pathway. Cancer Research 72, 1363–1372. https://doi.org/10.1158/0008-5472.CAN-11-2684

Chen, Y., Harrington, B.S., Lau, K.C.N., Burke, L.J., He, Y., Iconomou, M., Palmer, J.S., Meade, B., Lumley, J.W., Hooper, J.D., 2017. Development of an enzyme-linked immunosorbent assay for detection of CDCP1 shed from the cell surface and present in colorectal cancer serum specimens. Journal of Pharmaceutical and Biomedical Analysis 139, 65–72. https://doi.org/10.1016/j.jpba.2017.02.047

Chong, C.R., Jänne, P.A., 2013. The quest to overcome resistance to EGFR-targeted therapies in cancer. Nat Med 19, 1389–1400. https://doi.org/10.1038/nm.3388

Chopra, S., Trepka, K., Sakhamuri, S., Carretero-González, A., Zhu, J., Egusa, E., Zhou, J., Leung, K., Zhao, N., Hooshdaran, N., Feng, F.Y., Wells, J.A., Chou, J., Evans, M.J., 2023. Theranostic Targeting of CUB Domain-Containing Protein 1 (CDCP1) in Multiple Subtypes of Bladder Cancer. Clin Cancer Res 29, 1232–1242. https://doi.org/10.1158/1078-0432.CCR-22-1973

Chow, N.-H., Chan, S.-H., Tzai, T.-S., Ho, C.-L., Liu, H.-S., 2001. Expression Profiles of ErbB Family Receptors and Prognosis in Primary Transitional Cell Carcinoma of the Urinary Bladder1. Clinical Cancer Research 7, 1957–1962.

Chow, N.-H., Liu, H.-S., Yang, H.-B., Chan, S.-H., Su, I.-J., 1997. Expression patterns of erbB receptor family in normal urothelium and transitional cell carcinoma. Virchows Archiv 430, 461–466. https://doi.org/10.1007/s004280050056

Ciardiello, F., Tortora, G., 2008. EGFR Antagonists in Cancer Treatment. New England Journal of Medicine 358, 1160–1174. https://doi.org/10.1056/NEJMra0707704

Cohn, R.L., Gasek, N.S., Kuchel, G.A., Xu, M., 2023. The heterogeneity of cellular senescence: insights at the single-cell level. Trends in Cell Biology 33, 9–17. https://doi.org/10.1016/j.tcb.2022.04.011

Cui, Haitao, Du, X., Liu, C., Chen, S., Cui, Haowen, Liu, H., Wang, J., Zheng, Z., 2021. Visfatin promotes intervertebral disc degeneration by inducing IL-6 expression through the ERK/JNK/p38 signalling pathways. Adipocyte 10, 201–215. https://doi.org/10.1080/21623945.2021.1910155

Dan Sun, R., Buttitta, L., 2017. States of G0 and the proliferation-quiescence decision in cells, tissues and during development. The International Journal of Developmental Biology 61, 357–366. https://doi.org/10.1387/ijdb.160343LB

Di, G., Liu, Y., Lu, Y., Liu, J., Wu, C., Duan, H.-F., 2014. IL-6 Secreted from Senescent Mesenchymal Stem Cells Promotes Proliferation and Migration of Breast Cancer Cells. PLOS ONE 9, e113572. https://doi.org/10.1371/journal.pone.0113572

Duggan, S., 2018. Caplacizumab: First Global Approval. Drugs 78, 1639–1642. https://doi.org/10.1007/s40265-018-0989-0

Effern, M., Glodde, N., Bawden, E., Liebing, J., Hinze, D., Tüting, T., Gebhardt, T., Hölzel, M., 2022. CRISPitope: A generic platform to model target antigens for adoptive T cell transfer therapy in mouse tumor models. STAR Protoc 3, 101038. https://doi.org/10.1016/j.xpro.2021.101038

Farhood, B., Najafi, M., Mortezaee, K., 2019. CD8+ cytotoxic T lymphocytes in cancer immunotherapy: A review. J Cell Physiol 234, 8509–8521. https://doi.org/10.1002/jcp.27782

Ferguson, K.M., 2008. Structure-Based View of Epidermal Growth Factor Receptor Regulation. Annual Review of Biophysics 37, 353–373. https://doi.org/10.1146/annurev.biophys.37.032807.125829

Fleury, H., Malaquin, N., Tu, V., Gilbert, S., Martinez, A., Olivier, M.-A., Sauriol, S.A., Communal, L., Leclerc-Desaulniers, K., Carmona, E., Provencher, D., Mes-

Masson, A.-M., Rodier, F., 2019. Exploiting interconnected synthetic lethal interactions between PARP inhibition and cancer cell reversible senescence. Nat Commun 10, 2556. https://doi.org/10.1038/s41467-019-10460-1

Gao, J., Liang, Y., Wang, L., 2022. Shaping Polarization Of Tumor-Associated Macrophages In Cancer Immunotherapy. Front Immunol 13, 888713. https://doi.org/10.3389/fimmu.2022.888713

Gazzaniga, S., Bravo, A.I., Guglielmotti, A., van Rooijen, N., Maschi, F., Vecchi, A., Mantovani, A., Mordoh, J., Wainstok, R., 2007. Targeting tumor-associated macrophages and inhibition of MCP-1 reduce angiogenesis and tumor growth in a human melanoma xenograft. J Invest Dermatol 127, 2031–2041. https://doi.org/10.1038/sj.jid.5700827

Gire, V., Dulić, V., 2015. Senescence from G2 arrest, revisited. Cell Cycle 14, 297–304. https://doi.org/10.1080/15384101.2014.1000134

Gonzalez-Meljem, J.M., Apps, J.R., Fraser, H.C., Martinez-Barbera, J.P., 2018. Paracrine roles of cellular senescence in promoting tumourigenesis. Br J Cancer 118, 1283–1288. https://doi.org/10.1038/s41416-018-0066-1

Gu, Z., Eils, R., Schlesner, M., 2016. Complex heatmaps reveal patterns and correlations in multidimensional genomic data. Bioinformatics 32, 2847–2849. https://doi.org/10.1093/bioinformatics/btw313

Guardiola, S., Varese, M., Sánchez-Navarro, M., Giralt, E., 2019. A Third Shot at EGFR: New Opportunities in Cancer Therapy. Trends in Pharmacological Sciences 40, 941–955. https://doi.org/10.1016/j.tips.2019.10.004

Hann, C.L., Daniel, V.C., Sugar, E.A., Dobromilskaya, I., Murphy, S.C., Cope, L., Lin, X., Hierman, J.S., Wilburn, D.L., Watkins, D.N., Rudin, C.M., 2008. Therapeutic Efficacy of ABT-737, a Selective Inhibitor of BCL-2, in Small Cell Lung Cancer. Cancer Research 68, 2321–2328. https://doi.org/10.1158/0008-5472.CAN-07-5031

Harrington, B.S., He, Y., Khan, T., Puttick, S., Conroy, P.J., Kryza, T., Cuda, T., Sokolowski, K.A., Tse, B.W., Robbins, K.K., Arachchige, B.J., Stehbens, S.J., Pollock, P.M., Reed, S., Weroha, S.J., Haluska, P., Salomon, C., Lourie, R., Perrin, L.C., Law, R.H.P., Whisstock, J.C., Hooper, J.D., 2020. Anti-CDCP1 immuno-

conjugates for detection and inhibition of ovarian cancer. Theranostics 10, 2095–2114. https://doi.org/10.7150/thno.30736

He, S.-M., Sun, S., Chen, A.-Q., Lv, S.-J., Qiu, C.-Z., Wei, M.-L., Liu, W., Liu, H.-R., Zhang, L., Ren, D.-L., 2022. Hypoxia regulates cytokines expression and neutrophils migration by ERK signaling in zebrafish. Fish Shellfish Immunol 125, 212–219. https://doi.org/10.1016/j.fsi.2022.05.006

He, Y., Wortmann, A., Burke, L.J., Reid, J.C., Adams, M.N., Abdul-Jabbar, I., Quigley, J.P., Leduc, R., Kirchhofer, D., Hooper, J.D., 2010. Proteolysis-induced N-terminal Ectodomain Shedding of the Integral Membrane Glycoprotein CUB Domain-containing Protein 1 (CDCP1) Is Accompanied by Tyrosine Phosphorylation of Its C-terminal Domain and Recruitment of Src and PKCδ *. Journal of Biological Chemistry 285, 26162–26173. https://doi.org/10.1074/jbc.M109.096453

Heitmann, J.S., Hagelstein, I., Hinterleitner, C., Roerden, M., Jung, G., Salih, H.R., Märklin, M., Kauer, J., 2020. Identification of CD318 (CDCP1) as novel prognostic marker in AML. Ann Hematol 99, 477–486. https://doi.org/10.1007/s00277-020-03907-9

Herranz, N., Gil, J., 2018. Mechanisms and functions of cellular senescence. J Clin Invest 128, 1238–1246. https://doi.org/10.1172/JCI95148

Hiraoka, K., Zenmyo, M., Watari, K., Iguchi, H., Fotovati, A., Kimura, Y.N., Hosoi, F., Shoda, T., Nagata, K., Osada, H., Ono, M., Kuwano, M., 2008. Inhibition of bone and muscle metastases of lung cancer cells by a decrease in the number of monocytes/macrophages. Cancer Science 99, 1595–1602. https://doi.org/10.1111/j.1349-7006.2008.00880.x

Hollifield, A.L., Arnall, J.R., Moore, D.C., 2020. Caplacizumab: an anti–von Willebrand factor antibody for the treatment of thrombotic thrombocytopenic purpura. American Journal of Health-System Pharmacy 77, 1201–1207. https://doi.org/10.1093/ajhp/zxaa151

Hooper, J.D., Zijlstra, A., Aimes, R.T., Liang, H., Claassen, G.F., Tarin, D., Testa, J.E., Quigley, J.P., 2003. Subtractive immunization using highly metastatic human tumor cells identifies SIMA135/CDCP1, a 135 kDa cell surface phosphorylated glycoprotein antigen. Oncogene 22, 1783–1794. https://doi.org/10.1038/sj.onc.1206220

Hu, D.-N., Zhang, R., Iacob, C.E., Yao, S., Yang, S.-F., Chan, C.-C., Rosen, R.B., 2024. Effects of Toll-like receptor 1 and 2 agonist Pam3CSK4 on uveal melanocytes and relevant experimental mouse model. Experimental Eye Research 239, 109749. https://doi.org/10.1016/j.exer.2023.109749

Huang, W., Hickson, L.J., Eirin, A., Kirkland, J.L., Lerman, L.O., 2022. Cellular senescence: the good, the bad and the unknown. Nat Rev Nephrol 18, 611–627. https://doi.org/10.1038/s41581-022-00601-z

Huber, W., Carey, V.J., Gentleman, R., Anders, S., Carlson, M., Carvalho, B.S., Bravo, H.C., Davis, S., Gatto, L., Girke, T., Gottardo, R., Hahne, F., Hansen, K.D., Irizarry, R.A., Lawrence, M., Love, M.I., MacDonald, J., Obenchain, V., Oleś, A.K., Pagès, H., Reyes, A., Shannon, P., Smyth, G.K., Tenenbaum, D., Waldron, L., Morgan, M., 2015. Orchestrating high-throughput genomic analysis with Bioconductor. Nat Methods 12, 115–121. https://doi.org/10.1038/nmeth.3252

Hughes, C.E., Nibbs, R.J.B., 2018. A guide to chemokines and their receptors. FEBS J 285, 2944–2971. https://doi.org/10.1111/febs.14466

Jain, A., Kaczanowska, S., Davila, E., 2014. IL-1 Receptor-Associated Kinase Signaling and Its Role in Inflammation, Cancer Progression, and Therapy Resistance. Front Immunol 5, 553. https://doi.org/10.3389/fimmu.2014.00553

Jamaspishvili, T., Berman, D.M., Ross, A.E., Scher, H.I., De Marzo, A.M., Squire, J.A., Lotan, T.L., 2018. Clinical implications of PTEN loss in prostate cancer. Nat Rev Urol 15, 222–234. https://doi.org/10.1038/nrurol.2018.9

Jin, B., Odongo, S., Radwanska, M., Magez, S., 2023. NANOBODIES®: A Review of Diagnostic and Therapeutic Applications. International Journal of Molecular Sciences 24, 5994. https://doi.org/10.3390/ijms24065994

Jochems, F., Thijssen, B., Conti, G.D., Jansen, R., Pogacar, Z., Groot, K., Wang, L., Schepers, A., Wang, C., Jin, H., Beijersbergen, R.L., Oliveira, R.L. de, Wessels, L.F.A., Bernards, R., 2021. The Cancer SENESCopedia: A delineation of cancer cell senescence. Cell Reports 36. https://doi.org/10.1016/j.celrep.2021.109441

Josephs, D.H., Bax, H.J., Karagiannis, S.N., 2015. Tumour-associated macrophage polarisation and re-education with immunotherapy. Front Biosci (Elite Ed) 7, 293–308. https://doi.org/10.2741/E735

Kadomoto, S., Izumi, K., Mizokami, A., 2021. Macrophage Polarity and Disease Control. Int J Mol Sci 23, 144. https://doi.org/10.3390/ijms23010144

Kaefer, A., Yang, J., Noertersheuser, P., Mensing, S., Humerickhouse, R., Awni, W., Xiong, H., 2014. Mechanism-based pharmacokinetic/pharmacodynamic meta-analysis of navitoclax (ABT-263) induced thrombocytopenia. Cancer Chemother Pharmacol 74, 593–602. https://doi.org/10.1007/s00280-014-2530-9

Kajiwara, K., Yamano, S., Aoki, K., Okuzaki, D., Matsumoto, K., Okada, M., 2021. CDCP1 promotes compensatory renal growth by integrating Src and Met signaling. Life Science Alliance 4. https://doi.org/10.26508/lsa.202000832

Kamoun, A., de Reyniès, A., Allory, Y., Sjödahl, G., Robertson, A.G., Seiler, R., Hoadley, K.A., Groeneveld, C.S., Al-Ahmadie, H., Choi, W., Castro, M.A.A., Fontugne, J., Eriksson, P., Mo, Q., Kardos, J., Zlotta, A., Hartmann, A., Dinney, C.P., Bellmunt, J., Powles, T., Malats, N., Chan, K.S., Kim, W.Y., McConkey, D.J., Black, P.C., Dyrskjøt, L., Höglund, M., Lerner, S.P., Real, F.X., Radvanyi, F., Aine, M., Al-Ahmadie, H., Allory, Y., Bellmunt, J., Bernard-Pierrot, I., Black, P.C., Castro, M.A.A., Chan, K.S., Choi, W., Czerniak, B., Dinney, C.P., Dyrskjøt, L., Eriksson, P., Fontugne, J., Gibb, E.A., Groeneveld, C.S., Hartmann, A., Hoadley, K.A., Höglund, M., Kamoun, A., Kardos, J., Kim, J., Kim, W.Y., Kwiatkowski, D.J., Lebret, T., Lerner, S.P., Liedberg, F., Malats, N., McConkey, D.J., Mo, Q., Powles, T., Radvanyi, F., Real, F.X., de Reyniès, A., Robertson, A.G., Siefker-Radtke, A., Sirab, N., Seiler, R., Sjödahl, G., Taber, A., Weinstein, J., Zlotta, A., 2020. A Consensus Molecular Classification of Muscle-invasive Bladder Cancer. European Urology 77, 420–433. https://doi.org/10.1016/j.eururo.2019.09.006

Keam, S.J., 2023. Ozoralizumab: First Approval. Drugs 83, 87–92. https://doi.org/10.1007/s40265-022-01821-0

Khan, T., Kryza, T., Lyons, N.J., He, Y., Hooper, J.D., 2021. The CDCP1 Signaling Hub: A Target for Cancer Detection and Therapeutic Intervention. Cancer Res 81, 2259–2269. https://doi.org/10.1158/0008-5472.CAN-20-2978

Kobayashi, Y., Togashi, Y., Yatabe, Y., Mizuuchi, H., Jangchul, P., Kondo, C., Shimoji, M., Sato, K., Suda, K., Tomizawa, K., Takemoto, T., Hida, T., Nishio, K., Mitsudomi, T., 2015. EGFR Exon 18 Mutations in Lung Cancer: Molecular Predictors of Augmented Sensitivity to Afatinib or Neratinib as Compared with First- or Third-

Generation TKIs. Clinical Cancer Research 21, 5305–5313. https://doi.org/10.1158/1078-0432.CCR-15-1046

Koll, F.J., Banek, S., Kluth, L., Köllermann, J., Bankov, K., Chun, F.K.-H., Wild, P.J., Weigert, A., Reis, H., 2023. Tumor-associated macrophages and Tregs influence and represent immune cell infiltration of muscle-invasive bladder cancer and predict prognosis. Journal of Translational Medicine 21, 124. https://doi.org/10.1186/s12967-023-03949-3

Kollmorgen, G., Niederfellner, G., Lifke, A., Spohn, G.J., Rieder, N., Vega Harring, S., Bauss, F., Burtscher, H., Lammers, R., Bossenmaier, B., 2013. Antibody mediated CDCP1 degradation as mode of action for cancer targeted therapy. Molecular Oncology 7, 1142–1151. https://doi.org/10.1016/j.molonc.2013.08.009

Kopczynski, M., Rumienczyk, I., Kulecka, M., Statkiewicz, M., Pysniak, K., Sandowska-Markiewicz, Z., Wojcik-Trechcinska, U., Goryca, K., Pyziak, K., Majewska, E., Masiejczyk, M., Wojcik-Jaszczynska, K., Rzymski, T., Bomsztyk, K., Ostrowski, J., Mikula, M., 2021. Selective Extracellular Signal-Regulated Kinase 1/2 (ERK1/2) Inhibition by the SCH772984 Compound Attenuates In Vitro and In Vivo Inflammatory Responses and Prolongs Survival in Murine Sepsis Models. Int J Mol Sci 22, 10204. https://doi.org/10.3390/ijms221910204

Kryza, T., Khan, T., Puttick, S., Li, C., Sokolowski, K.A., Tse, B.W., Cuda, T., Lyons, N., Gough, M., Yin, J., Parkin, A., Deryugina, E.I., Quigley, J.P., Law, R.H.P., Whisstock, J.C., Riddell, A.D., Barbour, A.P., Wyld, D.K., Thomas, P.A., Rose, S., Snell, C.E., Pajic, M., He, Y., Hooper, J.D., 2020. Effective targeting of intact and proteolysed CDCP1 for imaging and treatment of pancreatic ductal adenocarcinoma. Theranostics 10, 4116–4133. https://doi.org/10.7150/thno.43589

Kurz, D.J., Decary, S., Hong, Y., Erusalimsky, J.D., 2000. Senescence-associated β-galactosidase reflects an increase in lysosomal mass during replicative ageing of human endothelial cells. Journal of Cell Science 113, 3613–3622. https://doi.org/10.1242/jcs.113.20.3613

Ladanyi, M., Pao, W., 2008. Lung adenocarcinoma: guiding EGFR-targeted therapy and beyond. Mod Pathol 21, S16–S22. https://doi.org/10.1038/modpathol.3801018

Lahmar, Q., Keirsse, J., Laoui, D., Movahedi, K., Van Overmeire, E., Van Ginderachter, J.A., 2016. Tissue-resident versus monocyte-derived macrophages in the tumor

microenvironment. Biochimica et Biophysica Acta (BBA) - Reviews on Cancer, The role of the immune system in cancer: from mechanisms to clinical applications 1865, 23–34. https://doi.org/10.1016/j.bbcan.2015.06.009

Leach, D., 2023. Urological Cancers, in: White, M., Perrin, A. (Eds.), Stoma Care Specialist Nursing: A Guide for Clinical Practice. Springer International Publishing, Cham, pp. 117–137. https://doi.org/10.1007/978-3-031-07799-9_8

Leonardo, A.D., Linke, S.P., Clarkin, K., Wahl, G.M., 1994. DNA damage triggers a prolonged p53-dependent G1 arrest and long-term induction of Cip1 in normal human fibroblasts. Genes Dev. 8, 2540–2551. https://doi.org/10.1101/gad.8.21.2540

Levantini, E., Maroni, G., Del Re, M., Tenen, D.G., 2022. EGFR signaling pathway as therapeutic target in human cancers. Seminars in Cancer Biology, Targeting Cellular Signaling Pathways 85, 253–275. https://doi.org/10.1016/j.semcancer.2022.04.002

Lim, S.Y., Yuzhalin, A.E., Gordon-Weeks, A.N., Muschel, R.J., 2016. Targeting the CCL2-CCR2 signaling axis in cancer metastasis. Oncotarget 7, 28697–28710. https://doi.org/10.18632/oncotarget.7376

Linggi, B., Carpenter, G., 2006. ErbB receptors: new insights on mechanisms and biology. Trends in Cell Biology 16, 649–656. https://doi.org/10.1016/j.tcb.2006.10.008

Locati, M., Curtale, G., Mantovani, A., 2020. Diversity, Mechanisms and Significance of Macrophage Plasticity. Annu Rev Pathol 15, 123–147. https://doi.org/10.1146/annurev-pathmechdis-012418-012718

Lopez-Beltran, A., Cookson, M.S., Guercio, B.J., Cheng, L., 2024. Advances in diagnosis and treatment of bladder cancer. BMJ 384, e076743. https://doi.org/10.1136/bmj-2023-076743

Love, M.I., Huber, W., Anders, S., 2014. Moderated estimation of fold change and dispersion for RNA-seq data with DESeq2. Genome Biology 15, 550. https://doi.org/10.1186/s13059-014-0550-8

Mantovani, A., Marchesi, F., Malesci, A., Laghi, L., Allavena, P., 2017. Tumour-associated macrophages as treatment targets in oncology. Nat Rev Clin Oncol 14, 399–416. https://doi.org/10.1038/nrclinonc.2016.217

Mantovani, A., Sozzani, S., Locati, M., Allavena, P., Sica, A., 2002. Macrophage polarization: tumor-associated macrophages as a paradigm for polarized M2 mononuclear phagocytes. Trends in Immunology 23, 549–555. https://doi.org/10.1016/S1471-4906(02)02302-5

Matulewicz, R.S., Steinberg, G.D., 2020. Non—muscle-invasive Bladder Cancer: Overview and Contemporary Treatment Landscape of Neoadjuvant Chemoablative Therapies. Rev Urol 22, 43–51.

Mikuła-Pietrasik, J., Niklas, A., Uruski, P., Tykarski, A., Książek, K., 2020. Mechanisms and significance of therapy-induced and spontaneous senescence of cancer cells. Cell. Mol. Life Sci. 77, 213–229. https://doi.org/10.1007/s00018-019-03261-8

Miselis, N.R., Wu, Z.J., Van Rooijen, N., Kane, A.B., 2008. Targeting tumor-associated macrophages in an orthotopic murine model of diffuse malignant mesothelioma. Molecular Cancer Therapeutics 7, 788–799. https://doi.org/10.1158/1535-7163.MCT-07-0579

Mooso, B.A., Vinall, R.L., Mudryj, M., Yap, S.A., White, R.W. deVere, Ghosh, P.M., 2015. The Role of EGFR Family Inhibitors in Muscle Invasive Bladder Cancer: A Review of Clinical Data and Molecular Evidence. Journal of Urology. https://doi.org/10.1016/j.juro.2014.07.121

Mosca, L., Ilari, A., Fazi, F., Assaraf, Y.G., Colotti, G., 2021. Taxanes in cancer treatment: Activity, chemoresistance and its overcoming. Drug Resistance Updates 54, 100742. https://doi.org/10.1016/j.drup.2020.100742

Mullard, A., 2022. FDA approves second BCMA-targeted CAR-T cell therapy. Nature Reviews Drug Discovery 21, 249–249. https://doi.org/10.1038/d41573-022-00048-8

Muñoz-Espín, D., Cañamero, M., Maraver, A., Gómez-López, G., Contreras, J., Murillo-Cuesta, S., Rodríguez-Baeza, A., Varela-Nieto, I., Ruberte, J., Collado, M., Serrano, M., 2013. Programmed cell senescence during mammalian embryonic development. Cell 155, 1104–1118. https://doi.org/10.1016/j.cell.2013.10.019

Nakashima, K., Uekita, T., Yano, S., Kikuchi, J.-I., Nakanishi, R., Sakamoto, N., Fukumoto, K., Nomoto, A., Kawamoto, K., Shibahara, T., Yamaguchi, H., Sakai, R., 2017. Novel small molecule inhibiting CDCP1-PKCδ pathway reduces tumor

metastasis and proliferation. Cancer Sci 108, 1049–1057. https://doi.org/10.1111/cas.13218

Ngambenjawong, C., Gustafson, H.H., Pun, S.H., 2017. Progress in tumor-associated macrophage (TAM)-targeted therapeutics. Advanced Drug Delivery Reviews, Immuno-engineering: The Next Frontier in Therapeutics Delivery 114, 206–221. https://doi.org/10.1016/j.addr.2017.04.010

Ocaña-Guzman, R., Vázquez-Bolaños, L., Sada-Ovalle, I., 2018. Receptors That Inhibit Macrophage Activation: Mechanisms and Signals of Regulation and Tolerance. Journal of Immunology Research 2018, 8695157. https://doi.org/10.1155/2018/8695157

Ohtani, N., 2022. The roles and mechanisms of senescence-associated secretory phenotype (SASP): can it be controlled by senolysis? Inflamm Regen 42, 11. https://doi.org/10.1186/s41232-022-00197-8

Oliveira, S., Heukers, R., Sornkom, J., Kok, R.J., van Bergen en Henegouwen, P.M.P., 2013. Targeting tumors with nanobodies for cancer imaging and therapy. Journal of Controlled Release 172, 607–617. https://doi.org/10.1016/j.jconrel.2013.08.298

Pao, W., Miller, V.A., Politi, K.A., Riely, G.J., Somwar, R., Zakowski, M.F., Kris, M.G., Varmus, H., 2005. Acquired Resistance of Lung Adenocarcinomas to Gefitinib or Erlotinib Is Associated with a Second Mutation in the EGFR Kinase Domain. PLOS Medicine 2, e73. https://doi.org/10.1371/journal.pmed.0020073

Papadimitrakopoulou, V.A., Wu, Y.-L., Han, J.-Y., Ahn, M.-J., Ramalingam, S.S., John, T., Okamoto, I., Yang, J.C.-H., Bulusu, K.C., Laus, G., Collins, B., Barrett, J.C., Chmielecki, J., Mok, T.S.K., 2018. Analysis of resistance mechanisms to osimertinib in patients with EGFR T790M advanced NSCLC from the AURA3 study. Annals of Oncology 29, viii741. https://doi.org/10.1093/annonc/mdy424.064

Paul, D., Stern, O., Vallis, Y., Dhillon, J., Buchanan, A., McMahon, H., 2023. Cell surface protein aggregation triggers endocytosis to maintain plasma membrane proteostasis. Nat Commun 14, 947. https://doi.org/10.1038/s41467-023-36496-y

Peter, A.E., Sandeep, B.V., Rao, B.G., Kalpana, V.L., 2020. Calming the Storm: Natural Immunosuppressants as Adjuvants to Target the Cytokine Storm in COVID-19. Front Pharmacol 11, 583777. https://doi.org/10.3389/fphar.2020.583777

Popivanova, B.K., Kostadinova, F.I., Furuichi, K., Shamekh, M.M., Kondo, T., Wada, T., Egashira, K., Mukaida, N., 2009. Blockade of a chemokine, CCL2, reduces chronic colitis-associated carcinogenesis in mice. Cancer Res 69, 7884–7892. https://doi.org/10.1158/0008-5472.CAN-09-1451

Prasanna, P.G., Citrin, D.E., Hildesheim, J., Ahmed, M.M., Venkatachalam, S., Riscuta, G., Xi, D., Zheng, G., Deursen, J. van, Goronzy, J., Kron, S.J., Anscher, M.S., Sharpless, N.E., Campisi, J., Brown, S.L., Niedernhofer, L.J., O'Loghlen, A., Georgakilas, A.G., Paris, F., Gius, D., Gewirtz, D.A., Schmitt, C.A., Abazeed, M.E., Kirkland, J.L., Richmond, A., Romesser, P.B., Lowe, S.W., Gil, J., Mendonca, M.S., Burma, S., Zhou, D., Coleman, C.N., 2021. Therapy-Induced Senescence: Opportunities to Improve Anticancer Therapy. JNCI: Journal of the National Cancer Institute 113, 1285–1298. https://doi.org/10.1093/jnci/djab064

Rannikko, J.H., Hollmén, M., 2024. Clinical landscape of macrophage-reprogramming cancer immunotherapies. Br J Cancer 131, 627–640. https://doi.org/10.1038/s41416-024-02715-6

Robinson, M.D., Oshlack, A., 2010. A scaling normalization method for differential expression analysis of RNA-seq data. Genome Biol 11, R25. https://doi.org/10.1186/gb-2010-11-3-r25

Roca, H., Varsos, Z.S., Sud, S., Craig, M.J., Ying, C., Pienta, K.J., 2009. CCL2 and interleukin-6 promote survival of human CD11b+ peripheral blood mononuclear cells and induce M2-type macrophage polarization. J Biol Chem 284, 34342–34354. https://doi.org/10.1074/jbc.M109.042671

Roger, L., Tomas, F., Gire, V., 2021. Mechanisms and Regulation of Cellular Senescence. International Journal of Molecular Sciences 22, 13173. https://doi.org/10.3390/ijms222313173

Roninson, I.B., 2003. Tumor Cell Senescence in Cancer Treatment1. Cancer Research 63, 2705–2715.

Rossiello, F., Herbig, U., Longhese, M.P., Fumagalli, M., d'Adda di Fagagna, F., 2014. Irreparable telomeric DNA damage and persistent DDR signalling as a shared causative mechanism of cellular senescence and ageing. Current Opinion in Genetics & Development, Molecular and genetic bases of disease 26, 89–95. https://doi.org/10.1016/j.gde.2014.06.009

Ruhland, M.K., Loza, A.J., Capietto, A.-H., Luo, X., Knolhoff, B.L., Flanagan, K.C., Belt, B.A., Alspach, E., Leahy, K., Luo, J., Schaffer, A., Edwards, J.R., Longmore, G., Faccio, R., DeNardo, D.G., Stewart, S.A., 2016. Stromal senescence establishes an immunosuppressive microenvironment that drives tumorigenesis. Nat Commun 7, 11762. https://doi.org/10.1038/ncomms11762

Ruth, J.H., Gurrea-Rubio, M., Athukorala, K.S., Rasmussen, S.M., Weber, D.P., Randon, P.M., Gedert, R.J., Lind, M.E., Amin, M.A., Campbell, P.L., Tsou, P.-S., Mao-Draayer, Y., Wu, Q., Lanigan, T.M., Keshamouni, V.G., Singer, N.G., Lin, F., Fox, D.A., 2021. CD6 is a target for cancer immunotherapy. JCI Insight 6, e145662, 145662. https://doi.org/10.1172/jci.insight.145662

Saleh, T., Carpenter, V.J., Tyutyunyk-Massey, L., Murray, G., Leverson, J.D., Souers, A.J., Alotaibi, M.R., Faber, A.C., Reed, J., Harada, H., Gewirtz, D.A., 2020. Clearance of therapy-induced senescent tumor cells by the senolytic ABT-263 via interference with BCL-XL–BAX interaction. Molecular Oncology 14, 2504–2519. https://doi.org/10.1002/1878-0261.12761

Saponaro, M., Flottmann, S., Eckstein, M., Hommerding, O., Klümper, N., Corvino, D., Hosni, S., Schmidt, A., Mönig, N., Schmidt, D., Ellinger, J., Toma, M., Kristiansen, G., Bald, T., Alimonti, A., Ritter, M., Hölzel, M., Alajati, A., 2023. CDCP1 expression is frequently increased in aggressive urothelial carcinoma and promotes urothelial tumor progression. Sci Rep 13, 73. https://doi.org/10.1038/s41598-022-26579-z

Sarkis, J., Vannier, E., Mjaess, G., Pochet, C., Albisinni, S., Quackels, T., Roumeguère, T., 2022. Neoadjuvant Immunochemotherapy in the Treatment of Nonmetastatic Muscle-Invasive Bladder Cancer: A Systematic Review. Immunotherapy. https://doi.org/10.2217/imt-2022-0039

Schalken, J., Fitzpatrick, J.M., 2016. Enzalutamide: targeting the androgen signalling pathway in metastatic castration-resistant prostate cancer. BJU Int 117, 215–225. https://doi.org/10.1111/bju.13123

Schmid-Burgk, J.L., Höning, K., Ebert, T.S., Hornung, V., 2016. CRISPaint allows modular base-specific gene tagging using a ligase-4-dependent mechanism. Nat Commun 7, 12338. https://doi.org/10.1038/ncomms12338

Schwarze, S.R., Fu, V.X., Desotelle, J.A., Kenowski, M.L., Jarrard, D.F., 2005. The Identification of Senescence-Specific Genes during the Induction of Senescence in Prostate Cancer Cells. Neoplasia 7, 816–823.

Serrano, M., Lin, A.W., McCurrach, M.E., Beach, D., Lowe, S.W., 1997. Oncogenic ras Provokes Premature Cell Senescence Associated with Accumulation of p53 and p16INK4a. Cell 88, 593–602. https://doi.org/10.1016/S0092-8674(00)81902-9

Shapouri-Moghaddam, A., Mohammadian, S., Vazini, H., Taghadosi, M., Esmaeili, S.-A., Mardani, F., Seifi, B., Mohammadi, A., Afshari, J.T., Sahebkar, A., 2018. Macrophage plasticity, polarization, and function in health and disease. Journal of Cellular Physiology 233, 6425–6440. https://doi.org/10.1002/jcp.26429

Shi, Y., Au, J.S.-K., Thongprasert, S., Srinivasan, S., Tsai, C.-M., Khoa, M.T., Heeroma, K., Itoh, Y., Cornelio, G., Yang, P.-C., 2014. A Prospective, Molecular Epidemiology Study of *EGFR* Mutations in Asian Patients with Advanced Non–Small-Cell Lung Cancer of Adenocarcinoma Histology (PIONEER). Journal of Thoracic Oncology 9, 154–162. https://doi.org/10.1097/JTO.0000000000000033

Sica, A., Erreni, M., Allavena, P., Porta, C., 2015. Macrophage polarization in pathology. Cell Mol Life Sci 72, 4111–4126. https://doi.org/10.1007/s00018-015-1995-y

Sigismund, S., Avanzato, D., Lanzetti, L., 2018. Emerging functions of the EGFR in cancer. Molecular Oncology 12, 3–20. https://doi.org/10.1002/1878-0261.12155

Siva, A.C., Wild, M.A., Kirkland, R.E., Nolan, M.J., Lin, B., Maruyama, T., Yantiri-Wernimont, F., Frederickson, S., Bowdish, K.S., Xin, H., 2008. Targeting CUB domain-containing protein 1 with a monoclonal antibody inhibits metastasis in a prostate cancer model. Cancer Res 68, 3759–3766. https://doi.org/10.1158/0008-5472.CAN-07-1657

Stecca, C., Mitin, T., Sridhar, S.S., 2023. The Role of Neoadjuvant Chemotherapy in Bladder Preservation Approaches in Muscle-Invasive Bladder Cancer. Semin Radiat Oncol 33, 51–55. https://doi.org/10.1016/j.semradonc.2022.10.006

Storer, M., Mas, A., Robert-Moreno, A., Pecoraro, M., Ortells, M.C., Di Giacomo, V., Yosef, R., Pilpel, N., Krizhanovsky, V., Sharpe, J., Keyes, W.M., 2013. Senescence is a developmental mechanism that contributes to embryonic growth and patterning. Cell 155, 1119–1130. https://doi.org/10.1016/j.cell.2013.10.041

Szebeni, G.J., Vizler, C., Kitajka, K., Puskas, L.G., 2017. Inflammation and Cancer: Extra- and Intracellular Determinants of Tumor-Associated Macrophages as Tumor Promoters. Mediators Inflamm 2017, 9294018. https://doi.org/10.1155/2017/9294018

Tan, Y., Zhao, N., Xie, Q., Xu, Z., Chai, J., Zhang, X., Li, Y., 2023. Melatonin attenuates cholestatic liver injury via inhibition of the inflammatory response. Mol Cell Biochem 478, 2527–2537. https://doi.org/10.1007/s11010-023-04682-7

Tang, X., Mo, C., Wang, Y., Wei, D., Xiao, H., 2013. Anti-tumour strategies aiming to target tumour-associated macrophages. Immunology 138, 93–104. https://doi.org/10.1111/imm.12023

Taubert, H., Eckstein, M., Epple, E., Jung, R., Weigelt, K., Lieb, V., Sikic, D., Stöhr, R., Geppert, C., Weyerer, V., Bertz, S., Kehlen, A., Hartmann, A., Wullich, B., Wach, S., 2021. Immune Cell-Associated Protein Expression Helps to Predict Survival in Muscle-Invasive Urothelial Bladder Cancer Patients after Radical Cystectomy and Optional Adjuvant Chemotherapy. Cells 10, 159. https://doi.org/10.3390/cells10010159

te Poele, R.H., Okorokov, A.L., Jardine, L., Cummings, J., Joel, S.P., 2002. DNA damage is able to induce senescence in tumor cells in vitro and in vivo. Cancer Res 62, 1876–1883.

Tonry, C., Finn, S., Armstrong, J., Pennington, S.R., 2020. Clinical proteomics for prostate cancer: understanding prostate cancer pathology and protein biomarkers for improved disease management. Clinical Proteomics 17, 41. https://doi.org/10.1186/s12014-020-09305-7

Tsao, P., Cao, T., von Zastrow, M., 2001. Role of endocytosis in mediating downregulation of G-protein-coupled receptors. Trends in Pharmacological Sciences 22, 91–96. https://doi.org/10.1016/S0165-6147(00)01620-5

Turdo, F., Bianchi, F., Gasparini, P., Sandri, M., Sasso, M., De Cecco, L., Forte, L., Casalini, P., Aiello, P., Sfondrini, L., Agresti, R., Carcangiu, M.L., Plantamura, I., Sozzi, G., Tagliabue, E., Campiglio, M., 2016. CDCP1 is a novel marker of the most aggressive human triple-negative breast cancers. Oncotarget 7, 69649–69665. https://doi.org/10.18632/oncotarget.11935

Ullrich, A., Coussens, L., Hayflick, J.S., Dull, T.J., Gray, A., Tam, A.W., Lee, J., Yarden, Y., Libermann, T.A., Schlessinger, J., Downward, J., Mayes, E.L.V., Whittle, N., Waterfield, M.D., Seeburg, P.H., 1984. Human epidermal growth factor receptor cDNA sequence and aberrant expression of the amplified gene in A431 epidermoid carcinoma cells. Nature 309, 418–425. https://doi.org/10.1038/309418a0

Urological Cancers, n.d.

Wadosky, K.M., Koochekpour, S., 2016. Molecular mechanisms underlying resistance to androgen deprivation therapy in prostate cancer. Oncotarget 7, 64447–64470. https://doi.org/10.18632/oncotarget.10901

Wang, C., Zhang, S., Huang, L., Liu, J., Zhou, Q., Du, G., Lao, S., 2022. Chemerin promotes MAPK/ERK activation to induce inflammatory factor production in rat synoviocytes. Exp Ther Med 24, 684. https://doi.org/10.3892/etm.2022.11620

Wang, H., Yung, M.M.H., Ngan, H.Y.S., Chan, K.K.L., Chan, D.W., 2021. The Impact of the Tumor Microenvironment on Macrophage Polarization in Cancer Metastatic Progression. Int J Mol Sci 22, 6560. https://doi.org/10.3390/ijms22126560

Wang, L., Lankhorst, L., Bernards, R., 2022. Exploiting senescence for the treatment of cancer. Nat Rev Cancer 22, 340–355. https://doi.org/10.1038/s41568-022-00450-9

Wang, L., Oliveira, R.L. de, Wang, C., Neto, J.M.F., Mainardi, S., Evers, B., Lieftink, C., Morris, B., Jochems, F., Willemsen, L., Beijersbergen, R.L., Bernards, R., 2017. High-Throughput Functional Genetic and Compound Screens Identify Targets for Senescence Induction in Cancer. Cell Reports 21, 773–783. https://doi.org/10.1016/j.celrep.2017.09.085

Wang, X., Wong, S.C., Pan, J., Tsao, S.W., Fung, K.H., Kwong, D.L., Sham, J.S., Nicholls, J.M., 1998. Evidence of cisplatin-induced senescent-like growth arrest in nasopharyngeal carcinoma cells. Cancer Res 58, 5019–5022.

Weichhart, T., Hengstschläger, M., Linke, M., 2015. Regulation of innate immune cell function by mTOR. Nat Rev Immunol 15, 599–614. https://doi.org/10.1038/nri3901

Weinberg, R.A., 1995. The retinoblastoma protein and cell cycle control. Cell 81, 323–330. https://doi.org/10.1016/0092-8674(95)90385-2

Wickham, H., 2016. ggplot2: Elegant Graphics for Data Analysis, 2nd ed. Springer.

Wortmann, A., He, Y., Deryugina, E.I., Quigley, J.P., Hooper, J.D., 2009. The cell surface glycoprotein CDCP1 in cancer—Insights, opportunities, and challenges. IUBMB Life 61, 723–730. https://doi.org/10.1002/iub.198

Wu, H., Schiff, D.S., Lin, Y., Neboori, H.J.R., Goyal, S., Feng, Z., Haffty, B.G., 2014. Ionizing Radiation Sensitizes Breast Cancer Cells to Bcl-2 Inhibitor, ABT-737, through Regulating Mcl-1. Radiat Res 182, 618–625. https://doi.org/10.1667/RR13856.1

Yarden, Y., Sliwkowski, M.X., 2001. Untangling the ErbB signalling network. Nat Rev Mol Cell Biol 2, 127–137. https://doi.org/10.1038/35052073

Yokota, S., Chosa, N., Matsumoto, S., Satoh, K., Ishisaki, A., 2022. Extracellular adenosine 5'-diphosphate promotes MCP-1/CCL2 expression via the P2Y13 purinergic receptor/ERK signaling axis in temporomandibular joint-derived mouse fibroblast-like synoviocytes. Mol Biol Rep. https://doi.org/10.1007/s11033-022-08125-2

Yonesaka, K., Tanizaki, J., Maenishi, O., Haratani, K., Kawakami, H., Tanaka, K., Hayashi, H., Sakai, K., Chiba, Y., Tsuya, A., Goto, H., Otsuka, E., Okida, H., Kobayashi, M., Yoshimoto, R., Funabashi, M., Hashimoto, Y., Hirotani, K., Kagari, T., Nishio, K., Nakagawa, K., 2022. HER3 Augmentation via Blockade of EGFR/AKT Signaling Enhances Anticancer Activity of HER3-Targeting Patritumab Deruxtecan in EGFR-Mutated Non–Small Cell Lung Cancer. Clinical Cancer Research 28, 390–403. https://doi.org/10.1158/1078-0432.CCR-21-3359

Yosef, R., Pilpel, N., Tokarsky-Amiel, R., Biran, A., Ovadya, Y., Cohen, S., Vadai, E., Dassa, L., Shahar, E., Condiotti, R., Ben-Porath, I., Krizhanovsky, V., 2016. Directed elimination of senescent cells by inhibition of BCL-W and BCL-XL. Nat Commun 7, 11190. https://doi.org/10.1038/ncomms11190

Yunna, C., Mengru, H., Lei, W., Weidong, C., 2020. Macrophage M1/M2 polarization. Eur J Pharmacol 877, 173090. https://doi.org/10.1016/j.ejphar.2020.173090

Zacarias-Fluck, M.F., Morancho, B., Vicario, R., Luque Garcia, A., Escorihuela, M., Villanueva, J., Rubio, I.T., Arribas, J., 2015. Effect of Cellular Senescence on the Growth of HER2-Positive Breast Cancers. JNCI: Journal of the National Cancer Institute 107, djv020. https://doi.org/10.1093/jnci/djv020

Zeisberger, S.M., Odermatt, B., Marty, C., Zehnder-Fjällman, A.H.M., Ballmer-Hofer, K., Schwendener, R.A., 2006. Clodronate-liposome-mediated depletion of tumour-associated macrophages: a new and highly effective antiangiogenic therapy approach. Br J Cancer 95, 272–281. https://doi.org/10.1038/sj.bjc.6603240

Zhang, Q., Sioud, M., 2023. Tumor-Associated Macrophage Subsets: Shaping Polarization and Targeting. Int J Mol Sci 24, 7493. https://doi.org/10.3390/ijms24087493

Zhang, X., Gureasko, J., Shen, K., Cole, P.A., Kuriyan, J., 2006. An Allosteric Mechanism for Activation of the Kinase Domain of Epidermal Growth Factor Receptor. Cell 125, 1137–1149. https://doi.org/10.1016/j.cell.2006.05.013

Zhang, Z., Lee, J.C., Lin, L., Olivas, V., Au, V., LaFramboise, T., Abdel-Rahman, M., Wang, X., Levine, A.D., Rho, J.K., Choi, Y.J., Choi, C.-M., Kim, S.-W., Jang, S.J., Park, Y.S., Kim, W.S., Lee, D.H., Lee, J.-S., Miller, V.A., Arcila, M., Ladanyi, M., Moonsamy, P., Sawyers, C., Boggon, T.J., Ma, P.C., Costa, C., Taron, M., Rosell, R., Halmos, B., Bivona, T.G., 2012. Activation of the AXL kinase causes resistance to EGFR-targeted therapy in lung cancer. Nat Genet 44, 852–860. https://doi.org/10.1038/ng.2330

Zheng, J.H., Nguyen, V.H., Jiang, S.-N., Park, S.-H., Tan, W., Hong, S.H., Shin, M.G., Chung, I.-J., Hong, Y., Bom, H.-S., Choy, H.E., Lee, S.E., Rhee, J.H., Min, J.-J., 2017. Two-step enhanced cancer immunotherapy with engineered Salmonella typhimurium secreting heterologous flagellin. Science Translational Medicine 9, eaak9537. https://doi.org/10.1126/scitranslmed.aak9537

Zhu, Y., Tchkonia, T., Fuhrmann-Stroissnigg, H., Dai, H.M., Ling, Y.Y., Stout, M.B., Pirtskhalava, T., Giorgadze, N., Johnson, K.O., Giles, C.B., Wren, J.D., Niedernhofer, L.J., Robbins, P.D., Kirkland, J.L., 2016. Identification of a novel senolytic agent, navitoclax, targeting the Bcl-2 family of anti-apoptotic factors. Aging Cell 15, 428–435. https://doi.org/10.1111/acel.12445

Zi, H., He, S.-H., Leng, X.-Y., Xu, X.-F., Huang, Q., Weng, H., Zhu, C., Li, L.-Y., Gu, J.-M., Li, X.-H., Ming, D.-J., Li, X.-D., Yuan, S., Wang, X.-H., He, D.-L., Zeng, X.-T., 2021. Global, regional, and national burden of kidney, bladder, and prostate cancers and their attributable risk factors, 1990-2019. Mil Med Res 8, 60. https://doi.org/10.1186/s40779-021-00354-z

9 Acknowledgements

This acknowledgments section does not want to be the typical monotonous and overly polite script written by an academic student. The path that has brought me to this day has not been always easy and joyful.

I want to start by recognizing my PI, Dr. Abdullah Alajati. I wholeheartedly thank him for granting me the opportunity to start a Ph.D. His support, trust, and the intellectual and economic freedom he provided me have been invaluable to express myself in my journey through science.

Since I profoundly value time as one of the most precious resources of the human being, a thanks go to my supervisors Prof. Dr. Med. Michael Hölzel, Prof. Dr. Nicola Aceto, Prof. Dr. Med. Manuel Ritter, and Prof. Dr. Med. Jörg Ellinger for dedicating some of theirs to participate to meetings and reports over my research progresses.

A great role in the achievement of my Ph.D. has been played by my colleagues, Sana, Doris, Karin, Anja and Ngoc. Firstly, they are the forger of a lively and enjoyable working atmosphere. Since the average human spends 90,000 hours over a lifetime at work, which means around 36% of their waking hours, an ambiance of camaraderie at work is surely essential for ensuring a clear mind in our daily lives and helps psychologically to maintain compliance with our goals. Moreover, they have always been there for technical help and/or scientific support whenever I was confronted with the need for a helping hand or a good suggestion.

Since we know that the road to stardom is not only paved by good working practice and environment but also by stable mental health in our personal space, a special thanks goes to Anja and Ngoc who spent hours listening to my breakdowns in the lab. A similar thank goes to my friends Nicole, Allegra, Silvia, and Chiara. To cite Richard Paul Evans, a U.S. writer that I actually have not read at all, “It is in the dark times that the light of friendship shines brightest”. In simple words, their support and bits of advice have shone in my darkest moments during these four years. P.S.: They are also the best companions for sneaky travels, alcoholic rendezvous, and dancing nights.

Lastly, I want to thank my big and often crazy Italian family. I will begin with my parents, Mara and Francesco, as they essentially started the biological process that brought my conscious self into this world and invested all their time, money, and energy in creating the woman I am today. It might feel scary sometimes to be alive in a world that seems collapsing slowly, but they also educated me so I would have the right amount of empathy, optimism and anger to try to be better and care about what and who surrounds me. I thank my brother Samuele for two aspects: the simple and innate act of being my brother, and for being resilient to me just being me. A thanks goes also to my grandparents, Sergio and Adriana, my aunts, Michela and Daniela, and cousins, Giorgia, Chiara and Daniele, who taught me that in this world you are never alone when you have the warmth of a home to come back to.

10 Curriculum vitae

Publications:

Richard Weiten, Theadora Engler, Hubert Schorle, Jörg Ellinger, **Miriam Saponaro**, Abdullah Alajati, Daniel Nettersheim, Isabella Syring-Schmandke. „The New Tumour Biomarker miRNA-371-3p Influences Cisplatin Sensitivity of Testicular Germ Cell Tumour Cell Lines“. Journal of Cellular and Molecular Medicine 28, Nr. 24 (December 2024): e70314. https://doi.org/10.1111/jcmm.70314.

Sara Zumerle, Miles Sarill, **Miriam Saponaro**, Manuel Colucci, Liliana Contu, Edoardo Lazzarini, Roberta Sartori, Camilla Pezzini, Anna Rinaldi, Anna Scanu, Jacopo Sgrignani, Patrizia Locatelli, Marianna Sabbadin, Aurora Valdata, Daniela Brina, Isabella Giacomini, Beatrice Rizzo, Alessandra Pierantoni, Saman Sharifi, Silvia Bressan, Claudia Altomare, Yulia Goshovska, Chiara Giraudo, Roberto Luisetto, Luca Iaccarino , Cristina Torcasio, Simone Mosole, Emiliano Pasquini, Andrea Rinaldi, Laura Pellegrini, Gregorio Peron, Matteo Fassan, Stefano Masiero, Andrea Maria Giori, Stefano Dall'Acqua, Johan Auwerx, Pietro Cippà, Andrea Cavalli, Marco Bolis, Marco Sandri, Lucio Barile, Monica Montopoli, Andrea Alimonti. „Targeting Senescence Induced by Age or Chemotherapy with a Polyphenol-Rich Natural Extract Improves Longevity and Healthspan in Mice“. Nature Aging 4, Nr. 9 (September 2024): 1231–48. https://doi.org/10.1038/s43587-024-00663-7.

Manuel Colucci, Sara Zumerle, Silvia Bressan, Federico Gianfanti, Martina Troiani, Aurora Valdata, Mariantonietta D’Ambrosio, Emiliano Pasquini, Angelica Varesi, Francesca Cogo, Simone Mosole, Cristina Dongilli, Maria Andrea Desbats, Liliana Contu, Ajinkya Revankdar, Jingjing Chen, Madhuri Kalathur, Maria Luna Perciato, Rossella Basilotta, Laczko Endre, Stefan Schauer, Alaa Othman, Ilaria Guccini, **Miriam Saponaro**, Luisa Maraccani, Nicolò Bancaro, Ping Lai, Lei Liu, Nicolò Pernigoni, Federico Mele, Sara Merler, Lloyd C Trotman, Greta Guarda, Bianca Calì, Monica Montopoli, Andrea Alimonti. „Retinoic Acid Receptor Activation Reprograms Senescence Response and Enhances Anti-Tumor Activity of Natural Killer Cells“. Cancer Cell 42, Nr. 4 (April 2024): 646-661.e9. https://doi.org/10.1016/j.ccell.2024.02.004.

Sana Hosni, Viola Kilian, Niklas Klümper, Daniela Gabbia, Katharina Sieckmann, Dillon Corvino, Anja Winkler, **Miriam Saponaro**, Karin Wörsdörfer, Doris Schmidt, Oliver Hahn,

Ilaria Zanotto, Marina Bertlich, Marieta Toma, Tobias Bald, Markus Eckstein, Michael Hölzel, Matthias Geyer, Manuel Ritter, Dagmar Wachten, Sara De Martin, Abdullah Alajati. „Adipocyte Precursor-Derived NRG1 Promotes Resistance to FGFR Inhibition in Urothelial Carcinoma“. Cancer Research 84, Nr. 5 (March 2024): 725–40. https://doi.org/10.1158/0008-5472.CAN-23-1398.

Miriam Saponaro, Sina Flottmann, Markus Eckstein, Oliver Hommerding, Niklas Klümper, Dillon Corvino, Sana Hosni, Anja Schmidt, Nicolas Mönig, Doris Schmidt, Jörg Ellinger, Marieta Toma, Glen Kristiansen, Tobias Bald, Andrea Alimonti, Manuel Ritter, Michael Hölzel, Abdullah Alajati. „CDCP1 Expression Is Frequently Increased in Aggressive Urothelial Carcinoma and Promotes Urothelial Tumor Progression“. Scientific Reports 13, Nr. 1 (January 2023): 73. https://doi.org/10.1038/s41598-022-26579-z.

Veronica Cocetta, Jessica Cadau, **Miriam Saponaro**, Isabella Giacomini, Stefano Dall'Acqua, Stefania Sut, Daniela Catanzaro, Genny Orso, Giorgia Miolo, Luca Menilli, Andrea Pagetta, Eugenio Ragazzi, Monica Montopoli. „Further Assessment of Salvia Haenkei as an Innovative Strategy to Counteract Skin Photo-Aging and Restore the Barrier Integrity“. Aging 13, Nr. 1 (January 2021): 89–103. https://doi.org/10.18632/aging.202464.

Miriam Saponaro, Isabella Giacomini, Giulia Morandin, Veronica Cocetta, Eugenio Ragazzi, Genny Orso, Ilaria Carnevali, Massimiliano Berretta, Mariangela Mancini, Francesco Pagano, Monica Montopoli. „Serenoa Repens and Urtica Dioica Fixed Combination: In-Vitro Validation of a Therapy for Benign Prostatic Hyperplasia (BPH)“. International Journal of Molecular Sciences 21, Nr. 23 (December 2020): 9178. https://doi.org/10.3390/ijms21239178.

Daniela Gabbia, **Miriam Saponaro**, Samantha Sarcognato, Maria Guido, Nicola Ferri, Maria Carrara, Sara De Martin. „Fucus Vesiculosus and Ascophyllum Nodosum Ameliorate Liver Function by Reducing Diet-Induced Steatosis in Rats“. Marine Drugs 18, Nr. 1 (January 2020): 62. https://doi.org/10.3390/md18010062.